Molecular Selective Interface for an Implantable Glucose Sensor Based on the Viscosity Variation of a Sensitive Fluid Containing Dextran and Concanavalin A

THÈSE N^{O} 4248 (2008)

PRÉSENTÉE LE 19 DÉCEMBRE 2008

À LA FACULTE SCIENCES ET TECHNIQUES DE L'INGÉNIEUR
LABORATOIRE DE PRODUCTION MICROTECHNIQUE 2
PROGRAMME DOCTORAL EN SYSTÈMES DE PRODUCTION ET ROBOTIQUE

ÉCOLE POLYTECHNIQUE FÉDÉRALE DE LAUSANNE

POUR L'OBTENTION DU GRADE DE DOCTEUR ÈS SCIENCES

PAR

Antoine BARRAUD

acceptée sur proposition du jury:

Prof. M.-O. Hongler, président du jury
Prof. P. Ryser, directeur de thèse
Prof. P. Diem, rapporteur
Prof. Ph. Renaud, rapporteur
Dr F. Robin, rapporteur

ÉCOLE POLYTECHNIQUE
FÉDÉRALE DE LAUSANNE

Suisse
2009

Abstract

Diabetes mellitus is a globally growing disease with more than 180 million cases worldwide and no cure exists. In order to minimize the many medical complications, tight glucose monitoring has been shown to be the best alternative. Many diabetics require insulin injections to regulate their glucose level and, as of today, the insulin quantity to be delivered can only be determined on the basis of finger stick measurements. Such measurements are painful and insufficient, and therefore continuous glucose monitoring systems are necessary. A few devices are recently available for 2 - 7 days of use, but since these devices adopt a semi-invasive principle, they are not suited for long term (e.g. 1 year) monitoring. In practice, it is necessary for a long term sensor to be implanted and such a device does not exist yet.

A novel method has been recently developed in our laboratory to continuously monitor the glucose concentration in the subcutaneous interstitial fluid. The method uses an implanted rotating microviscometer to measure the viscosity variations of a glucose-sensitive fluid due to the glucose concentration changes. The present work investigates solutions for a biocompatible interface between the living tissues and the sensitive fluid enclosed in the device. Because the sensitive fluid contains two necessary molecules, dextran and concanavalin A, the interface has to selectively retain these two solutes whilst being permeable to glucose.

On the basis of the requirements of the sensor, a wide literature search and theoretical considerations, two selective interfaces have been selected among the most actual technologies: hybrid membranes composed of a nanoporous alumina membrane coated with poly(poly(ethylene glycol) methacrylate) (PPEGMA) brushes and nanoporous polyethylene films, which have different advantages from each other. A theoretical model for the transient diffusion of a solute through membranes permitted to quantify the membrane performance.

Both selective interfaces have been characterized systematically and their selectivity to a test protein has been demonstrated. Furthermore, the link between the diffusion rate of glucose and the protein retention threshold has been highlighted, which enabled to determine the membrane performance without complex analysis. The optimized hybrid porous alumina-PPEGMA selective interface revealed sufficient retention properties of dextran and ConA in diffusion cells over 48 hours.

In a second step, the hybrid selective interface has been integrated to a

latest implantable sensor demonstrator and the interface performance has been investigated under an environment mimicking the *in vivo* conditions. Since the integrated demonstrator showed a good ability to respond to glucose variations *in vitro*, the system has been transferred for *in vivo* experimentation. An *in vivo* test has been carried out over 5 days in a rat model, and the implantation as well as the transcutaneous data acquisition have been successfully demonstrated. Finally, the sensor capability to respond to glucose variation in a rat model has been shown and solutions for further development of the device are proposed.

Keywords: biofouling, biocompatibility, continuous glucose monitoring, Concanavalin A, dextran, dialysis, glucose concentration sensing, glycemia, glucose affinity sensor, selective interface, microviscometer, nanoporous membrane, long term implantable sensor, biosensor, interstitial implantable sensor, diabetes management, membrane, *in vivo*, minimally invasive, molecular selectivity, diabetes technology, coaxial viscometer.

Résumé

Le diabète est une maladie grandissante qui s'étend à 180 millions de cas dans le monde et aucun remède n'existe. Afin de minimiser les nombreuses complications, il a été démontré qu'une gestion fine de la glycémie reste la meilleure alternative. Beaucoup de diabétiques ont besoin d'injections d'insuline pour réguler leur glycémie et, de nos jours, le dosage ne peut être déterminé qu'en se basant sur des mesures par prélèvement d'une goutte de sang. De telles mesures sont douloureuses et insuffisantes. Par conséquent, un système qui mesure en continu la glycémie est nécessaire. Quelques dispositifs sont disponibles depuis peu pour une utilisation sur 2 à 7 jours, mais puisque ceux-ci ont recours à une méthode semi-invasive, ils ne sont pas adaptés à une utilisation à long terme (p. ex. 1 an). En pratique, il est nécessaire qu'un capteur long terme soit implanté, et un tel appareil n'existe pas encore.

Une nouvelle méthode a été récemment mise au point dans notre laboratoire pour mesurer en continu la concentration de glucose dans le fluide interstitiel sous-cutané. La méthode utilise un implant qui consiste en un micro-viscosimètre rotatif pour mesurer les variations de viscosité d'un fluide sensible aux changements de concentration de glucose. Le travail présenté examine des solutions pour une interface biocompatible entre les tissus vivants et le fluide sensible contenu dans le dispositif. Puisque le liquide sensible contient deux molécules indispensables, le dextrane et la concanavaline A, l'interface doit sélectivement retenir ces deux composants tout en étant perméable au glucose.

En se basant sur les besoins du capteur, une recherche littéraire élargie et des considérations théoriques, deux interfaces sélectives ont été choisies parmi les technologies les plus récentes : des membranes hybrides composées d'une membrane en alumine revêtue de poils en poly(poly(ethylene glycol) methacrylate) (PPEGMA) et des films de polyéthylène nanoporeux, qui présentent chacun des avantages différents. Un modèle théorique pour la diffusion transitoire d'un soluté au travers d'une membrane nous a permis de quantifier les performances des interfaces.

Les deux interfaces sélectives ont été caractérisées systématiquement et leur sélectivité à une protéine test a été démontrée. De plus, le lien entre le taux de diffusion du glucose et le seuil de rétention d'une protéine a été mis en avant, ce qui a permis de déterminer la performance de la membrane sans une analyse complexe. L'interface sélective hybride composée

d'alumine poreuse et de PPEGMA a présenté des propriétés de rétention suffisantes du dextrane et de la concanavaline A dans des cellules de diffusion sur 48 heures.

Dans un deuxième temps, l'interface sélective hybride a été intégrée à un nouveau démonstrateur du capteur de glucose implantable. La performance de l'interface a été examinée dans un environnement imitant les conditions *in vivo*. Etant donné que le démonstrateur intégré a montré une bonne capacité à répondre aux variations de glucose *in vitro*, le système a été transféré pour une expérimentation *in vivo*. Ce test a été effectué sur une durée de 5 jours dans un modèle de rat, l'implantation ainsi que l'acquisition de données transcutanée ont été démontrés avec succès. Finalement, la capacité du capteur à répondre aux variations de glycémie dans un modèle de rat a été montrée. Des solutions pour un futur développement du dispositif sont proposées.

Mots clés: bioencombrement, biocompatibilité, mesure de glucose en continu, concanavaline A, dextrane, dialyse, détection de la concentration de glucose, glycémie, capteur de glucose, interface sélective, micro-viscosimètre, membrane nanoporeuse, capteur implantable long terme, biocapteur, capteur implantable sous-cutané, gestion du diabète, membrane, *in vivo*, peu invasif, sélectivité moléculaire, technologie du diabète, viscosimètre coaxial.

Acknowledgements

I would like to express my gratitude to all those who gave me the possibility to complete this thesis. Especially to Prof. Peter Ryser who offered me the opportunity to work at the Laboratoire de Production Microtechnique at the EPFL and to Eric Meurville the project leader who has always offered me his valuable advice, friendly help and support in difficult times.

I owe my most sincere gratitude to Dr. Nao Takano and Dr. Simon Kuenzi for the many hours of brainstorming and their precious help with measurements and lab equipments.

I am also grateful to Dr. Nao Takano, Eric Meurville, Dr. Franck Robin, Dr. Simon Kuenzi and Prof. Peter Ryser for the proofreading and constructive criticism of my thesis and to Dr. Laurent Lavanant for helping me with the polymer chemistry.

During this work I have collaborated with many friends and colleagues to whom I wish to express my warmest thanks: Caroline, Christian, Christophe, David, Elodie, Eric, Fabrice, Frank, Giancarlo, Ismaël, Jean-Pierre, Julien, Karine, Laurent, Léandre, Mina, Morgane, Nao, Nela, Niki, Olivier, Sadasing, Simon, Sophie, Svend, Sylvain, Thomas and Yannick. Thanks to Karine Genoud for her valuable comments and help in administrative papers.

My sincere thanks are due to the official referees, for their detailed review and constructive criticism of this thesis. I thank the Swiss Innovation Promotion Agency CTI/KTI for funding this thesis under the project number 7537.2 ESPP-LS. I also thank Sensile Medical AG for the direct funding during the last year.

Last, but definitely not least, I wish to thank all my friends and family for their support and the good times during these years at EPFL. Without them, this adventure would by far not have been as enjoyable as it was. I especially thank my parents for their continuous encouragements, Fanny for the wonderful moments and support, and my siblings and nephews Charlotte, Martin, Louise, Aliénor and Augustin for the great moments together.

Contents

List of Figures

List of Tables

Chapter 1

Introduction

1.1 Background & motivations

The World Health Organization[1] (WHO) estimates that more than 180 million people worldwide have diabetes. This number is likely to more than double by 2030. The world prevalence is mapped in figure 1.1. In 2005, an estimated 1.1 million people died from diabetes type 1. Almost 80% of diabetes deaths occur in low and middle-income countries. Almost half of diabetes deaths occur in people under the age of 70 years; 55% of diabetes deaths are in women. WHO projects that diabetes deaths will increase by more than 50% in the next 10 years without urgent action. Most notably, diabetes deaths are projected to increase by over 80% in upper-middle income countries between 2006 and 2015. In many countries in Asia, the Middle East, Oceania and the Caribbean, diabetes affects 12-20% of the adult population.

Diabetes is increasing faster in the world's developing economies than in developed countries. The developing countries will bear the brunt of this epidemic in the 21^{st} century, with 80% of all new cases of diabetes expected to appear in the developing countries by 2025. If present trends persist, by 2025 the majority will be in the 45-64 age group. In a generation, diabetes has had a six-fold increase. Seven out of ten countries with the highest number of people living with diabetes are in the developing world. With an estimated 35 million people with diabetes, India has the world's largest diabetes population.

Diabetes is a silent epidemic that claims as many lives each year as HIV/AIDS. In 2007, diabetes caused 3.5 million deaths globally[2].

Diabetes mellitus can now be found in almost every population in the world and epidemiological evidence suggests that, without effective prevention and control programmes, diabetes will likely continue to increase

[1] http://www.who.int

[2] http://www.worlddiabetesfoundation.org

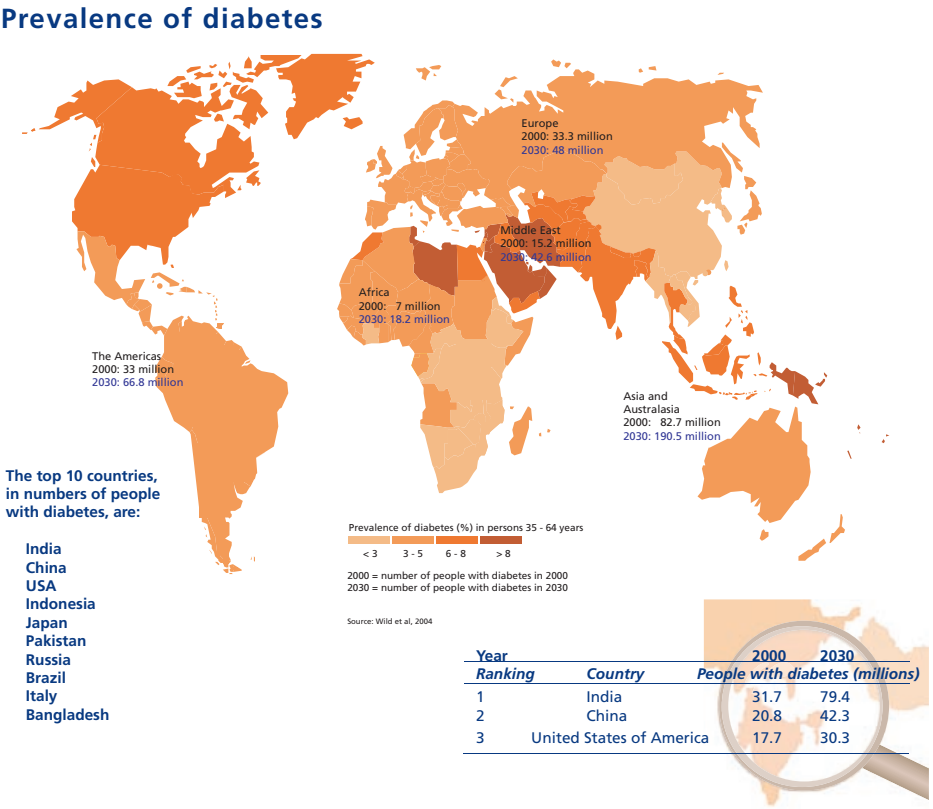

Figure 1.1: World map of the diabetes prevalence in the active population. Source: World Health Organization

globally.

Before insulin was discovered in 1921, diabetes was a deadly illness. Today, there is still no cure for diabetes, the best way to avoid health complication is to manage the illness through tight glucose monitoring together with insulin injections. Less acute cases of type 2 diabetes can manage it through an adapted diet and lifestyle, or simple oral medication can be prescribed.

The first company to introduce a blood glucose measurement system for home use was A.R.M. in 1965[3]. The Dextrostix were paper strips covered with a chemical reagent whose color was changing with the addition of a drop of blood. The reaction had to be timed for one minute, and was then washed off. The strip developed a color which was compared to a

[3]http://www.mendosa.com/history.htm

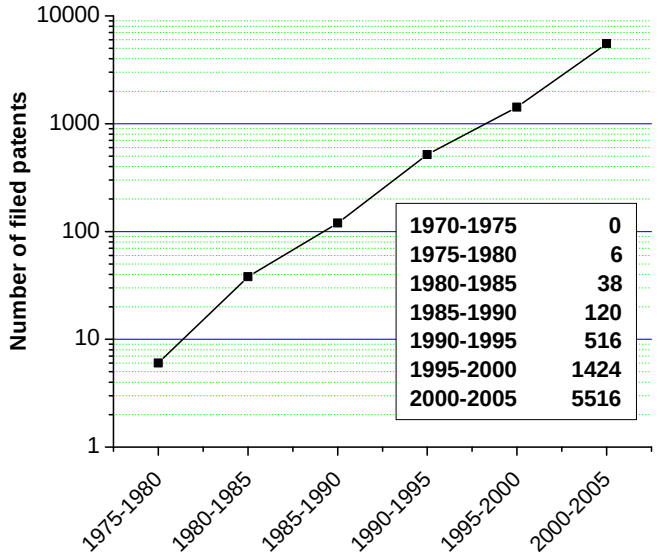

Figure 1.2: Number of patents filed in the United States on non-invasive glucose measuring techniques. The U.S. patents make up about 80% of the worldwide list.
Source: http://www.mendosa.com/noninvasive_glucose.pdf

color chart for glucose concentration determination. The system was not quantitative, but gave an approximation of the blood glucose level. In addition, it was more designed for physician's office than home use. Later in 1970, realizing that the Dextrostix were difficult to read, Anton Hubert Clemens developed a reflectance meter. The instrument measured the color of the reflected light from the Dextrostix strips and made their use more convenient.

Today, at the beginning of the 21^{st} century, not much has changed in the world of glucose measuring techniques. Of course, the meters have become more accurate, smaller and require less blood volume. But there is still no painless solution commercially available to measure the blood glucose concentration. The research for an alternative method, which would prevent diabetics to prick their fingers, has been going on for the last 30 years. Today the motivation is growing drastically, and it becomes an evidence if one looks at the increasing number of filed patents in the United States on the topic of non-invasive glucose measuring methods, see figure 1.2.

It stands to reason that the motivation toward better glucose measuring techniques is also economical. In 2007, the glucose monitoring market is estimated worldwide to over six billion US dollars and it is obvious that

the massive demand from patients will guarantee an immediate financial success for the organization that finally finds a solution.

As actual non-invasive measuring method fail providing a reliable device, research groups are focusing on long-term implantable glucose sensors, also called minimally invasive. Such a device would allow a constant monitoring of the human glycemia and would considerably improve the quality of life of diabetics. Moreover, it would generalize the real-time closed-loop insulin regulation. Such a system, joining a glucose sensor and an insulin pump, is called an artificial pancreas.

In 2008 no one has succeeded in bringing a long-term implantable glucose sensor to commercial realization. Most insulin dependent diabetics still rely on 2 - 6 glucose measurements per day to manage their insulin injections, like thirty years ago. Therefore a implantable device would represent a major breakthrough in the diabetes management and overall health of the patients.

Our team, through the **I**mplantable **GLU**cose **S**ensor (IGLUS) project, aims at the realization of such a long-term implantable glucose sensor.

1.2 Diabetes

In this section, an overview of diabetes is presented. We intend to give basic information about the disease and its different forms, and shortly present the different complications.

Diabetes mellitus is recognized as a group of heterogeneous disorders with the common elements of hyperglycaemia and glucose intolerance due to insulin deficiency, impaired effectiveness of insulin action, or both.

Diabetes mellitus is classified on the basis of aetiology and clinical presentation of the disorder into three main types: Type 1 diabetes, Type 2 diabetes, gestational diabetes and other specific types[4].

1.2.1 Type 1

Type 1 diabetes results from cellular-mediated autoimmune destruction of pancreatic islet β-cells causing the loss of insulin production. It ranks as the most common chronic childhood disease in developed nations, but occurs at all ages and the clinical presentation can vary with age. Figure 1.3 presents a schematic of the the glucose regulation.

Type 1 diabetes in an adult may masquerade as Type 2 diabetes at presentation with a slow deterioration in metabolic control, and subsequent progression to insulin dependency. This form is called latent autoimmune

[4] http://www.eatlas.idf.org

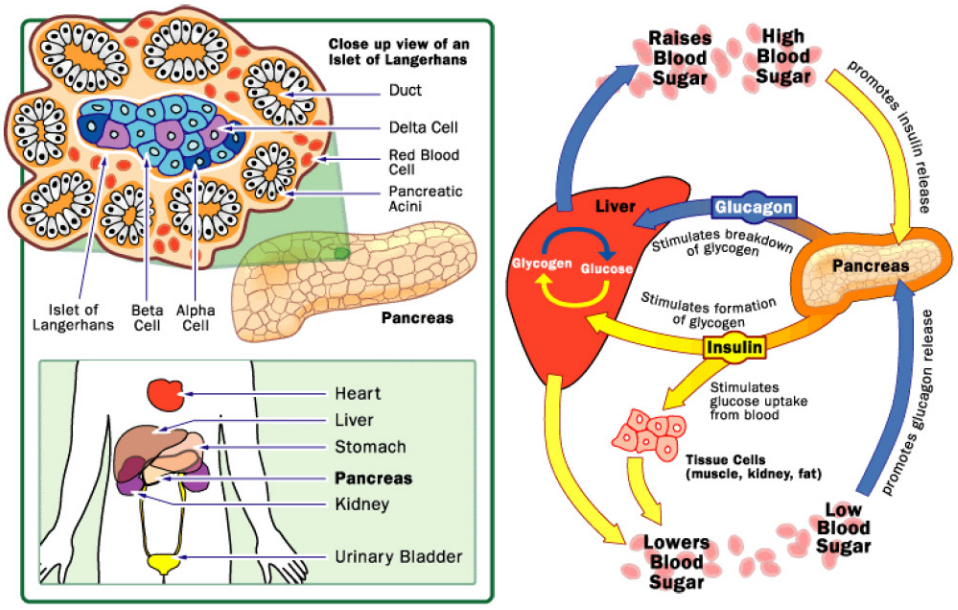

Figure 1.3: The pancreas has many islets that contain insulin-producing β-cells and glucagon-producing α-cells. Insulin and glucagon have opposite effects on liver and other tissues for controlling blood-glucose levels. Source: http://health.howstuffworks.com/diabetes1.htm

diabetes mellitus in adults (LADA). LADA falls within Type 1 autoimmune diabetes, but in a slowly progressive form, in the new WHO classification.

The predominant cause of hyperglycaemia in Type 1 diabetes is the autoimmune destruction of the β-cells, which leads to absolute dependence on insulin treatment and a high rate of complications typically occurring at relatively young ages.

1.2.2 Type 2

Type 2 diabetes is characterized by insulin resistance and relative insulin deficiency, either of which may be present at the time that diabetes becomes clinically manifest. The specific reasons for the development of these abnormalities are not yet known.

The diagnosis of Type 2 diabetes usually occurs after the age of 40 years although the age of onset is often a decade earlier in populations with a high diabetes prevalence. People with Type 2 diabetes may not show any symptoms for many years and the diagnosis is often made from associated complications or incidentally through an abnormal blood or urine glucose test.

Type 2 diabetes is often, but not always, associated with obesity, which

itself can cause insulin resistance and lead to elevated blood sugar levels. It is strongly familial, but major susceptibility genes have not yet been identified. In contrast to Type 1 diabetes, persons with Type 2 diabetes are not dependent on exogenous insulin and are not ketosis-prone, but may require insulin for control of hyperglycaemia if this is not achieved with diet alone or with oral hypoglycaemic agents.

Type 2 diabetes constitutes about 85% to 95% of all diabetes in developed countries, and accounts for an even higher percentage in developing countries. It is now a common and serious global health problem, which, for most countries, has evolved in association with rapid cultural and social changes, ageing populations, increasing urbanization, dietary changes, reduced physical activity and other unhealthy lifestyle and behavioural patterns.

1.2.3 Gestational

The most widely accepted definition of gestational diabetes mellitus (GDM) is "carbohydrate intolerance of varying degrees of severity with onset or first recognition during pregnancy". This definition applies regardless of whether insulin is used for treatment or the condition persists after pregnancy. It does not exclude the possibility that unrecognized glucose intolerance may have occurred before the pregnancy.

It is widely believed that differences in reported prevalence of GDM parallel the differences that have been found in the frequency of Type 2 diabetes among different populations. Nonetheless GDM is increasing in prevalence in concert with the worldwide rise in Type 2 diabetes.

1.2.4 Complications of diabetes

While insulin allows a person with Type 1 diabetes to stay alive, it does not cure the disease, nor does it prevent the development of serious complications, which can be many and varied. High blood sugar levels eventually damage blood vessels, nerves, and organ systems in the body. Among the potential complications of diabetes are:

Cardiovascular disease
Cardiovascular disease, a range of blood vessel system diseases that includes both stroke and heart attack, is the major cause of death in people with diabetes. The two most common types of cardiovascular disease are coronary heart disease, caused by fatty deposits in the arteries that feed the heart, and hypertension, or high blood pressure. Research shows that people with diabetes are more likely to have high cholesterol and hypertension, both of which cause damage to the cells lining the artery walls. Researchers

think high blood glucose contributes to both of these conditions.

Hypoglycemia

Hypoglycemia, low blood sugar, is a dangerous condition for people with diabetes. It can be triggered by not eating often enough, eating too little food, too much physical activity without eating, or too much insulin. People with diabetes can usually tell when their blood sugar is low. But the more episodes of hypoglycemia you have, the harder it gets for your body to detect the next episode. In severe forms, hypoglycemia can lead to unconsciousness or even death. For patients with Type 1 diabetes, fear of hypoglycemia is a major obstacle to maintaining tight blood glucose control.

Nephropathy

Diabetic kidney disease, also known as diabetic nephropathy, is one of the most common and most devastating complications of diabetes. It is a slow deterioration of the kidneys and kidney function which, in severe cases, can eventually result in kidney failure, also known as end-stage renal disease, or ESRD. About one third of people with Type 1 diabetes develop nephropathy.

Neuropathy

Neuropathy, or nerve damage, affects more than 60% of people with Type 1 diabetes. The impact of nerve damage can range from slight inconvenience to major disability and even death. Diabetic neuropathy leads to loss of feeling and sometimes pain and weakness in the feet, legs, hands, and arms, and is the most common cause of amputations not caused by accident in the United States. In one type of neuropathy, known as autonomic neuropathy, high glucose levels injure the autonomic nervous system, which controls bodily functions such as breathing, circulation, urination, sexual function, temperature regulation, and digestion. Autonomic neuropathy may result in various types of digestive problems, diarrhea, erectile dysfunction, a rapid heartbeat, and low blood pressure.

Retinopathy

Diabetic retinopathy is the most common and serious eye-related complication of diabetes. It is a progressive disease that destroys small blood vessels in the retina, eventually causing vision problems. In its most advanced form (known as "proliferative retinopathy") it can cause blindness. Nearly all people with Type 1 diabetes show some symptoms of diabetic retinopathy, usually after about 20 years of living with diabetes; approximately 20 to 30% of them develop the advanced form.

1.2.5 Glucose concentration range in blood

The blood glucose concentration (or blood sugar concentration or glucose level) is tightly regulated in the human body. In non-diabetics, the concen-

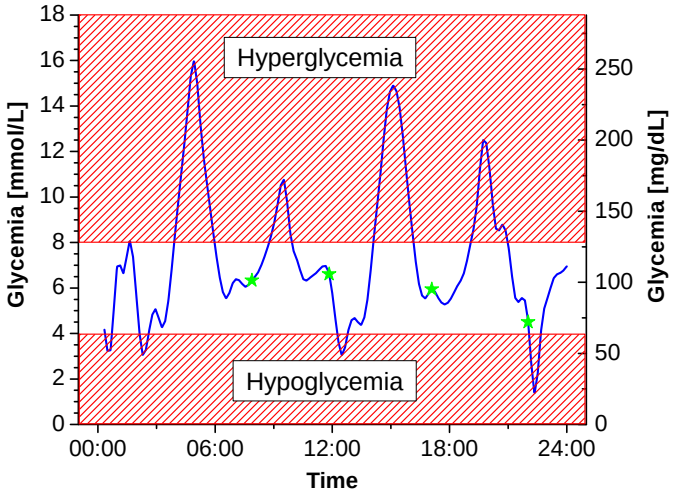

Figure 1.4: Glycemia evolution of a diabetic over one day. The green points represent the points-in-time monitoring obtained with finger-stick measurements, and the blue curve the real glycemia.

tration is maintained between 4 and 8 mM (72 to 144 mg/dl). The total amount of glucose in the circulating blood is therefore between 3.3 to 7 g (assuming an ordinary adult blood volume of 5 l). This amount is rather low compared to the body needs. As a comparison, 1dl of Coca-Cola has 30 g of sugar. As a general rule, the glucose concentration is at its lowest level in the morning before the first meal, and rises after every meal.

Diabetics have a much broader range of blood glycemia depending on the way they manage the condition. If not or poorly controlled, the blood glucose level can, in extreme cases, reach 50 mM (900 mg/dl). An example of the glycemia excursion of a diabetic over day is depicted in figure 1.4.

Hypoglycemia is defined below a threshold of 4 mM (72 mg/dl). Above a concentration of 8 mM (144 mg/dl), it is considered as a hyperglycemia. In between, the term normoglycemia is used. There is no absolute definition for the two thresholds, since these values can differ slightly depending on the patient and physician.

Commercially available strip glucose meters have a typical measuring range of 0.6 to 33.3 mM (10-600 mg/dl).

1.3 Needs for glucose regulation

Many of the complications of diabetes can be prevented through tight control of glucose levels. Two landmark studies on diabetes treatment were the Diabetes Control and Complications Trial (DCCT), completed by the National Institutes of Health in 1993 among 1'400 Type 1 diabetes patients,

and the United Kingdom Prospective Diabetes Study (UKPDS) completed in 1998 with 5'000 Type 2 diabetes patients. These studies demonstrated that tight glucose control, involving various therapeutic interventions as well as three or more glucose measurements daily, substantially reduced morbidity and mortality among these diabetes patient populations.

In addition, the DCCT showed that intensive glucose control dramatically delays or prevents the eye, nerve, and kidney complications of Type 1 diabetes. A paradigm shift in the way Type 1 diabetes is controlled was based on this finding. As researchers continued to follow study participants, they found that tight glucose control also prevents or delays the cardiovascular complications of Type 1 diabetes, such as heart attack and stroke[5].

Even before a closed-loop artificial pancreas is available, continuous glucose monitoring (CGM) is expected to help people with diabetes better manage glucose levels. In fact, clinical studies [21] have shown that patients using CGMs spend much more time in the normal glucose range compared with patients using conventional finger-stick blood glucose methods. With tighter control, as measured by long-term hemoglobin A1c testing, their risk of complications should drop dramatically.

1.4 The market

In 2007 the glucose monitoring market is estimated worldwide to be over six billion dollars. Earlier, in 2004, the market was estimated at 5 billions, mostly shared by four big companies as presented in figure 1.5.

As for the economic burden of the disease, 5 to 10% of the world's healthcare budget is currently spent on diabetes, and by 2025 this figure could reach 40% in some countries if predictions of diabetes prevalence are fulfilled[6]. Most of the economic costs of diabetes are attributable to the various complications linked to it, with up to two-thirds of people with diabetes in certain countries developing serious chronic complications. The American Diabetes Association estimated in 2007 diabetes costs to be $174 billion each year for the United States, $58 billion thereof generated by indirect costs. Health expenditure due to diabetes for Europe was $120 billion in 2007. While increasing in incidence, diabetes already represents a substantial burden to health systems. For Switzerland, costs caused by this disease currently represent 5 - 10% of the health expenses. A device that can lower the costs is ensured to rapidly take market shares.

[5]Source: http://www.nih.gov
[6]Source: http://www.idf.org

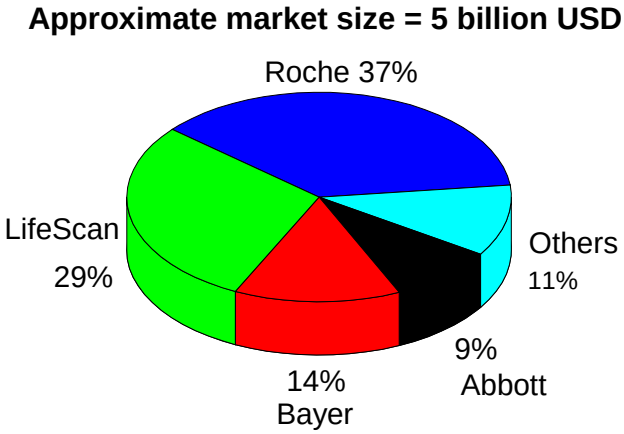

Figure 1.5: Glucose test sensor market in 2004. Source: Abbott Laboratories.

1.5 This work

As described in section 1.1, diabetes mellitus is a globally growing disease. In order to minimize the medical complications, tight glucose monitoring is required. As of today, however, the insulin quantity to be delivered can only be determined on the basis of finger stick measurements. CGM devices are recently available for 2 - 7 days of use, but since these devices adopt a semi-invasive principle, they are not suited for long term (e.g. 1 year) monitoring. In practice, it is necessary for a long term sensor to be implanted and such a device does not exist yet.

The IGLUS is an implant type sensor and is meant for a continuous use over 1 year. The original idea of the IGLUS comes from Dr. Sigi Straessler, Dr. med. Klaus Ganz and Prof. Dr. Peter Ryser, and has been engineered by members of the Laboratoire de Production Microtechnique at EPFL.

The work presented in this thesis intends to develop a molecular selective interface (SI) for the IGLUS which is based on a glucose-sensitive fluid containing dextran and concanavalin A. The SI is one of the biggest pieces of the puzzle for the IGLUS to function, and is essential to be understood to design an optimum system. One of the other important pieces is a microviscometer, which was thoroughly investigated in a previous work [22], and consists of a novel method to continuously monitor the viscosity variations of the sensitive fluid due to the glucose concentration changes. The last piece of the puzzle is the sensitive fluid (SF).

Deeper in details, this work aims to select a better membrane for the IGLUS and to give tools for this purpose. We focused on the realization of a working IGLUS demonstrator *in vitro*, which is then applied to *in vivo* stud-

ies. In order to select an optimum membrane, the functioning of every component of the sensor must be well understood. Another task of this work is to choose the best known technologies for each component and integrate them to build the IGLUS demonstrator. The vision of the overall project is to create a commercial product, and therefore the choices must integrate existing and suitable technologies for production. The chosen SIs characterized in this work are a hybrid membrane composed of a nanoporous alumina membrane coated with poly(poly(ethylene glycol) methacrylate) brushes (PPEGMA) and a nanoporous polyethylene (PE) film. The hybrid membrane was developed by Dr. Laurent Lavanant in the laboratory of Prof. Dr. Harm-Anton Klok. And the PE films were developed by Prof. Dr. Hiroki Uehara.

In the following, a state-of-the-art in glucose measuring technologies is presented to start with, and the IGLUS concept and functioning are descibed. Then the basics and requirements to design the SI are introduced and followed by the results of characterization of the chosen SI through glucose diffusion and protein retention measurements in diffusion cells. Afterwards, the *in vitro* assessment of the SI on a latest IGLUS demonstrator is discussed. The last part of this work describes the first application of the IGLUS to *in vivo* environment and the related results are analyzed for future improvement.

Chapter 2

State of the art in glucose measuring technologies

2.1 Introduction

The glucose concentration in the body can be measured by various techniques, which are applied either to the interstitial fluid or to the blood. They can be summarized in 3 groups: electrochemical, spectroscopic and mechanical methods.

Nowadays, the standard measuring technique is the test strip, which relies on an electrochemical principle. Since a blood sample must be taken for every measurement, the method is painful and the frequency of measurements is limited. The only potential commercially available alternatives are semi-invasive needle sensors. These are quite new and cannot replace the test strips at present. The barriers are both scientific and regulatory[1]. Indeed their reliability is not sufficient and reference measurements still need to be done using strips. Due to the infection risks, the semi-invasive needle sensors are short-term sensors (2 - 7 days). A long-term solution can only be achieved with an implantable sensor, but no commercial product is available, nor any FDA[2] or CE[3] approved device. As discussed in section 1.3, continuous glucose monitoring (CGM) sensors represent the optimal way for glycemia regulation. It stands to reason that a long-term CGM sensor would make very rich its inventors. Often companies prematurely disclosed that they were close to a solution, but were not. Now, diabetics, investors and researchers are suspiciously awaiting a working device for over thirty years [23]. It is difficult to gather reliable information from the

[1] http://www.jdrf.org

[2] U.S. Food and Drug Administration, responsible agency for the safety regulation of medical devices in USA.

[3] "Conformité Européenne", certification required for medical devices in the European Union.

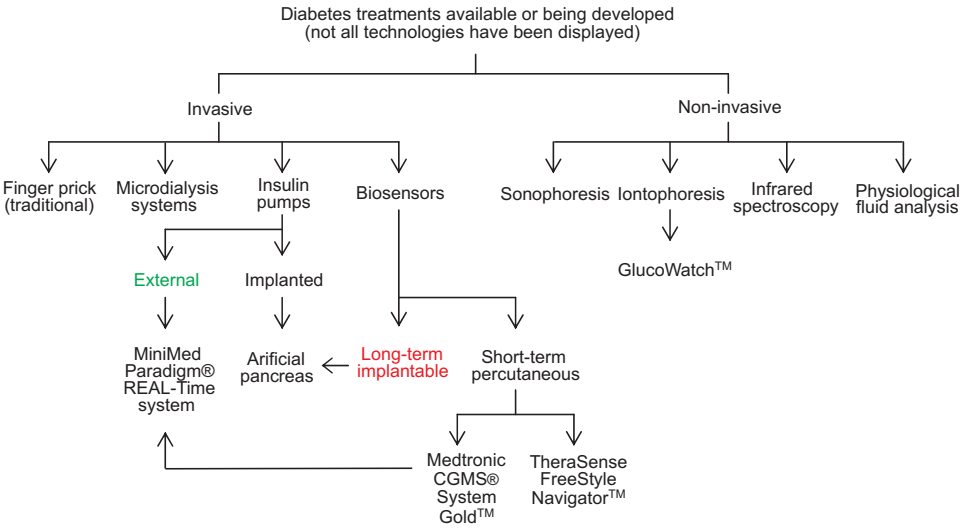

Figure 2.1: Schematic of the different glucose measuring techniques and the key commercial products [1].

web sites of companies, therefore the present state-of-the-art is based on scientific publications. Web sites are solely useful to have an overview of the current products, as they tend to be too optimistic for marketing purposes. However an independent web site keeps an objective list of the current companies working on glucose monitoring: http://www.mendosa.com/-meters.htm.

The different glucose measuring techniques and their related commercially available devices are briefly described in the following sections. Figure 2.1 describes the different glucose measuring techniques together with the key commercial products.

2.2 Electrochemical test strips

In 2008, the only reliable and approved glucose measurement for diabetes management is the electrochemical test strip. This method requires the patient to take a blood sample of 0.3 to 1 μl (depending on devices) and place it on a disposable test strip, which is connected to an electronic device (meter) for data acquisition. The test strip contains a capillary that absorbs a reproducible amount of blood on an enzyme electrode containing glucose oxidase (GO). The enzyme is reoxidized with an excess of ferrocyanide ion as schematized in figure 2.2. The total charge passing through the electrode is measured and is proportional to the concentration of glucose. Some glucose meters use another enzyme, the glucose dehydrogenase (GD).

Over twenty five different meters are available commercially. But four

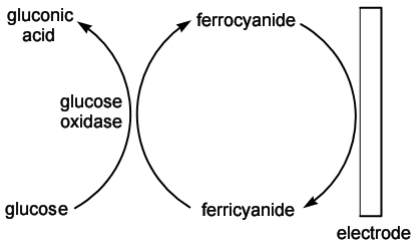

Figure 2.2: The electrochemical reaction in a glucose monitoring test strip [2].

Table 2.1: Recent strip glucose meter from the four market leaders. GO and GD stand for glucose oxidase and glucose dehydrogenase respectively.

Brand	**Glucose meter**	**Blood sample**	**Chemical reaction**
Roche diagnostics	Accu-chek Aviva/Advantage	0.6 μl	GO
Abbott diabetes care	FreeStyle/Flash/ Freedom	0.3 μl	GD
Bayer	Contour/Breeze 2	0.6/1 μl	GO
Lifescan	UltraSmart/ UltraMini	1 μl	GO

major companies share almost 90% of the market. The latest glucose meters from these companies are listed in table 2.1. The accuracy of such meters is approximatively $\pm$15%. This gives an estimate of the required accuracy for glucose sensors.

Some recent glucose meters, like the Precision Xtra from Abbott Diabetes Care, integrate the measurement of β-hydroxybutyrate (β-ketone) concentration in the blood to detect ketoacidosis, because diabetic ketoacidosis is a life-threatening complication if not treated. Urine ketone test strips are the only alternative.

2.3 Non-invasive sensors

As people suffering from diabetes need to measure frequently their glycemia frequently, a system capable of a painless and continuous measurement is highly demanded. It would avoid the pain caused by the finger pricking and allow a tight control of the glycemia. A measuring method which does not mechanically penetrate the skin or a body cavity is commonly named non-invasive. Such a method would highly ease and enhance the diabetes management or at least increase patients' compliance.

Table 2.2: Non-invasive optical, acoustic and electromagnetic glucose detection methods.

Technique	**Definition**	Ref.
Polarimetry	A reflected polarized light beam, usually through the eye, contains information on the glucose concentration.	[26, 27, 28]
Near Infrared (NIR) absorption and scattering	Absorption or emission in the 0.7 to 2.5 μm region of the spectrum.	[29, 30, 31, 32]
Raman spectroscopy	Probes the vibrational modes of glucose with inelastic scattering of light.	[33, 34, 35, 36]
Photoacoustic	The photoacoustic effect is based on the generation of acoustic waves as a consequence of light absorption.	[37, 38, 39, 40, 41]
Optical coherent tomography	Low-coherence interferometry with backscattered light from the tissue using super bright LEDs or lasers with extremely short pulses. The light spectrum is in the range of 10 - 15 μm.	[42, 43, 44]
Impedance spectroscopy	Dielectric investigation of cellular membranes (influenced by glucose). Electromagnetic frequency spectrum: 1 to 200 MHz.	[45, 46, 47]

Currently developed non-invasive methods are mainly spectroscopic and of the following types: optical, acoustic and electric. The general measurement principle can be summarized as follows: a zone of skin or of the eye is probed by sending a signal, and a signature is detected within the response, which is obtained either by reflection, diffusion or scattering. D-glucose can be detected through numerous spectroscopic signatures, but the difficulty is to extract its signature in the complex environment that is the body. The usual test sites are finger tips, forearm, ear lobe and eye. Many different non-invasive techniques have been reviewed [24, 25] and an overview is presented in table 2.2.

Though many different spectroscopic techniques exist, none has been successfully integrated in a commercial working glucose meter yet. All methods suffer from the fact that glucose has a chemical composition similar to other components of its environment, and do not have the property to show an important response to any of the methods. In other word, none of these techniques is sufficiently selective to glucose to precisely detect its

presence.

The only non-invasive glucose sensor that currently has an FDA approval is the GlucoWatch G2 Biographer from Cygnus. The device requires a daily calibration and is only meant to monitor the glycemia trends. One limitation is that the GlucoWatch system is not able to cope with sweat at the measurement site. Due to such limitations, the product is no longer on the market.

Besides these methods, other approaches to non-invasive glucose monitoring are investigated. Some try to extract a small sample of interstitial fluid through the skin by applying vacuum[4] through the skin. Others apply a small electric current to the skin (ionophoresis) [31, 48, 49, 50, 51]. It results that uncharged particles such as glucose are carried by electroosmosis to the cathode. However, as it is the case for the GlucoWatch, the skin is often covered by sweat or other secretions which interfere with the measurements, therefore the device requires recurrent calibrations.

2.4 Semi-invasive sensors

Semi-invasive glucose sensors are external devices with a probe inserted through the skin into the subcutaneous tissues. In general, the probe consists of a flexible needle or thin flexible probe and is disposed after a limited time, between one to seven days for the actual sensors. The measurement in the interstitial fluid of the subcutaneous tissue is suitable because it has been demonstrated that there is a good correlation between the glucose concentration in the interstitial fluid and the blood glucose concentration [52, 53]. This correlation is subject to a lag time of 5 to 30 minutes depending on the implantation site.

The existing sensors employ different measuring methods. One category measures the glucose concentration at the tip of a needle while another extract a small amount of interstitial fluid. A third category uses a dialysis type needle.

Needle type sensors are now present on the market, but only available under medical prescription. Health care professionals use them for their diabetic patients in order to have a clearer view of the glycemia evolution throughout the day. The system gives a continuous glycemic profile which fills in the gaps left by punctual measurements, and can reveal hidden patterns, like frequent episodes of hypoglycemia (see figure 1.4). But, at present, it is not meant for an every day use.

Needle glucose sensors still suffer from a poor reliability and accuracy, especially in the hypoglycemic range [54, 55]. Even though several products have obtained the CE mark or FDA certification, they are not approved

[4] http://www.iit.edu/∼ipro331f04/ultrasound.html

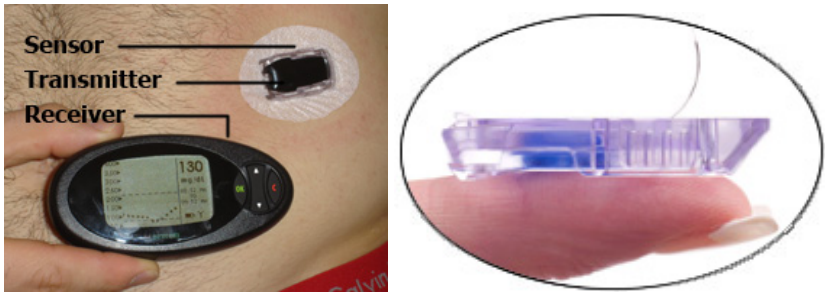

Figure 2.3: Dexcom STS semi-invasive electrochemical sensor. The image on the right shows the sensor and the flexible needle which is inserted into the skin.

to replace the finger stick method, only to supplement it or to serve as "glucose trend monitors".

Besides the motivation to replace daily glucose testing, efforts have been taken to develop a reliable short-term glucose sensor for use in clinical environment, especially in intensive care units.

The main recent semi-invasive techniques and products are given below and are separated in three categories: electrochemical, optical and mechanical methods.

2.4.1 Electrochemical needle glucose sensors

All FDA or CE approved devices are listed in table 2.3 and are based on the glucose oxidase (GO) electrochemical method, which is described in section 2.2. Electrochemical sensors are known to be a rapid and rather reliable method in the short-term range. The accuracy of the cited continuous glucose sensors is in the range of 14-20% [56]. As an example, the minimally invasive sensor from Dexcom is shown in figure 2.3.

The GlucoDay from Menarini is particular because it uses the combination of two dialysis membranes and a GO-based sensor. A dialysis hollow fiber (regenerated cellulose) with a molecular weight cut-off (MWCO) of 15 - 20 kDa is inserted subcutaneously. A perfusion solution flows in the fiber and transports the glucose to the GO electrochemical sensor. The GO probe is covered with a second dialysis membrane (cellulose ester) with a MWCO of 100 Da, which prevents some interferant constituents of the interstitial fluid (ascorbic and uric acid) from reaching the electrode. In summary, the GlucoDay distributes the dialysis process to two membranes, the hollow fiber having a high MWCO and a high diffusivity to glucose, and a membrane with a very low MWCO (very selective) and a poor glucose diffusivity. The slow glucose diffusivity of the latter membrane is not an issue since it directly covers the probe and hence the response time remains

Table 2.3: Semi-invasive sensors: FDA or CE approved continuous glucose monitoring devices. GO stands for glucose oxidase.

	CGMS Gold	GlucoDay-S	Guardian TGMS
Company	Medtronic	Menarini	Medtronic
Approval	1999 FDA	2002 CE	2004 FDA
Method	GO μ-electrode	Dialysis + GO	GO μ-electrode
Life time	72 h	48 h	72 h
Calibration	4/day	first day	4/day
Test freq.	5 min	5 min	5 min

	Guardian RT	STS Sensor	FreeSytle Navigator
Company	Medtronic	DexCom	Abbott
Approval	2005 FDA	2006 FDA	2008 FDA
Method	GO μ-electrode	GO probe	GO probe
Life time	72 h	7 days	5 days
Calibration	max 5/day	every 12h	4 /5 days
Test freq.	5 min	5 min	1 minute

rapid.

2.4.2 Optical needle glucose sensors

The optical needle glucose sensor developed by Ballerstadt *et al.* [57] is based on a fluorescence measurement. The principle is based on the reversible binding of fluorescent-labeled concanavalin A (ConA) to glucose inside a colored Sephadex bread [58]. The fluorescent dye Alexa647 is grafted to ConA and emits in the red visible light range (670 nm). The fluorescent compound is placed at the tip of a glucose permeable needle which is connected through an optical fiber to an external electronic device. The company BioTex[5] is currently developing the device. The current restriction of the method are the long-term stability and the decay of the fluorescence intensity.

Pasic *et al.* [59, 60] proposed to measure the interstitial glucose concentration using a dialysis hollow fiber coupled to a fiber optics sensor. The glucose level is detected via oxygen consumption which occurs as a consequence of the enzymatic reaction between glucose and immobilized GO. Using an optical fiber, the probe is connected to an oxygen meter that uses a phase-shift method for the determination of the luminescence decay time which is then converted to oxygen concentration. A representation of the probe is given in figure 2.4. This device is intended for intensive care units

[5]http://www.biotexmedical.com

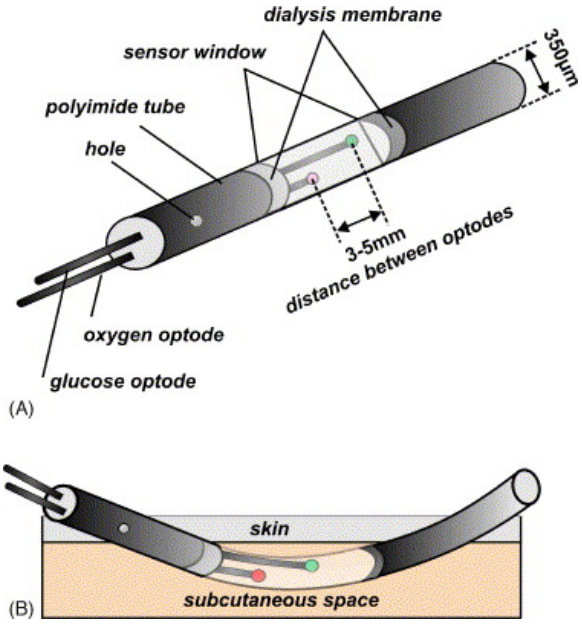

Figure 2.4: A) Schematic representation of the hybrid sensor. Both the oxygen and the glucose concentration are measured through optic-fibers. B) The sensor is implanted subcutaneously for a duration of 24 h.

since, compared to other GO-based systems, the sensitivity loss due to oxygen is compensated.

Another interesting concept has been developed by GluMetrics LLC. Their device, the GluCath^{TM}, contains a glucose-sensitive boronic acid-based polymer that fluoresces in the presence of glucose[6]. The polymer is embodied in a catheter inserted into the venous periphery, and the system allows a direct monitoring of blood glucose for up to 48 h. The targeted market is critically ill patients in intensive care units. They pretend to avoid stability issues due to oxygen interference by working without an enzyme-based reaction. This device is still under development, and no *in vivo* results are available.

No needle glucose sensor based on optical method currently holds a FDA or CE approval. Nonetheless, several serious candidates are present in the semi-invasive glucose monitoring area.

2.4.3 Mechanical needle glucose sensors

A needle glucose sensor based on a chemico-mechanical principle has been developed by the swiss company Disetronic[7] under the trade name Gluc-

[6] http://www.Glumetrics.com
[7] http://www.disetronic.com

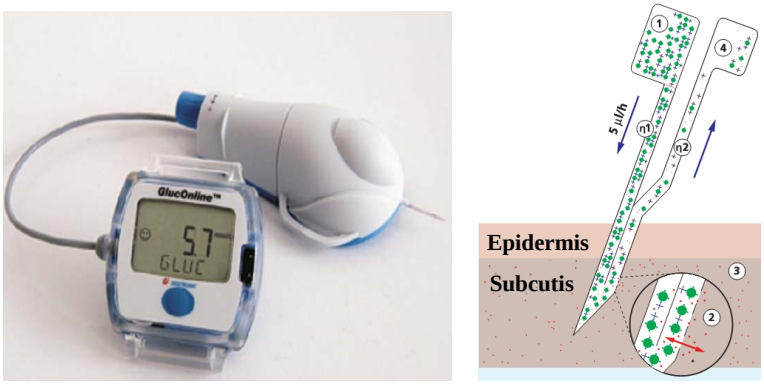

A) B)

Figure 2.5: A) GlucOnline device prototype from Disetronic. B) Schematic view of measuring principle. 1) Reservoir and pump. 2) Microdialysis through semi-permeable membrane. 3) Subcutaneous tissue. 4) Collecting vessel. The viscosity is measured via the two pressure sensors $\eta 1$ and $\eta 2$, and gives the glucose concentration.
Source: www.disetronic.com.

Online. This company was acquired by Roche in 2003 and the project was sold to Sensile Medical AG. The semi-invasive needle sensor measures the viscosity variations of a glucose-sensitive fluid. The fluid is based on the competitive binding affinity of the ConA lectin with glucose and dextran. The needle encloses a dialysis hollow fiber in which the sensitive fluid flows. A pump initiates the flow and the viscosity is determined by measuring the pressure difference at both ends of the fiber via two pressure sensors. The device is shown in figure 2.5. For every measurement, a new dose of the sensitive fluid is used. The GlucOnline is dedicated to intensive car units and can monitor glucose levels subcutaneously over 5 days.

The GlucOnline sensor has served as an inspiration to design our implantable glucose sensor, the IGLUS. The IGLUS is based on a similar glucose-sensitive fluid but uses a different method to measure the viscosity. As detailed in section 3.3, the IGLUS uses a rotational microviscometer and the sensitive fluid is kept during the sensor life time. The device is implantable and therefore is suitable for a long-term activity.

2.5 Implantable sensors

Among existing implantable sensors, one can distinguish two groups: the minimally invasive and the invasive sensors. The invasive category requires surgery in order to be implanted. As for the minimally invasive

ones, they can be implanted subcutaneously with a syringe-trocar upon a local anesthesia. The IGLUS belongs to the minimally invasive implantable sensors.

Since 1997, Animas corp.[8] (acquired by Johnson & Johnson in 2005) has been working on a long-term implantable continuous glucose sensor which can be classified in the invasive category. They decided not to base their sensor on the enzymatic method to avoid the known stability and drift issues. The Animas sensor measures the near-infrared absorption of blood and they target a sensor life time of over 5 years. The rather large device (twice the size of a pacemaker) is surgically implanted under the skin, and a probe, connected to the main device through an optical fiber, is inserted in a blood vessel. The system has the advantage of indicating directly the blood glycemia. However, the information about the sensor has disappeared from Animas web site, which is not a sign of success.

The methods used for minimally invasive implantable sensors are electrochemical, spectroscopic or mechanical, and are similar to the ones used for non-invasive and semi-invasive sensors. A substantial number of devices has been recently reviewed [61], and the Diabetes Monitor web site[9] lists the many companies working on such systems. However, as of today no device has been approved by the FDA or CE mark.

An interesting technology, based on fluorescence measurement, is developed in competition by two companies, Dexcom[10] and Sensors for Medicine and Science (SMSI)[11]. The devices embed the excitation source (LED) in the sensing element which is a matrix containing fluorescent indicator molecules (fluorophore). SMSI has a FDA pre-market approval application process underway. Surprisingly, Dexcom has recently abandoned its long-term implantable glucose sensor and now focuses its efforts on the short-term needle sensor (see section 2.4.1).

Finally, three devices are classified in the mechanical implantable sensors. The IGLUS (our sensor), which uses a rotatory microviscometric measurement of viscosity-variable fluid containing dextran and ConA. The sensor of Zhao *et al.* [62] uses a similar glucose-sensitive fluid, but measures the viscosity with a vibrating cantilever. The latter uses a regenerated cellulose membrane as a selective interface, but no data showing a continuous monitoring have been published yet.

The third device is from Lei *et al.* [63]. The basic device structure is a passive (inductor/capacitor (LC)) micromachined resonator coupled to a stimuli-sensitive hydrogel, which is confined between a stiff nanoporous membrane and a thin glass diaphragm. As glucose molecules pass through the nanoporous membrane, the hydrogel swells and deflects the flexible

[8] http://www.animascorp.com
[9] http://www.diabetesmonitor.com/meters.htm
[10] http://www.dexcom.com
[11] http://www.s4ms.com

glass diaphragm, which is the movable plate of the variable capacitor in the totally integrated passive LC resonator. The corresponding change in resonant frequency can be remotely detected. The nanoporous membrane used to cap the hydrogel is an anodic alumina membrane with 200 nm pores and a thickness of 60 μm (from Whatman International), and the glucose-sensitive hydrogel is based on phenylboronic acid. We believe this sensor to be a very promising technology, since it eliminates the necessity of a molecular selective interface to retain the sensing molecule (boronic acid), since it is covalently linked to a gel. The technology is at the proof-of-concept stage.

Chapter 3

The IGLUS viscosity based glucose sensor

3.1 Introduction

Over the last thirty years, in the race for continuous glucose monitoring (CGM), all spectroscopic and electromagnetic glucose detection methods have failed providing a long-term device. The electrochemical methods, based on enzyme-catalyzed reactions, are nowadays used for discrete measurements and short-term CGM devices, but have some significant drawbacks which make them not suitable for long-term CGM. First, glucose is irreversibly consumed by enzymatic reaction during detection, which might change the equilibrium glucose concentration in tissue and influence the actual measured glucose level. Furthermore, the rate of glucose consumption is diffusion limited. Any changes in diffusion layers (e.g. by cell deposition, capsule formation) on the sensor surface affect the diffusion rate, i.e. the device sensitivity [64]. In order to overcome such drawbacks, our laboratory proposed a viscosity-based glucose sensor, the IGLUS (Implantable GLUcose Sensor), which was invented by Dr. Sigi Straessler, Dr. med. Klaus Ganz and Prof. Dr. Peter Ryser [65].

Our glucose sensing technology is based on the rheological property of an aqueous solution which changes its viscosity with the glucose concentration [66]. The sensitive fluid (SF) is enclosed in a small cylindrical capsule with a small cylindrical rotor, making the entity a small rotating viscometer. The capsule is partially surrounded with a semipermeable nanoporous membrane which allows the glucose concentration equilibrium with the surroundings. In order to measure the viscosity of the SF, the sensing capsule is magnetically coupled to another capsule, the drive, which is driven by coils and electronics as an electrical motor. Ultimately, the measured viscosity values could be sent via RF communication to an integrated PC-based base station. A fully integrated implanted sensor is

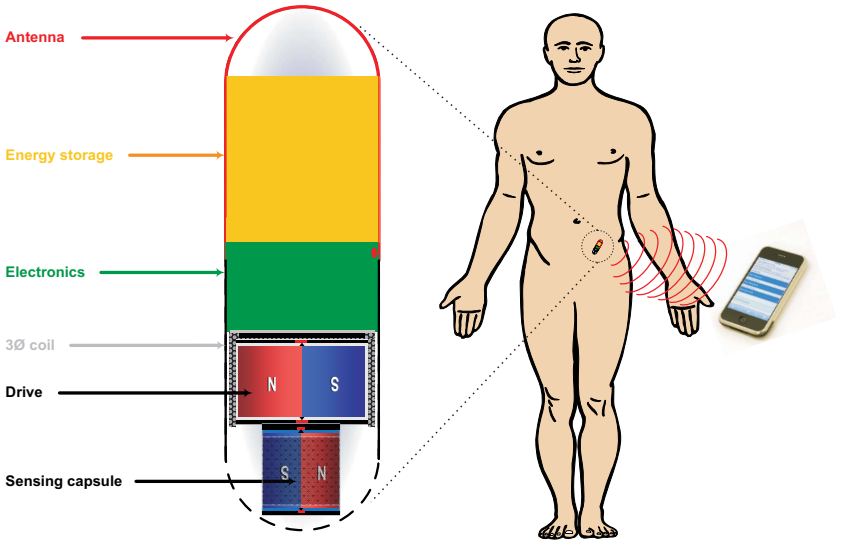

Figure 3.1: Concept of implantable autonomous glucose sensor.

now under development and the concept is shown in figure 3.1.

The system is designed to be able to track the variation rate of glucose levels and warn the user to impede hypo- or hyperglycaemia. The targeted operational life of the sensor implant is 6-12 months, after which it would need to be replaced. The concept shown in figure 3.1 foresees the implantation site in the abdomen because medical studies have shown that the lag time is reduced in the abdomen and is of the order of 4-10 min [67]. The response time in this case is mainly determined by the time lag with which the interstitial fluid glucose level follows the blood glucose level.

This measuring technique presents two important advantages. First, the SF is very selective to glucose due to the properties of the concanavalin A (ConA). Second, the method is very sensitive at low glucose concentration, which is crucial to prevent hypoglycemia. We believe that the method has a better long-term stability than electrochemical methods. Furthermore, there are no weak signals to measure as in spectroscopic glucose measuring methods.

Since the sensor fully integrated with its electronic is still at the concept stage and under development, we worked with a simplified system where only the sensing capsule is implanted and the acquisition system is in an external hand-held reader which allows the viscosity measurements through the skin. The reader communicates with a computer allowing the user to monitor glucose levels continuously or on demand. The system is detailed further in section 7.2.2.

3.2 IGLUS project organization

The IGLUS is a multidisciplinary research project and therefore requires to associate scientists of different fields. The organization of the different groups is shown in figure 3.2.

The project is centered on the micro-engineering team since it is the initiator of the project and does the integration of the different technologies to get a fully working system. As illustrated in figure 3.2, this interdisciplinary project consists of four major research subjects:
a) The micro-engineering is done at the Laboratoire de Production Microtechnique (LPM) at the EPFL by Julien Chassot, Olivier Haldimann, Sadasing Kowlessur, Dr. Simon Kuenzi, Eric Meurville, Jean-Pierre Rougnon, and myself (Antoine Barraud), supervised by Prof. Peter Ryser and Eric Meurville. The micro-electronics for the future autonomous implant is being investigated by Léandre Bolomey at the LPM under the supervision of Eric Meurville.
b) The SF has been developed in a collaboration between the LPM, the Laboratory of Regenerative Medicine and Pharmacobiology (Dr. Nela Angelova and Dr. Christine Wandrey) and Sensile Medical AG (Dr. Uwe Beyer and Dr. Richard Meier). The developed SF has been further adapted for the IGLUS requirements by Dr. Simon Kuenzi and Dr. Nao Takano.
c) The characterization of the selective interface (SI) is being investigated by Dr. Nao Takano and myself (Antoine Barraud) at the LPM. Since the SI is designed to be in contact with the subcutaneous tissue, this part has been done in close collaboration with Dr. Laurent Lavanant at the Laboratoire des Polymères at EPFL who investigates the surface modification of membranes.
d) The *in vivo* tests are performed in a close collaboration with the Centre d'application du vivant and ISREC institute of the EPFL. There are mainly two fields investigated within the *in vivo* tests:
- the biocompatibility test of the sensor components and histological analysis are performed by Dr. Jessica Dessimoz from the Histology Core Facility of the EPFL.
- the *in vivo* studies of our sensor are performed by Christophe Boss, Véronique Garea, Marcel Gyger, Pierre Latin, Dr. Nao Takano and myself (Antoine Barraud) under the supervision of Dr. Gisèle Ferrand, veterinary of the ISREC institute at EPFL.

The micro-viscometer and the acquisition system have been developed by Dr. Simon Kuenzi in his PhD thesis [22].

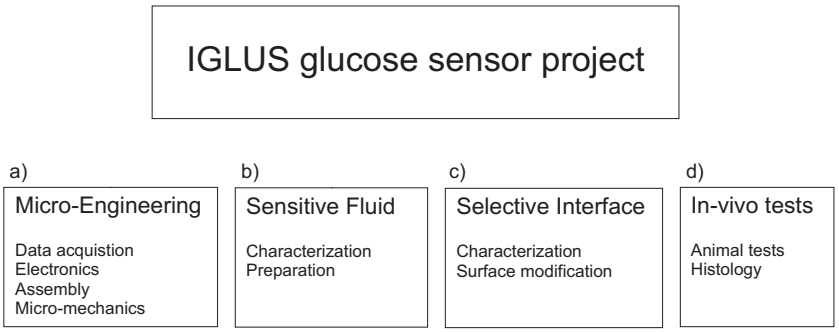

Figure 3.2: Structure of the IGLUS project.

3.3 Mechanical measuring principle

The mechanical measuring principle is a rotating microviscometer. A cylindrical rotor is enclosed in a cylindrical capsule, whose inner free space is filled by the fluid where viscosity must be determined. The cylindrical rotor is a diametrically magnetized magnet which can be actuated by electric coils. The coils create a rotating magnetic field which leads to the rotor rotation. A shear stress is thus applied to the fluid and is directly proportional to its dynamic viscosity. For Newtonian liquids, the shear stress is described as

$$\tau = \eta \frac{\partial u}{\partial x} \tag{3.1}$$

where τ is the shear stress, η the dynamic viscosity and $\frac{\partial u}{\partial x}$ the velocity gradient.

As illustrated in figure 3.3, the rotor is accelerated by the applied magnetic field up to a desired rotating velocity, at which the magnetic field is switched off. The rotor then decelerates due to the shear stress applied onto the fluid. The rotor velocity is measured by hall sensors and the deceleration curve is memorized for mathematical treatment. The deceleration curve is fitted with a decreasing exponential function $f(x) \sim e^{-\lambda t}$ in order to extract the damping factor λ. Calibration curves on calibrated oils and SF define the dynamic viscosity η and the glucose concentration.

In order to have a small volume of SF in the microviscometer, a system composed of two magnetically coupled microviscometer is employed. The system is composed of the drive capsule, with a bigger size and greater inertia, and the sensing capsule, whose size is minimized and hence has a low moment of inertia. It is important to minimize the volume of liquid in the sensing capsule because it minimizes the response time of the sensor to glucose variations. In addition, it is also preferable to keep the SF quantity small enough in order to avoid any risk that could be caused by leakage of the SF which has a certain toxicity. The last point is important for a future

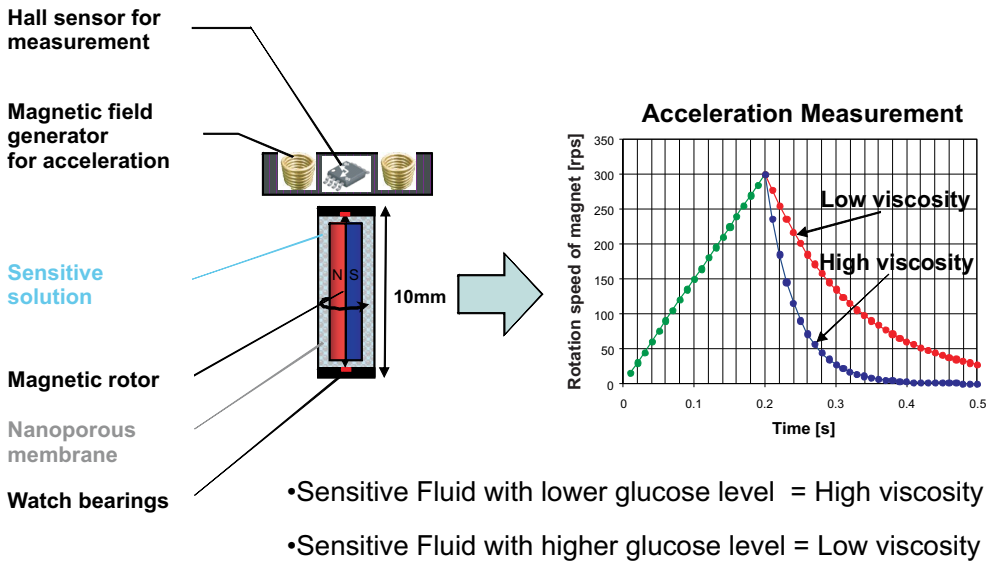

Figure 3.3: Measurement principle of the implantable glucose sensor.

authorization of a product (FDA and CE approvals). Considering these requirements, the drive capsule has been designed to provide a sufficient moment of inertia to the two coupled rotors system. The two rotors are strongly coupled and thus the measured damping factor λ_t results from these two rotors. A previous work [22] has shown that $\lambda_t = \lambda_d + \lambda_s$, where λ_d and λ_s are the damping factors of the drive and the sensing capsule respectively.

The viscosity of the SF being highly dependent on the temperature, the temperature has to be measured accurately. The temperature dependency of the SF is presented in section 3.4. During the period of this work, we chose to measure the temperature with a separated sensor. The measurement system is detailed in section 6.4.

3.4 Sensitive Fluid

3.4.1 Chemical mechanism

The sensitive fluid (SF) used within the sensor is the key for glucose recognition. It is based on the competing affinity of two saccharide species, glucose and dextran, to a specific saccharide-binding protein, concanavalin A (ConA). Dextran is a branched polysaccharide issued from bacteria [3] and ConA is a lectin protein extracted from the jack bean (*Canavalia ensiformis*) which affinity to glucose and mannose and their polysaccharides has been described by Goldstein *et al* [68]. The interaction of ConA with polysaccha-

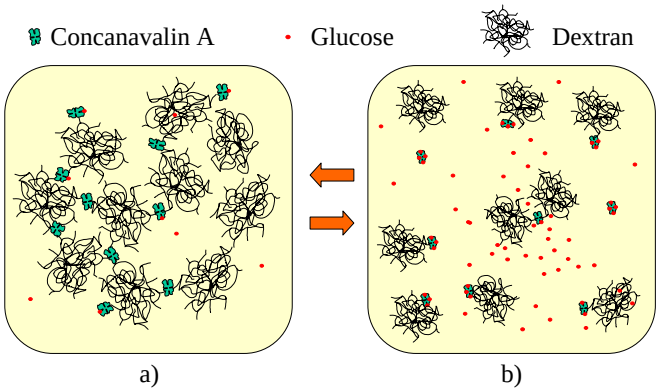

Figure 3.4: Chemical mechanism of glucose recognition in the SF. a) at low glucose concentration, b) at high glucose concentration.

rides involves the chain ends of the polymer, i.e. the ending glycosyl group of a branch (see binding site on dextran in section 3.4.2.B).

In 1979, Schultz and Sims [69] proposed to sense glucose using the properties of ConA as an alternative system to electrochemical methods and developed the first affinity sensor [70]. They used a fluorescence-labeled dextran to measure the glucose concentration by optical means. Another method, described by Ehwald and Ballerstadt in 1993 [66], measures the viscosity changes of a suitable aqueous dispersion of dextran and ConA. The method offers a sensitive, rapid and stable viscosity dependence on the glucose concentration.

The viscosity variation of the aqueous dextran-ConA dispersion happens as follows:
- In the absence of glucose, a ConA + dextran dispersion (*ca.* 0.7% ConA and 7% dextran [71]) is cross-linked by the dextran-ConA bonds and therefore highly viscous.
- Increasing the glucose concentration progressively removes the cross-links by replacing dextran-ConA bonds with glucose-ConA ones. A single glucose molecule being able to link to one ConA at a time, whereas dextran can link to several, the cross-linked structure is disintegrated and the dispersion viscosity decreases.

Figure 3.4 depicts the mechanism. The reversibility of the chemical process has been demonstrated [66]. This competing affinity principle may be also exploited for other measurement techniques such as infrared or fluorescence spectroscopy, by appropriate labeling of ConA and dextran.

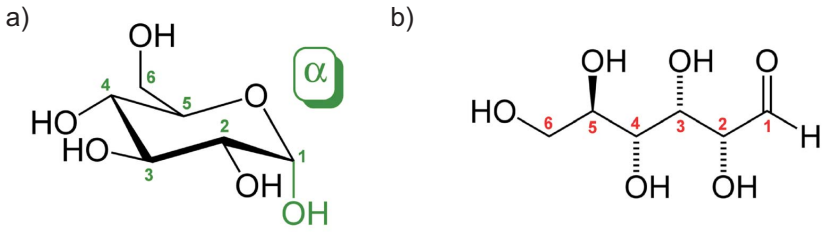

Figure 3.5: Illustration of two forms of D-glucose. a) α-D-glucose (or α-D-glucopyranose), b) open chain form of D-Glucose

3.4.2 Important components of the SF

In this work we employed the viscosimetric means with the SF. The major ingredients which have important roles in the SF are described in details in the following sections.

3.4.2.A Glucose

Glucose, also known as dextrose, D-glucose or D-glucopyranose, is a simple sugar (monosaccharide sugar, $C_6H_{12}O_6$), occurring widely in most plant and animal tissue [72]. We use the name D-glucose and is a short name for dextrorotatory glucose. It is one of the two stereoisomers of aldohexose and only D-glucose is biologically active. Aldohexose sugars have 4 chiral centers giving 2^4 = 16 stereoisomers. These are split into two groups, L and D, with 8 sugars in each. Glucose is one of these sugars, and L-glucose and D-glucose are two of the stereoisomers. Only 7 of these are found in living organisms, of which D-glucose (Glu), D-galactose (Gal), and D-mannose (Man) are the most important.

D-glucose contains six carbon atoms, one of which is part of an aldehyde group, and is therefore referred to as an aldohexose. In solution, the glucose molecule can exist in an open-chain (acyclic) form and a ring (cyclic) form (in equilibrium), see figure 3.5. The cyclic form is the result of a covalent bond between the aldehyde C atom and the C-5 hydroxyl group to form a six-membered cyclic hemiacetal. At pH 7 the cyclic form is predominant. In the solid phase, D-glucose assumes the cyclic form. Because the ring contains five carbon atoms and one oxygen atom, which resembles the structure of pyran, the cyclic form of glucose is also referred to as glucopyranose. In this ring, each carbon is linked to a hydroxyl side group with the exception of the fifth atom, which links to a sixth carbon atom outside the ring, forming a CH_2OH group.

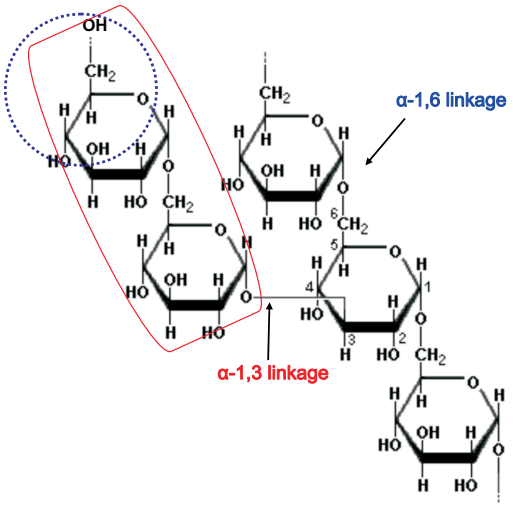

Figure 3.6: High molar mass branched dextran. Blue circle shows the terminal glucose residue recognized by ConA.

3.4.2.B Dextran

Dextran $(C_6H_{10}O_5)_n$ is an α-D-1,6-glucose-linked polysaccharide with side-chains mainly α-D-1,3-linked to the backbone units of the Dextran polymer. Other conformation exists and are discussed by Dimler *et al.* [73]. In common dextrans, the degree of branching is approximately 5% (i.e. 95% of α-D-1,6 links). The branches are mostly 1-2 glucose units long[1].

Dextran is obtained from fermentation of sucrose-containing media by the *Leuconostoc mesenteroides* bacteria and its molecular weight can vary from 12 to 600 million g/mol [74]. Optimization of this synthesis has shown the possibility of varying the branching links (α-D-1,3, α-D-1,2 or α-D-1,4) and increasing the degree of branching up to 14.7% as done by Kim *et al.* [75]. The production of dextran being possible by various bacterial species from two genera, *Leuconostoc* and *Streptococcus*, and by various conditions, the dextran properties varies for every manufacturers and production lots.

The role of the dextran in the SF is to create the viscosity when cross-linked by ConA. ConA has a specific affinity binding site to the end glucose residues of the dextran branches, as depicted in figure 3.6, and thus the degree of branching has an impact on the polymerization and the SF viscosity. The dextran molecules have to be retained inside the sensor and this is achieved by the membrane which has size exclusion properties for diffusion. It is therefore important to characterize the size distribution of the dextran molecules. Ioan *et al.* [3] have measured the radii of different dextrans and their results in pure water are shown in figure 3.7. The com-

[1] http://www.dextran.net

monly used radius is the hydrodynamic radius R_h or the Stokes radius, and is the radius of a hard sphere that diffuses at the same rate as the molecule. The behavior of this sphere includes hydration and shape effects. It is not restricted to the effective radius of the hydrated molecule in solution. Another less common measure is the radius of gyration R_g, which is the root mean square distance of the monomers from the center of gravity. The radius of gyration has the advantage to be easily determined experimentally with static light scattering as well as with small angle neutron- and x-ray scattering. R_h and R_g are similar as shown in figure 3.7.

As discussed previously in this section, dextran size distribution and degree of branching vary a lot from batch to batch and therefore we have decided to use only two specific types of dextrans: the dextran 2000 from Fluka and the dextran DXTB3M from Polymer Standard Service GmbH (PSS). These dextrans are expected to have a sufficiently large molecular weight to be retained by a selective membrane. Then, in order to assess the quality of the dextran 2000 kDa from Fluka which is sold without characteristics on the molecular weight (MW) distribution, we characterized it by Size-exclusion Chromatography (SEC) and we discovered a broad molecular weight distribution and peak at 200 kDa. The average MW is much lower than expected and the smaller molecules are suspected to leak through the membrane. Therefore we used a purified dextran from PSS, the dextran DXTB3M, which has a narrow MW distribution and a peak at 3200 kDa (see data sheet in appendix A). Unfortunately the degree of branching of these polymers are unknown from the manufacturers.

3.4.2.C Concanavalin A

Concanavalin A (ConA), illustrated in figure 3.8, is the most studied member of the legume lectin family. It was isolated from the jack bean (*Canavalia ensiformis*) and crystallized for the first time in 1919 by Sumner [76]. One of the most noteworthy properties of ConA is its affinity to α-D-glucopyranosyl and α-D-mannopyranosyl residues (α-D-glucose and α-D-mannose) and their derived polymers. It was described by Goldstein *et al.* [68] and, since then, numbers of publications on ConA characterization have been made. The sugar binding site is depicted in figure 3.9. The primary and tertiary structures are elucidated [77, 78], and the interactions between the subunits that form the crystalline quaternary structure have been well described [79]. Moreover, the topography of the binding site is described [80, 4], as depicted in figure 3.8. ConA crystallizes as a tetramer of identical 25'500 g/mol molecular weight protomers [81], some of which are fragmented [82, 83]. The quaternary structure in solution is pH and temperature dependent as it appears in dimer and tetramer configurations. The size of the ConA monomer has been studied at 2-Å resolution [84] and is reported to be a globular protein of overall dimensions $42 \times 40 \times 39$ Å. The

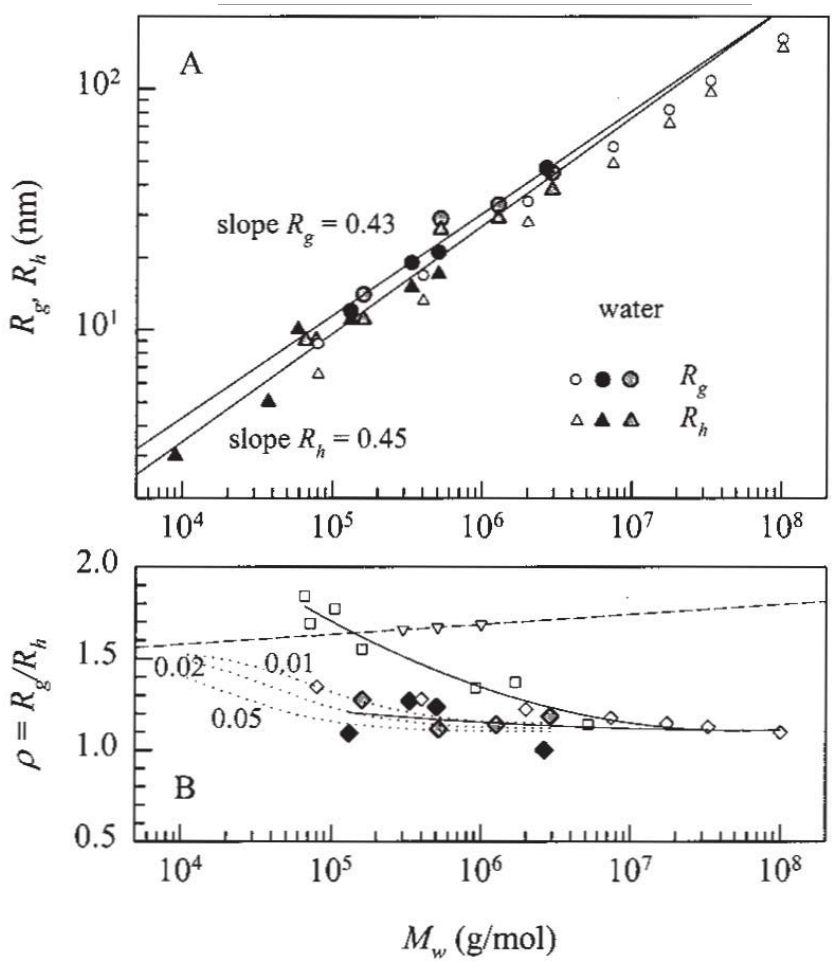

Figure 3.7: (A) Molar mass dependencies of the radius of gyration R_g (circular symbols) and the hydrodynamic radius R_h (triangular symbols) for different dextran samples in water: (▲), (●) dextrans-Sigma; (gray triangle), (gray circle) dextrans-degraded; (△), (○) dextrans-Nordmeier. B) The ratio $\rho = R_g/R_h$ of the two radii as a function of the molar mass M_w: (⧫) dextrans-Sigma; (gray tilted square) dextrans-degraded; (◇) dextrans-Nordmeier; (▽) pullulan-Nordmeier (dashed line: fit); (□) degraded starches. Source:[3]

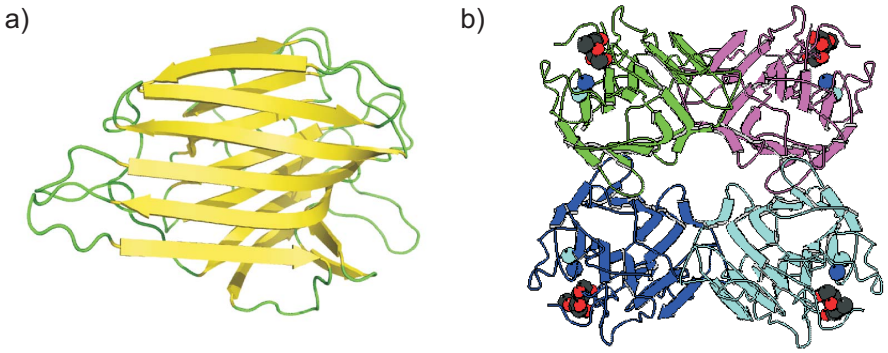

Figure 3.8: Concanavalin A 3D structures; a) the globular tertiary structure of the ConA monomer, b) the quaternary structure of the ConA tetramer where the S1 and S2 sites are represented by the blue spheres and the glucose molecules by the black and red spheres.

crystallographic size of the dimers is approximately $84 \times 40 \times 39$ Å and in water the hydrodynamic radius is R_h = 3.3 nm [84]. Finally the tetramer conformation has been studied [79] and is the result of the association of dimers. The crystallographic dimensions are $6 \times 7 \times 7$ nm [62] and the hydrodynamic radius is R_h = 4.4 nm. The dimensions of molecules are listed in table 3.1.

ConA exists as a dimer in solution at pH values below 5.5. Above pH 7 it exists mainly as a tetramer of identical subunits. In intermediate range both dimer and tetramer exist [85, 86, 87, 88] and some ConA seems to remain as dimer even above pH 7 [79, 89]. Each subunit of ConA has one specific carbohydrate-binding site [4]. The isoelectric point is in the pH range of 4.5-5.5. In literature, different pI values can be found for ConA because it exists in slightly different forms [90].

For the SF to work properly in an implantable glucose sensor, the saccharide-binding properties of ConA must stay constant. It has been known for quite a long time that the saccharide affinity of ConA depends on the presence of divalent metals within the protein [91]. These divalent metallic cations must remain in the protein and not be substituted by others, as we could expect the saccharide affinity to change. It is therefore important to describe the ConA activity as a function of different metal cations.

In its natural form, ConA contains two divalent cationic sites S1 and S2, occupied by Mn^{2+} and Ca^{2+} respectively, quite near the saccharide-binding site [92]. This fully metallised protein is in an active "locked" form (LMnCa). Upon leaching away of these cations (done by leaching e.g. with

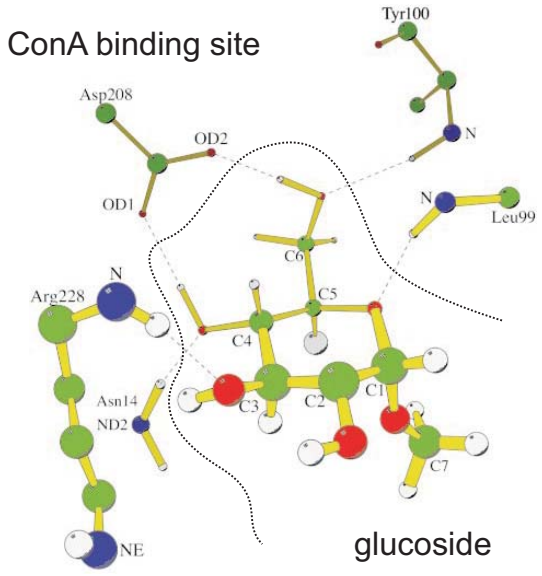

Figure 3.9: Hydrogen bonding interactions of glucoside in the binding site of concanavalin A. The hatched lines depict hydrogen bonds between the sugar and protein, and the doted line separates the two molecules. Source: [4]

EDTA[2] in acidic solutions) to give the metal-free "apportion", locked apo-ConA (L) progressively undergoes a structural transformation (conformation change) to an "unlocked" form (U), whose saccharide affinity is very low [93]. Subsequent exposure to free Mn^{2+} and Ca^{2+} leads to a reversal of these transformations, e.g. metal uptake followed by a conformation change back to the active locked form (LMnCa). The site occupation is essentially sequential, in that S1 must be occupied (normally Mn^{2+}) before the 2nd metal ion (normally Ca^{2+}) can go to S2 [93, 94]. The conformation of ConA is the most important factor, before the cation content, determining saccharide affinity [95]. Reaching the locked state is not an issue as long as ConA is fully metallised, because essentially all such ConA is in the locked state (LM1M2), due to a strong thermodynamic stabilization induced by locking. The protein must absolutely remain metallised, because the apoprotein (U) is reported to unfold irreversibly at low temperatures and high pH values: the onset of transformation is *ca.* 35˚C at pH 6.9.

The natural form of ConA (LMnCa), is quite stable: under normal physiological pH, the equilibrium concentrations of Ca^{2+} and Mn^{2+} required to keep ConA in this state are very low [93, 95, 96]. Moreover, the presence of saccharide (glucose or dextran), at normoglycemia (5 mM), strongly stabilizes metal bonding to ConA by a mass action effect, as evidenced from the

[2]EthyleneDiamineTetraAcetic acid

Table 3.1: Molecular size of the main constituents in the sensitive solution. R_W is the van der Waals radius and R_h the hydrodynamic or Stokes radius. The dimensions have been determined in the crystallin form.

Description	Molecular weight	Stokes radius or dimensions
Glucose	180.16 Da	$R_W = 0.76 - 0.85nm$[106]
Dextran 2000	2'000 kDa	$R_h = 27nm$ [3]
Dextran 200	200 kDa	$R_h = 15nm$ [3]
ConA monomer	25,5 kDa	$42 \times 40 \times 39$ Å[78]
ConA dimer	52 kDa	$84 \times 40 \times 39$ Å[84]
		$R_h = 3.3nm$
ConA tetramer	104 kDa	$6 \times 7 \times 7$nm [64]
		$R_h = 4.4nm$

equilibrium constants [96], a stabilization which occurs to various degrees for all metallised forms of ConA (see below).

In the case of a large concentration of Ca^{2+} and quasi absence of Mn^{2+}, both metal binding sites may be filled with Ca^{2+}, or, vice versa with Mn^{2+} [97, 96]. However, the corresponding equilibrium concentrations to maintain these LCaCa or LMnMn forms are much higher, and the thermal stability of such modified ConA is lower [98]. In other words, there is a strong thermodynamical advantage for the natural form vs. Mn^{2+} in S2 and especially Ca^{2+} in S1. However, this is not necessarily true for substitution of Mn^{2+} in S1 by another divalent transition metal ion such as Ni^{2+}, Co^{2+}, Zn^{2+}, Cu^{2+}, Cd^{2+}, or even Mg^{2+} [99]. Substitution by Zn^{2+} or Cu^{2+} is quite likely in the body, and also by Ca^{2+} and Mg^{2+}, although much less favorable for ConA [100, 95], because of their much higher concentration. Substitution of Mn^{2+} by Mg^{2+} is also observed, and it is reported that Mg^{2+} is actually more abundant in S1 of most natural lectins, including ConA [101]. Mg^{2+} is specific to S1 and has no significant affinity for S2.

The saccharide affinity of metallised, locked ConA (LM1M2) is almost independent of the metal ions M1 and M2 present in S1 and S2 [102, 95, 103]. This possibility of double metal binding (LM1M1) has been challenged by Sophianopoulos and Sophianopoulos [104, 105] for Mn^{2+}. However, double Mn^{2+} and Ca^{2+} binding [19] has been confirmed by a recent detailed study [20], who successfully isolated and crystallised both the LMnMn and LCaCa forms.

Respective affinities of ConA having different transition metals in S1 are not known. The only comparative equilibrium values found are for metallization of S1 of the apo-ConA with no Ca^{2+} or saccharide in solution [99], which is not really pertinent to our conditions.

Table 3.2: Product description and references for the SF. For a preparation, only one type of dextran is used at a time and also one antiseptic, either sodium azide or phenol.

Description	Product details	Ref.Num. and Brand
$C_6H_{12}O_6$	D-(+)-Glucose anhydrous	49138 Fluka
$(C_6H_{10}O_5)_n$	Dextran 2000 (Leuconostoc spp.)	95771 Fluka Sigma
$(C_6H_{10}O_5)_n$	Dextran broad/branched	dxtb3m PSS
ConA	Concanavalin A, type IV	C2010 Sigma
Tris buffer	Trizma pre-Set crystals, pH 7.4	T-7693 Sigma
NaN_3	Sodium azide	13412 Riedel-de Haen
C_6H_6O	Phenol	77610 Fluka
$MnCl_2$	Manganese(II) chloride tetrahydrate	31422 Riedel-de Haen
$CaCl_2$	Calcium chloride dehydrate puriss.	21101 Fluka
$NaCl$	Sodium chloride puriss.	71379 Fluka
$NaOH$	Sodium hydroxide purum p.a.	71691 Fluka
Water	Millipore water	-

3.4.3 Preparation and viscosity measurements

3.4.3.A Preparation of the sensitive fluid

The different constituents used for the SF preparation are listed in Table 3.2.

In the sensitive solution, the most important substances are dextran, ConA and glucose. These three substances create the special chemistry that allows the detection of the glucose concentration variation via the viscosity changes. Tris Buffer is used to stabilize the pH of the sensitive solution. Sodium azide or phenol is used as an antiseptic. Sodium azide is preferred for *in vitro* studies because it allows the use of UV spectrometry since phenol has an absorption peek at 280 nm which interferes with protein detection. Phenol is preferred for *in vivo* studies because it is less toxic and is accepted by the body in small quantities. Manganese chloride and calcium chloride are necessary to activate the ConA in order for the protein to link to saccharides (c.f. section 3.4.2.C). The sodium chloride is useful to enhance the solubility of ConA and corresponds to physiological conditions.

To prepare the sensitive solution we first prepare three different stock solutions (c.f. Table 3.3), which are then used for all preparations. Stock solutions 1 and 3 are known to be very stable, but there is a doubt for solution 2, thus if the solution 2 is older than two weeks, it is replaced. Depending on the choice of the antiseptic (*in vitro* or *in vivo* use), stock solution 1a or 1b is used.

The whole recipe consists of preparing two solutions, the dextran solution and the ConA solution, which are mixed at the end. The following

Table 3.3: Stock Solutions.

Solution	Description	Concentration
Stock solution 1a	Tris buffer pH 7.4 NaN_3 Glucose H_2O	20 mM 0.1%(w/w) 4 mM -
Stock solution 1b	Tris buffer pH 7.4 Phenol Glucose H_2O	20 mM 0.4%(w/w) 4 mM -
Stock solution 2	$MnCl_2$ $CaCl_2$ $NaCl$ H_2O	2 mM 2 mM 300 mM -
Stock solution 3	$NaOH$ H_2O	50 mM -

is an example procedure for a SF containing 3% dextran 2000, 0.6% ConA, 2 mM glucose and 0.1% (w/w) sodium azide. The preparation is for 10 ml of final product.

STEP 1) Solution A (dextran 2000 solution, total 6 g, density 1 g/ml.):

1. Solubilize 360 mg dextran 2000 in 5.64 g stock solution 1a.
2. Mix for at least 8h.
3. Control that the final weight is 6 g.

STEP 2) Solution B (ConA solution, total 6 g, density 1 g/ml.):

1. Solubilize 72 mg ConA in 5 g stock solution 2. (72mg corresponds to 1.2% in the Solution B).
2. Slowly adjust the pH of the solution to 7.4 by adding the stock solution 3. This is a critical process and it should be done carefully. We use a Tecan pump to add the stock solution 3 at a rate of 10 μl/min. The initial pH is usually between 4 and 5. If the transition is made too fast the ConA tends to be denaturated and precipitates. However this process should not take too long either, because ConA has a tendency to precipitate in the absence of dextran.
3. Correct the weight of the preparation to 6 g with stock solution 2.
4. Make sure the pH is 7.4.

5. Centrifuge the solution at 4600 min^{-1} for 10 min.

STEP 3) Mixing solutions A and B

1. Put 5 g of Solution A in a clean glass container.
2. Add 5 g of solution B filtered through a Millex HV 0.45 μm syringe filter.
3. Quickly mix both solutions. The solution may turn a bit milky during the first seconds.
4. After mixing, the solution should be clearer, and the viscosity should be much higher.
5. Check that the total weight is 10 g.
6. Gently mix the solution for 24 h before any viscosity measurement.
7. The sensitive solution is stored at room temperature.

3.4.3.B Viscosity properties of the prepared SFs

Measurement method

As a reference, we measured the viscosity of the prepared solution with a capillary viscometer. The choice of this method relies on the following requirements:

1. It has to be standard and commercially available
2. Accuracy has to be better than 1%
3. Small volume of necessary liquid due to high cost of constituents
4. Evaporation has to be minimized for viscosity stability over the measurement time
5. Stabilized temperature

In order to fulfill the last point, the capillary viscometer is placed in a temperature controlled vessel described in section 6.4. We used different capillaries with different diameters for different viscosity ranges acquired from Schott Instruments GmbH[3] and Cannon Instruments Company Inc.[4].

The viscosity properties of the SF as a function of dextran from Fluka and ConA concentrations have been studied systematically in a previous work [22]. The concentrations of these constituents have thus been chosen

[3] http://www.schottinstruments.com
[4] http://www.cannoninstrument.com

in order to suit the viscosity range for the sensor demonstrator, see chapter 6. As discussed in section 3.4.2.B, the Fluka dextran is polydisperse and contains smaller molecules than specified by the manufacturer. In order to ensure the dextran retention by the SI, we also used the dextran from PSS which is sold purified with a narrow peak at 3200 kDa. In the forthcoming experiments, we used different variants of SF and their reference viscosities have been measured and are presented in the followings.

The SFs are named after the concentrations of dextran and ConA as well as type of dextran. For example, the name SF36F stands for a SF prepared with 3% of Fluka dextran and 0.6% of ConA, and the name SF24P with 2% of PSS dextran and 0.4% of ConA.

SF36F - 3% dextran 2000 Fluka, 0.6% ConA

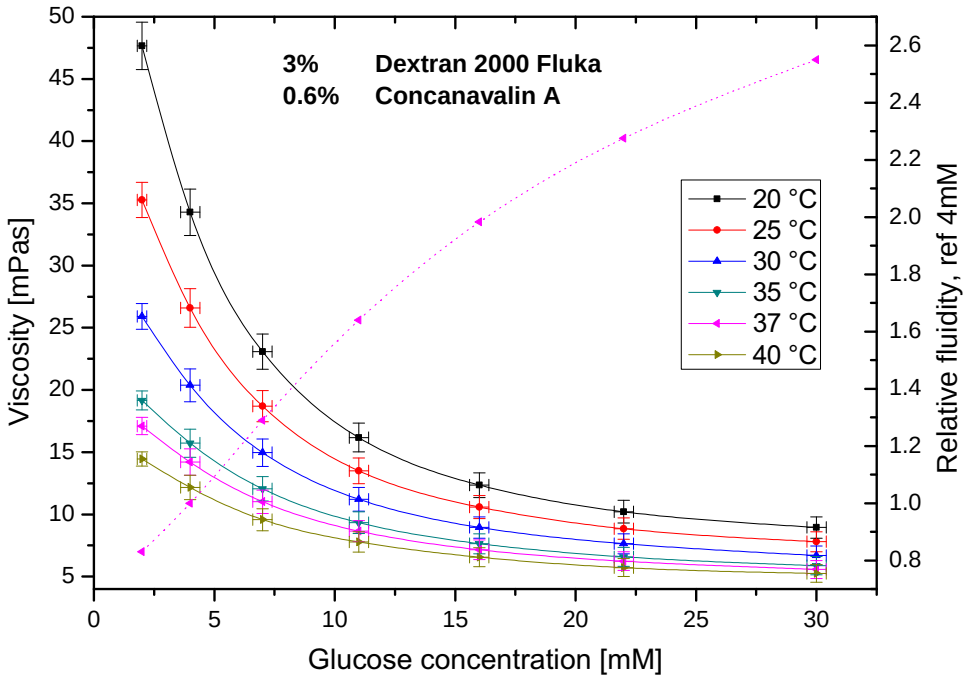

Figure 3.10: Viscosity characteristics of SF36F.

Table 3.4: Viscosity of sensitive fluid SF36F in $mPa \cdot s$.

	20°C	25°C	30°C	35°C	37°C	40°C
2mM	47.7	35.3	25.9	19.2	17.1	14.5
4mM	34.3	26.6	20.4	15.7	14.2	12.2
7mM	23.1	18.7	15.0	12.1	11.0	9.6
11mM	16.2	13.5	11.2	9.3	8.7	7.8
16mM	12.3	10.6	8.9	7.6	7.2	6.6
22mM	10.2	8.9	7.6	6.6	6.2	5.7
30mM	8.9	7.8	6.7	5.9	5.6	5.3

SF23P - 2% dextran 3200 PSS, 0.3% ConA

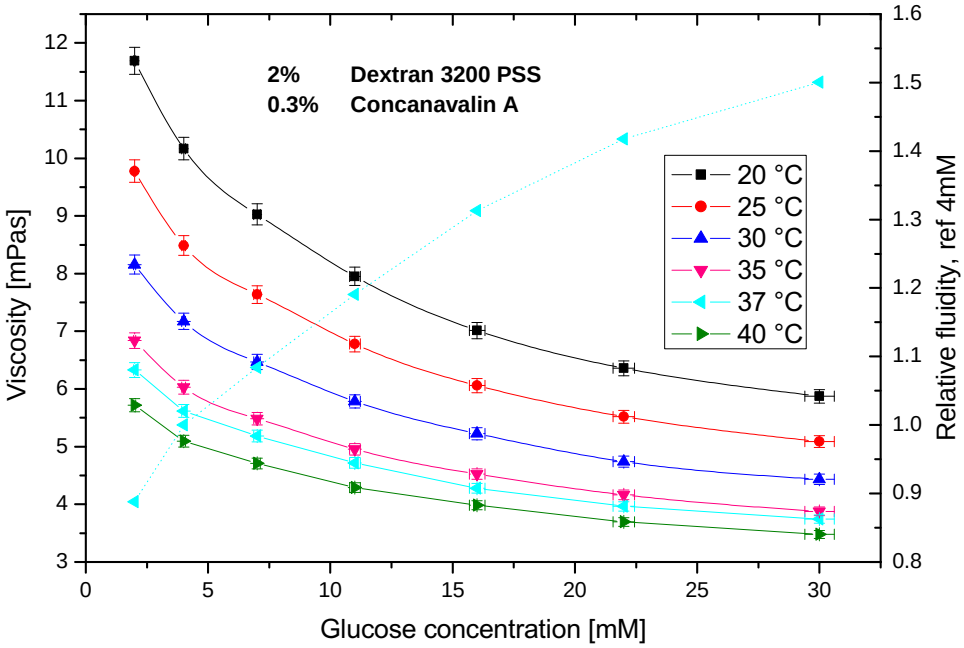

Figure 3.11: Viscosity characteristics of SF23P.

Table 3.5: Viscosity of sensitive fluid SF23P in $mPa \cdot s$.

	20°C	25°C	30°C	35°C	37°C	40°C
2 mM	11.7	9.8	8.2	6.8	6.3	5.7
4 mM	10.2	8.5	7.2	6.0	5.6	5.1
7 mM	9.0	7.6	6.5	5.5	5.2	4.7
11 mM	8.0	6.8	5.8	5.0	4.7	4.3
16 mM	7.0	6.1	5.2	4.5	4.3	4.0
22 mM	6.4	5.5	4.7	4.2	4.0	3.7
30 mM	5.9	5.1	4.4	3.9	3.7	3.5

SF24P - 2% dextran 3200 PSS, 0.4% ConA

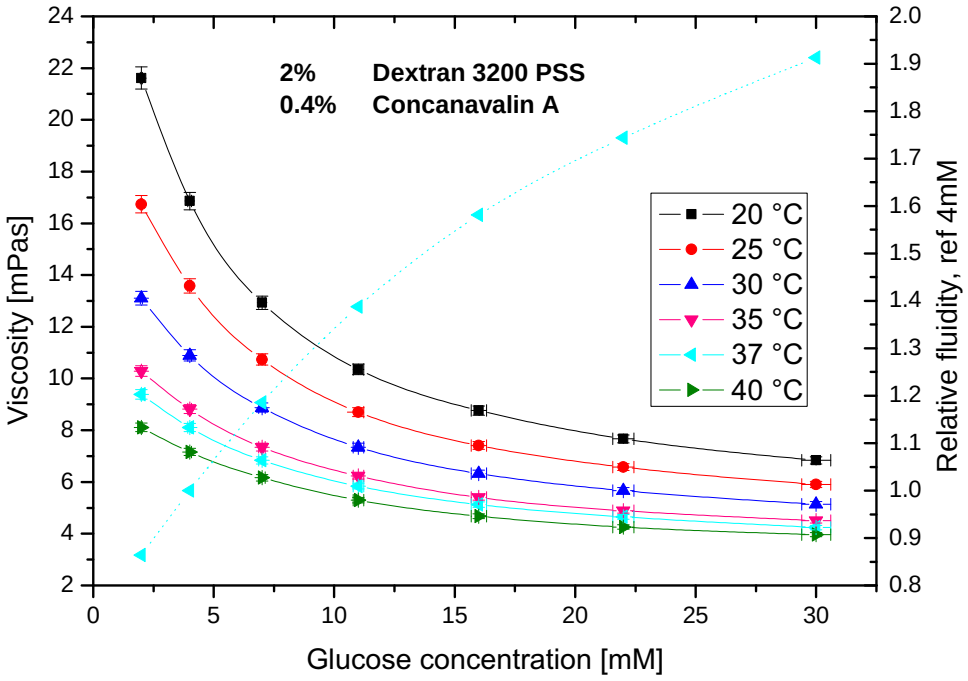

Figure 3.12: Viscosity characteristics of SF24P.

Table 3.6: Viscosity of sensitive fluid SF24P in $mPa \cdot s$.

	20°C	25°C	30°C	35°C	37°C	40°C
2 mM	21.6	16.7	13.1	10.3	9.4	8.1
4 mM	16.9	13.6	10.9	8.8	8.1	7.2
7 mM	12.9	10.7	8.9	7.3	6.8	6.2
11 mM	10.4	8.7	7.3	6.2	5.8	5.3
16 mM	8.8	7.4	6.3	5.4	5.1	4.7
22 mM	7.7	6.6	5.7	4.9	4.6	4.3
30 mM	6.8	5.9	5.1	4.5	4.2	4.0

SF36P - 3% dextran 3200 PSS, 0.6% ConA

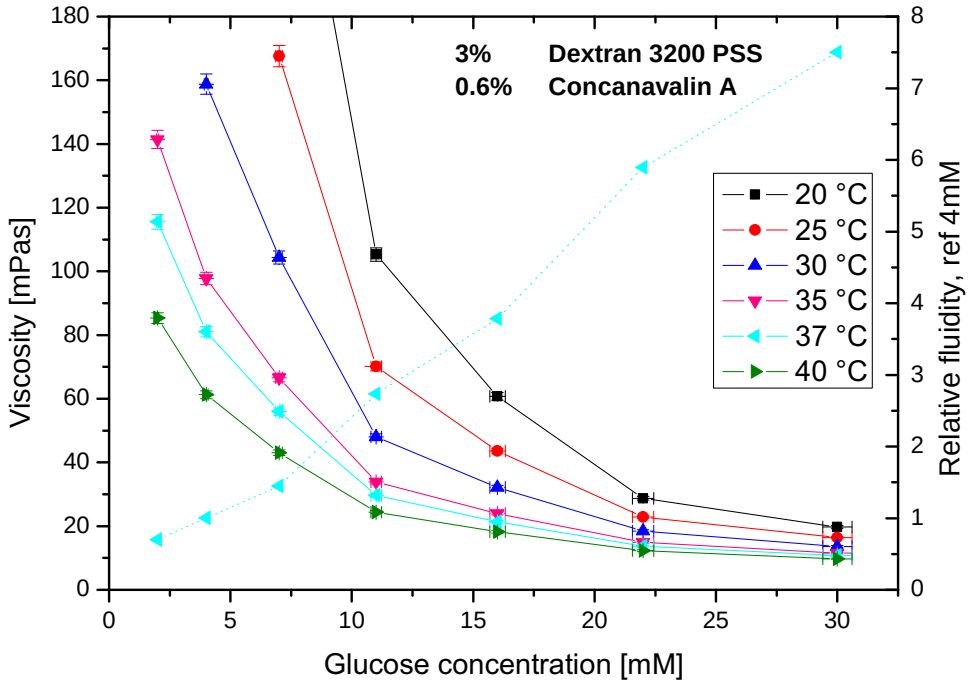

Figure 3.13: Viscosity characteristics of SF36P.

Table 3.7: Viscosity of sensitive fluid SF36P in $mPa \cdot s$.

	20°C	25°C	30°C	35°C	37°C	40°C
2 mM				141.4	115.6	85.3
4 mM			158.8	97.8	81.0	61.3
7 mM		167.6	104.4	66.6	56.0	43.0
11 mM	105.3	70.1	48.0	33.9	29.6	24.4
16 mM	60.7	43.6	32.1	24.0	21.4	18.2
22 mM	28.8	22.9	18.5	14.9	13.8	12.3
30 mM	19.7	16.4	13.6	11.5	10.8	9.7

Table 3.8: Effects of wound healing on sensor detection of small molecular weight blood borne analytes. [19]

	Hemostasis	Inflammation
	Minutes to hours	Days
Cause	Blood borne proteins and platelets adhere to sensor surface	Proteins and cells of immune system adhere to sensor surface
Effect	Membrane biofouling restricts analyte diffusion to sensing layer	Membrane biofouling restricts analyte diffusion to sensing layer

	Repair	Encapsulation
	Days to weeks	Weeks to months
Cause	Vascularized and gelatinous granulation tissue formation	Increasing avascularity and fibrocity of surrounding tissue
Effect	Increased analyte perfusion and diffusion to the sensor surface	Decreased analyte perfusion and diffusion to the sensor surface

3.5 Body-sensor interface

The IGLUS is designed to be implanted subcutaneously, therefore the outside walls of the sensor are directly in contact with the living tissues. The surgical procedure is followed by a healing process of the living tissues and can be summarized in four stages: hemostatis, inflammation, repair and encapsulation. The details are presented in table 3.8 and an illustration is shown in figure 3.14. Unfortunately theses processes lead to an alteration of the sensor operation and therefore have to be minimized. It is commonly known as biocompatibility. The first gesture adopted in surgery is to set the implant away from the wound with a trocar, but this only minimizes the issues caused by hemostasis and tissue repair. For an implanted sensor, the situation is more complicated than for passive implants, such a hip or knee implant, since the access to chemical solutes such as glucose must remain over time. The reasons for almost all actual sensors to fail after a few days of implantation are the biofouling and encapsulation [107, 5]. It is thus essential to apply chemical surface modification on our sensor in order to enable its long-term efficiency. The situation is illustrated in figure 3.15. In the frame of this work, we limited our research on the SI because it is the most crucial and difficult external area to develop.

In literature, with key words "membrane biofouling" or "membrane fouling", different methods to prevent the membrane fouling of a biosen-

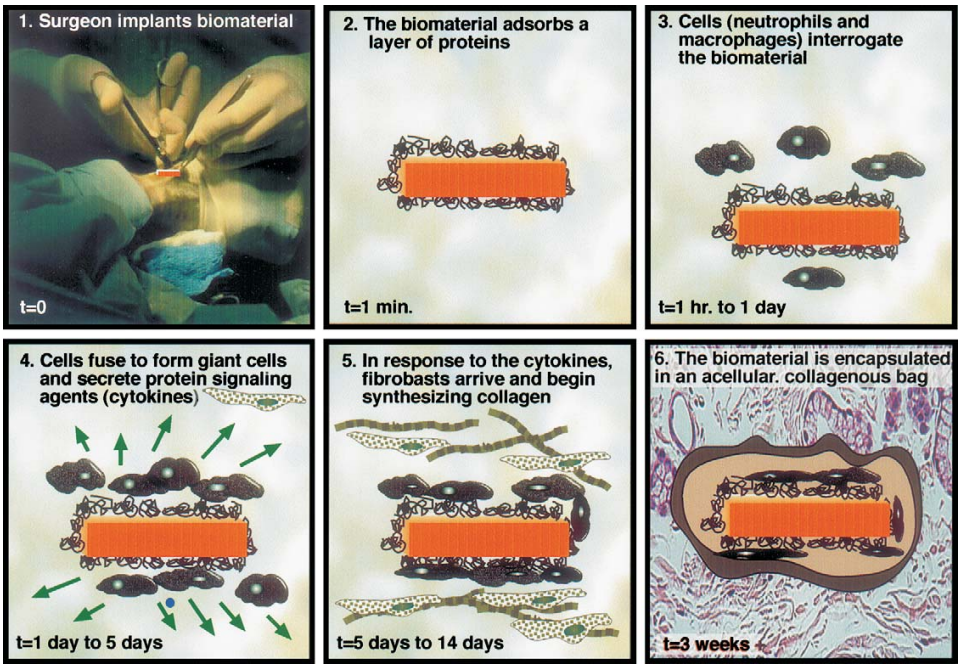

Figure 3.14: The foreign body reaction is the normal reaction of a higher organism to an implanted synthetic material and is schematically illustrated here. (1) A surgeon implants a biomaterial in a surgical site (an injury). (2) Quickly, the implant adsorbs a layer of proteins, the normal process for a solid surface in biological fluids. (3) Cells (neutrophils and then macrophages) interrogate and attack the "invader", i.e. the biomaterial. (4) When the macrophages find they cannot digest the implant, they fuse into giant cells to engulf the object. However, it is too large to completely ingest. The giant cells send out chemical messengers (cytokines) to call in other cells. (5) Fibroblast cells arrive and begin synthesizing collagen. (6) The end stage of the reaction has the implant completely encased in an acellular, avascular collagen bag. There are macrophages between the collagen sac and the implant [5].

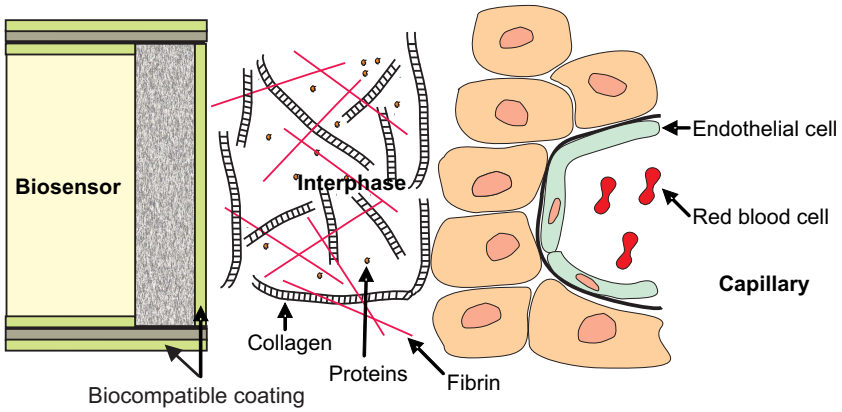

Figure 3.15: Illustration of the interface between body tissue and a glucose sensor.

sor have been recently reviewed [19]. The prevention of encapsulation is partially enclosed in the topic since it is believed that the adhering proteins are one of the main factors that modulates the longer term cellular and/or encapsulation response [107].

The choice of the best strategy for a SI with limit biofouling capabilities was first based on the requirements of the IGLUS sensor:

1. Allow selective transport of glucose in and out of the sensor and simultaneously prevent leakage of dextran and ConA out of the sensor. It must also prevent other proteins to penetrate the device.

2. Prevent fibrous encapsulation in the vicinity of the membrane to facilitate diffusion of glucose to the sensor device.

The possibilities of surface modifications found in literature are numerous but only two solutions remain potential as they have been highlighted by Lei *et al.* [63]. The two possibilities are the grafting of polyethylene glycol (PEG) [108] or a biomimetic coating such as hyaluronic acid (HA) [109]. Both techniques have the ability to create a super-hydrophilic surface that repels proteins culpable for biofouling. Though these techniques show potentials for biofouling, their effectiveness *in vivo* has not been fully explored.

Prior to selecting the surface modification method, the support, i.e. the selective membrane, was chosen. We chose a nanoporous anodic aluminium oxide (AAO) membrane (detailed in section 4.5), also called alumina membrane in literature. Since the membrane selection is an important topic of this thesis, it is presented in details in chapter 4.

The choice of the surface modification had to suit the nanoporous alumina membrane and has been made in a close collaboration with another group (see section 3.2). We chose a poly(poly(ethyleneglycol methacrylate)

(PPEGMA) coating as the best candidate because it is compatible with alumina and was available at EPFL. Our partner developed this coating and therefore the details of its chemistry are not presented here. In addition to its biofouling capabilities, the coating was also used to tune the membrane selectivity by pore filling.

Chapter 4

Understanding the selective interface

4.1 Introduction

The IGLUS implantable glucose sensor consists of three core technologies: the sensitive fluid (SF), the micro-viscometer and the selective interface (SI) between the inside and outside of the sensor. This chapter describes the investigations conducted to create a dedicated SI for the IGLUS.

The SI is a semi-permeable membrane whose role is to retain the essential molecules of the SF (ConA and dextran) inside the sensor whilst allowing glucose to diffuse freely in and out. In addition, the interface material has to be biocompatible and to minimize biofouling by preventing the non-specific adhesion of proteins. As presented in section 3.5, the membrane has to act as an interface between the SF and the surrounding living tissues which are composed of cells and the extracellular matrix, see figure 3.15.

This chapter aims to gather the necessary information to understand the physical and chemical processes in and around the SI. The first section details the requirements of the IGLUS for the interface. Subsequently a review of potential nanoporous supports for the interface is presented and the selected candidates are described. As a potential alternative, polyethylene (PE) films which have different mechanical properties are presented. Finally, a theoretical model for the diffusion of solutes through the interface is introduced.

4.2 Requirements for IGLUS

The IGLUS measures the viscosity of a fluid which varies with the glucose concentration. The sensor being implanted subcutaneously (see figure 4.1), it bathes in the interstitial fluid (IF). The SI has to fulfil three functions:

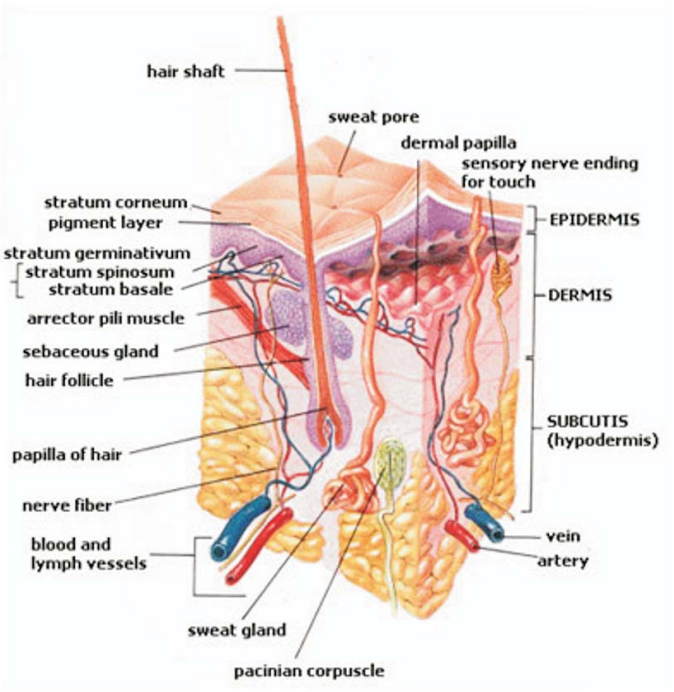

Figure 4.1: Cross-section of the human skin.

1. Maintain the rheological and glucose sensitive properties of the inner SF

2. Allow the glucose concentration equilibrium between the IF and the inner SF

3. Prevent biofouling of the membrane and nonspecific adhesion of proteins

The two first functions are necessary for the basic functioning of the sensor while the third function is required for a long term sensing functionality of the implanted sensor.

Maintaining the rheological and glucose sensitive properties of the SF means that the SF constituent molecules have to be retained inside the sensor whilst preventing some of the IF constituents to penetrate into the sensor. The main constituent molecules of both fluids are sketched in figure 4.2. On this figure, the relative sizes of the important molecules are shown. The main constituents of the SF are the dextran and the ConA, and for their activity to remain constant, their chemical environment needs to remain the same over time. Since the viscosity is the key of the sensing system, the only parameter that should induce viscosity changes must be glucose. In order to satisfy this last statement, the concentration of each

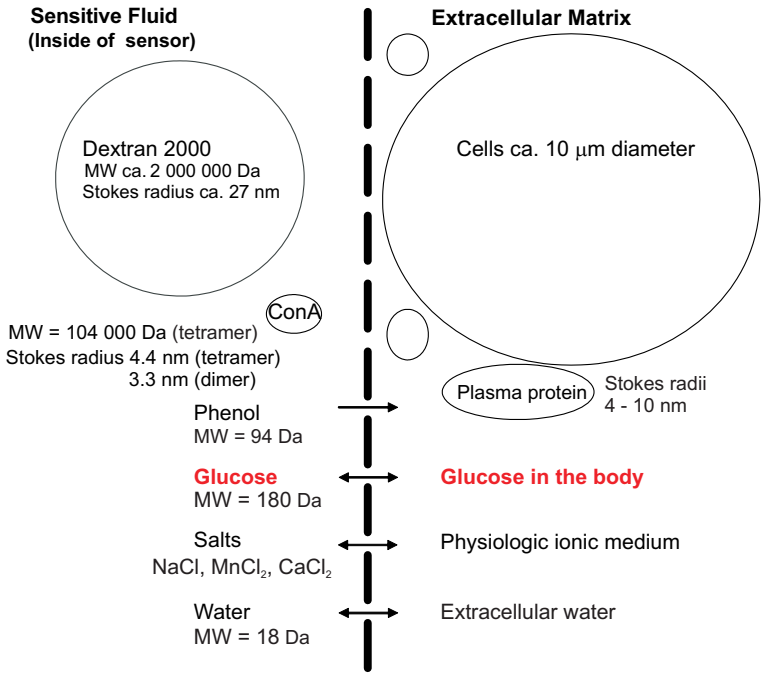

Figure 4.2: Illustration of the relative sizes of the molecules that the membranes has to select. MW is the molecular weight in Dalton.

molecule (except for glucose) must remain constant. In other words, the dextran and ConA molecules may not leak through the membrane and IF macromolecules (peptides and proteins) may not pass through the membrane either. As detailed in section 3.4, the SF activity depends on the pH and the ionic composition, therefore they also must remain constant.

As the first goal is to make the sensor operating *in vitro*, we focused on the two first functions because they are sufficient for a simplified *in vitro* environment model. In this work, the simplified *in vitro* environment model (SITEM) is a chemical environment where the IF is mimicked by a reference solution (RS) which is an isotonic solution of the SF for all of its constituents. In other words, the RS contains equal concentrations of ions and has the same pH and buffer as the SF. During *in vitro* experiments, the only component whose concentration is varied is D-glucose. The SITEM has been chosen to test the two first functions of the membrane mentioned above. It realizes a situation where the only chemical constituents which differ on both sides of the membrane are dextran and ConA.

The three functions of the membrane listed earlier cannot be studied simultaneously. Therefore we studied and characterized different membranes by testing separately their glucose permeability, dextran retention ability, protein retention ability. Finally, their retention capability of dex-

tran and ConA simultaneously was investigated.

The function of maintaining large molecules inside the sensor implies more than only selecting the chemical constituents. It also implies to strive against overpressures and mechanical stresses that can arise from the use and manipulations of the sensor. Moreover, the membrane has to resist the osmotic pressure which arises from the difference of chemical constituents on both sides of the membrane. Since some chemical constituents cannot diffuse through the membrane, an osmotic pressure remains and has to be sustained by the membrane. A swelling of the membrane would induce a dilution of the SF and modify the distance between the rotor and the membrane which has to remain constant in order to guarantee a constant shear stress for every measurement. Therefore the membrane has to be rigid.

4.3 Basic chemistry and physics of membranes

This section is intended to give the reader the necessary knowledge for understanding the basic chemical and physical phenomena relating to membranes.

4.3.1 Membrane surface chemistry

The **membrane chemistry** indicates the chemical nature and composition of the membrane surface, which is important because the chemical components of the medium are directly in contact with the surface of the membrane. The chemical makeup of the surface may often be different from the chemistry of the membrane bulk. The membrane chemistry determines important properties such as hydrophilicity (or hydrophobicity), surface electric charges, chemical and thermal resistance, binding affinity of solutes, biocompatibility, etc.

Because of the importance of the surface chemical properties, the membrane chemistry can be modified to improve the performances for specific applications. The modifications can be applied to the bulk (e.g. annealing of porous alumina membranes makes it resistant to water, see section 4.6), to the surfaces either by chemical treatment and/or grafting of a modifier (e.g. grafting of polymer brushes on anodic alumina membranes, see section 4.5). The surface modifications are applied through numerous methods [9] depending on the desired affinity with specific solutes.

The **hydrophilicity** (or hydrophobicity) of a surface is expressed by means of water contact angle. It is important because it determines the wetting properties of the solvent (in our case water). In the case of an hydrophilic surface, the membrane pores are spontaneously filled, whereas, when hydrophobic, the pores must be wetted by applying pressure or by

Table 4.1: Isoelectric points of selected membranes. [9].

Membrane material	Manufacturer	pI
Aluminium oxide	Whatman	4.4
Polysulfone	DDS	3.6
Polycarbonate	Whatman	2.5
Sulfonated polyslufone	DDS	<2.5
Cellulose acetate/nitrate	Millipore	2.2

using another solvent at start. For example, porous polyethylene is hydrophobic (high contact angle of water) but is easily wetted by ethanol (low contact angle of ethanol) and so, one can wet it by soaking in ethanol prior to water. Once wetted by ethanol, the membrane can be rinsed with water and since the two solvents are miscible, water replaces ethanol in the pores.

The **surface charges** of a membrane is another important aspect of the surface chemistry. The presence of net electrical negative or positive charges changes the character of the membrane-liquid interface. The nature of the charged groups is also important as the liquid-phase properties, such as pH and ionic strength, can vary these charges. When the charge of a surface or molecule is dependent from the pH, the isoelectric point is used to describe the charge state. By definition, the isoelectric point (pI) is the pH at which a particular molecule or surface carries no net electrical charge. The net charge can become more positive or negative when varying the pH of surrounding environment. The pI's of different commercial membranes are given in table 4.1. In particular the affinity of a biomolecule to be adsorbed or repelled by the surface is partially defined by the charge status of both surface and molecule. As discussed by Zeman and Zydney [9], this influences the molecular selectivity and fouling properties of a membrane.

4.3.2 Porous structure and pore sizes

In addition to the different materials for membranes, manufacturers have the ability to cast a number of different membrane structures. Various production methods are employed depending on both the material and the desired structure, especially for polymers [9]. For polymers, methods include air casting, immersion casting, melt casting, track-etching, stretching, radiation-induced polymerization and others. Casting may also be performed using another membrane as a substrate, often referred to as composite membranes. The structural characteristics of the membrane play a major role in determining permeability, retention capability and flux for filtration processes. More recent methods are able to produce composite and multi-layer membranes which provide dramatic increases in membrane capabilities compared to the isotropic membranes. Figure 4.3 shows the dif-

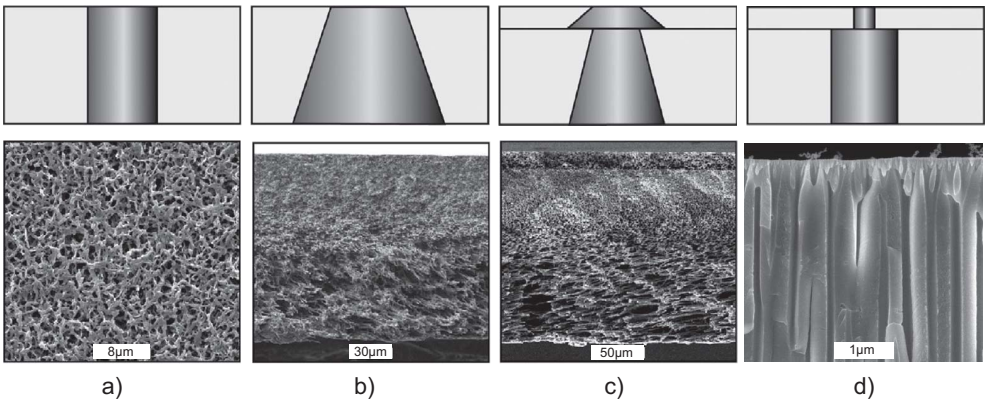

Figure 4.3: Cross-sectional view of different porous structures of membranes; a) isotropic and b) anisotropic membranes. More complex membranes co-cast structures c) of anisotropic or d) isotropic layers. a) to c) [6]

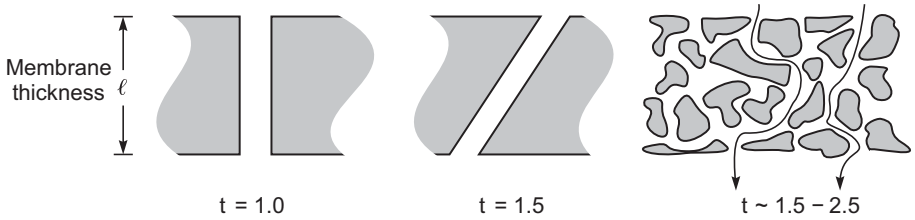

Figure 4.4: Cross-sections of porous membranes of different tortuosity t [7].

ferent membrane structures. Besides the polymer membranes, the anodic membranes, and in particular the anodic aluminium oxide membranes, can be structured as being asymmetrical. They are isotropic membranes and, when produced as bi-layer, are asymmetrical, each layer being isotropic, see figure 4.3.d. The anodic alumina membranes are presented in details in section 4.6.

The pore structure itself is also determinant for the membrane properties. Most of the membranes are made of polymers and their porous structure is the result of randomly situated and interconnected cavities. Some membranes, such as the anodic and track-etched have straight pores and this has an impact on the diffusions of solutes through the membrane. The form factor of pores is characterized by its tortuosity. The membrane tortuosity t reflects the average length of the pores compared to the membrane thickness. Simple cylindrical pores at right angles to the membrane surface have a tortuosity of one, that is, the average length of the pores is the membrane thickness, see figure 4.4. The more meandering the path through the membrane, the higher the tortuosity. Typical tortuosities are in the range of 1.5-2.5.

4.3.3 Membrane selectivity mechanisms

The intrinsic selectivity of the membrane is determined by the underlying pore size distribution and the membrane surface properties. For example, highly selective ultrafiltration membranes can be developed using electrically charged membranes that exhibit very high retention of proteins with the same polarity [110, 111]. Similarly, adsorptive membranes can provide highly selective separations based on the specific binding of various components. In details, the rejection of organic compounds represents a complex interaction of steric hindrance, electrostatic repulsion, solution effects on the membrane, and solute/membrane properties. Some interactions are fairly well understood. For example, the major mechanism of solute rejection by nanofiltration is physical sieving of solutes larger than the membrane molecular weight cut-off (MWCO). Other mechanisms of rejection such as electrostatic exclusion and hydrophobic-hydrophobic interactions between membrane and solute are considered important but are not as well understood [112]. For the ultrafiltration (larger molecules) range, physical sieving is not as predominant and the selectivity is a complex mechanism involving all the cited interactions. The major difference between nano- and ultrafiltration solutes is that when a molecule increases in size, such as polymers and polypeptides, the molecule dimensions depend on the tertiary structure which itself depends on the chemical environment. The molecule dimensions thus depends on the environment.

For the sieving mechanism to act correctly one could simply choose a membrane with pore much smaller than the dimensions of the molecules one wants to retain. In the case of a membrane for the IGLUS, we have to find a situation where glucose diffuses freely and other larger molecules such as the ConA dimer are completely retained. The difference of sizes between glucose and ConA dimer (see table 3.1) is only a factor 4-5 and thus we have to face the case where the molecule size and pore size are comparable. This situation is known as hindered molecular transport [113]. In this case we can define the ratio λ between molecular diameter d_{solute} and pore diameter d_{pore}:

$$\lambda = \frac{d_{solute}}{d_{pore}} \tag{4.1}$$

The results of the hindered diffusion observations are that the apparent diffusion coefficient D of the molecule in the pore is much lower than the bulk solution diffusion coefficient D_∞. The main results found in literature have been reviewed by Deen *et al.* [8] and a selection of plots is given in figure 4.5.

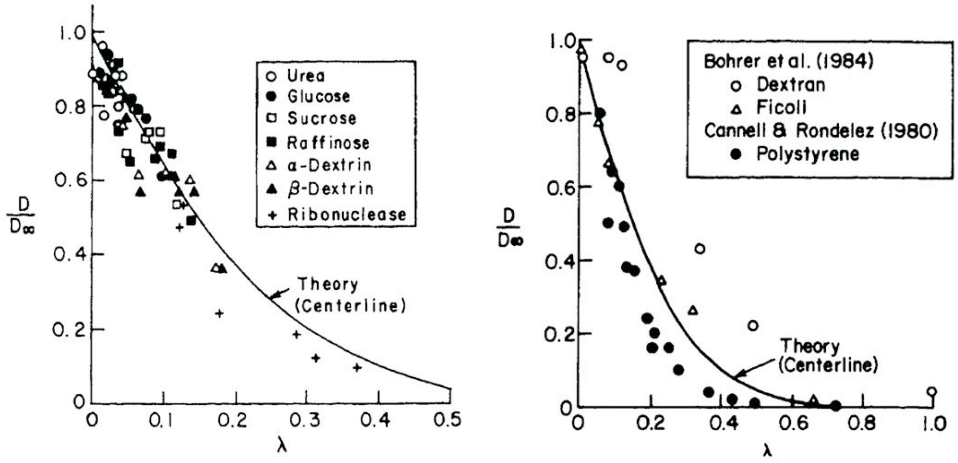

Figure 4.5: Experimental results of hindered diffusion in cylindrical track-etched pores. [8]

4.3.4 Size selectivity (dextrans, proteins)

As described in the last section, the pore size of a membrane is the major property for the size selectivity of a solute. Among the commercially available membranes, there are two ways of describing their size selectivity, either by their pore size or nominal MWCO which is typically defined as the molecular weight of a solute that has a retention coefficient of 90% (although this definition is not explicit and it can vary between 60% and 90% depending upon protocols used by various manufacturers [112]).

As shown in figure 4.6, there is a wide variety of membrane pore sizes and biomolecule sizes. The need of the IGLUS is among the dialysis and ultrafiltration membranes. The latter membranes are characterized by their manufacturer using either two proteins of different molecular weight (one retained and one passing solute) or a mixture of dextrans covering a large molecular weight range. When using proteins it is important to note the pH and surface charges as these have a significant impact on the hydrodynamic volume and hence sieving capability by membranes [114]. The common mixed dextran test [6] uses a mixture of dextrans with various molecular weights typically spanning a range of 1-2000 kDa. Samples of feed and filtrate taken under steady-state conditions are run on size exclusion chromatography and the resulting filtrate chromatogram is divided by the feed chromatogram to provide sieving as a function of retention time. Retention time is converted to dextran molecular weight with a calibration curve generated by running individual dextran standards. With both methods it is also important to note the mass transfer conditions if the measurements are done in filtration. Stirred cells will typically have much lower mass transfer coefficients than tangential flow ultrafiltration membranes,

which will impact the sieving performance [9].

The problem is that there is no general link between the pore size of membrane and the molecular weight of a molecule to ensure the selectivity. However correlations have been made between sieving of proteins, dextrans, and polyethylene glycols (PEG) based on their Stokes radius [9, 6] rather than the molecular weight (MW). An example in figure 4.7 shows the rejection differences as a function of the MW and the Stokes radius. Further details on the Stokes radius of dextrans and proteins are given in section 4.4.

4.3.5 Membrane functions: dialysis & filtration

A distinction must be done between the two different uses of a membrane: filtration and dialysis. For filtration one apply a pressure difference between both faces of the membranes which creates a flux of the solvent. For dialysis, no such pressure is applied. Dialysis can be thus defined as the diffusion of dissolved solutes across a semi-permeable membrane against a concentration gradient in an effort to achieve equilibrium. The results is that small solutes pass through the membrane while larger solutes are trapped on one side of the membrane. Having a flux of the solvent through the membranes impacts the molecular transport [115]. The IGLUS uses the membrane in the dialysis mode.

4.4 Properties of biomolecules

The biomolecules of interest for the IGLUS are dextran and the different proteins present inside and outside the sensor such as ConA (dimer and tetramer), albumin and fibrinogen. The properties of dextran are simple with respect to its environment since it is a neutral molecule. Its structure and Stokes radius have been presented in section 3.4.2.B. The properties of proteins are more complex and therefore an introduction is required.

The biological activity of a protein is determined by its unique three-dimensional structure and surface functionality. Proteins are biopolymers formed by a linear sequence of the 20 natural-occurring amino acids. The native state (or conformation) is stabilized primarily by hydrophobic interactions due to the unfavorable free energy associated with solvation of nonpolar groups by water. The net result is that the non-polar side chains tend to collapse together to form the protein hydrophobic core. Hydrogen bonds between weak acid donor groups (e.g. $N-H$ and $O-H$) and acceptor groups with one pair electrons stabilize the protein secondary structure including both α-helices and β-sheets. Positively-charged amino groups and negatively charged carboxylic acid groups are typically located along

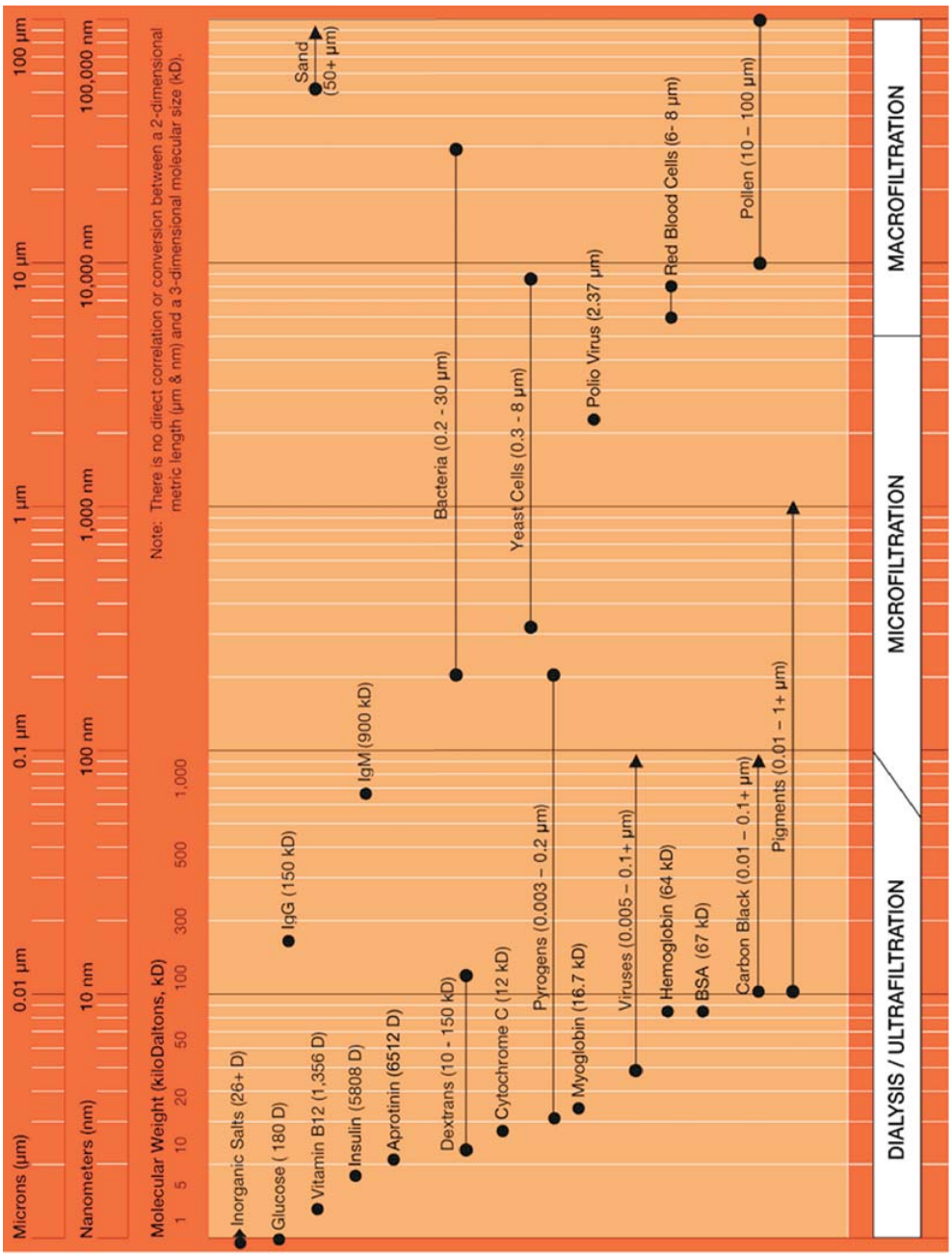

Figure 4.6: Relative size chart of membrane pore sizes and molecule sizes. Source: Spectrum Laboratories Inc.

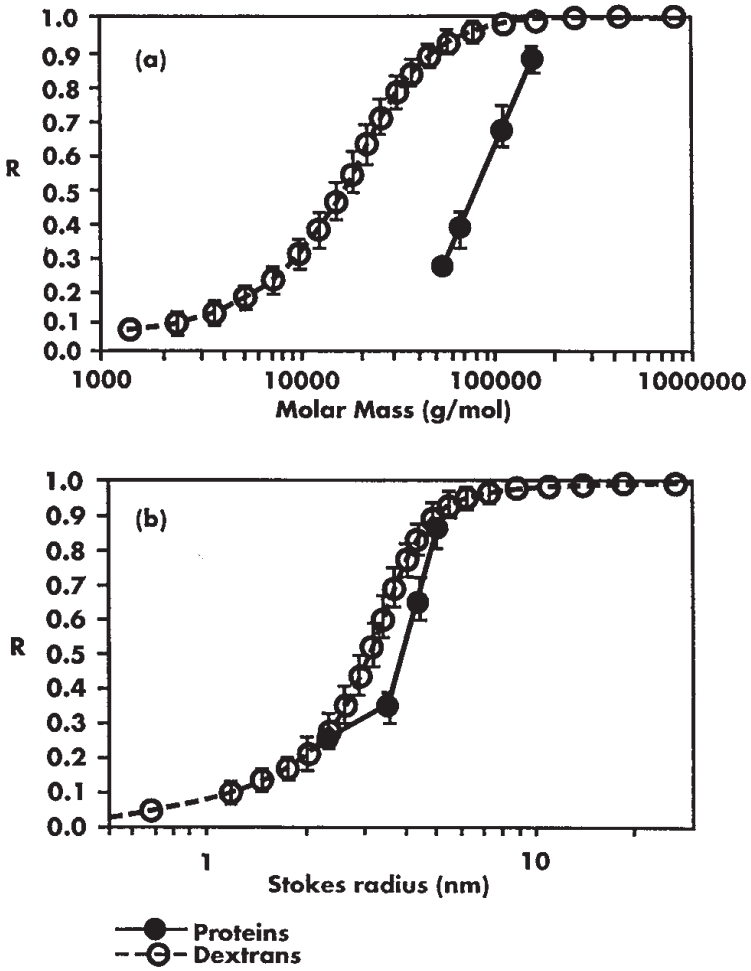

Figure 4.7: Measured values of rejection coefficients for dextrans and proteins plotted as a function of (a) molecular weight and (b) Stokes radius. The used membrane has an approximate 100 kDa MWCO and a low protein-binding surface. [9]

the protein exterior [116]. The net protein charge is determined by the number and pKa[1] of these acidic and basic amino acids. The isoelectric point (pI) is the pH at which the protein has no net electrical charge, typically determined by the equilibrium position in an isoelectric focusing gel or the lack of motion in an applied electric field. Since the three-dimensional geometry of a given protein can be quite complex, the hard sphere radius is usually estimated from the measured diffusion coefficient using the Stokes-Einstein equation:

$$R_h = \frac{kT}{6\pi\eta D} \tag{4.2}$$

where R_h is the Stokes or hydrodynamic radius, k the Boltzmann constant, T the temperature, η the dynamic viscosity of the medium and D the diffusion coefficient.

The effective radius of a protein in the context of membrane separation can be considerably larger than the hard sphere radius due to the presence of the diffuse ion cloud (the electrical double layer) that surrounds the charged protein in aqueous solution [117]. This effect can be quite dramatic, with the effective molecular weight of a protein (as determined by size exclusion chromatography) increasing by more than a factor of 20 as the solution ionic strength is reduced from 150 to 5mM [114].

The electric charges along the protein skeleton are the source of important differences in the tertiary structure with the dextran. Among them is the difference of Stokes radius as a function of the MW. The Stokes radius being related to the diffusion coefficient, it can be determined. This work has been done by Tyn *et al.* [118] and the diffusion coefficients of various proteins are plotted in figure 4.8. Young *et al.* [119] developed an equation for the proteins

$$D = 8.34 \cdot 10^{-8} \left(\frac{T}{\eta M^{\frac{1}{3}}} \right) \tag{4.3}$$

Where D is in $\frac{m^2}{s}$, T in Kelvin, η in $mPa \cdot s$ and M the molecular weight in Da.
When associating equation (4.2) and (4.3), we get the relation

$$R_h = 0.88 \cdot M^{\frac{1}{3}} \tag{4.4}$$

for proteins.

A similar relation as equation (4.3) has been experimentally established for dextrans [120]

$$D = 7.667 \cdot 10^{-9} M^{-0.47752} \tag{4.5}$$

where D is in $\frac{m^2}{s}$ and M in Da.

[1] Acid dissociation constant

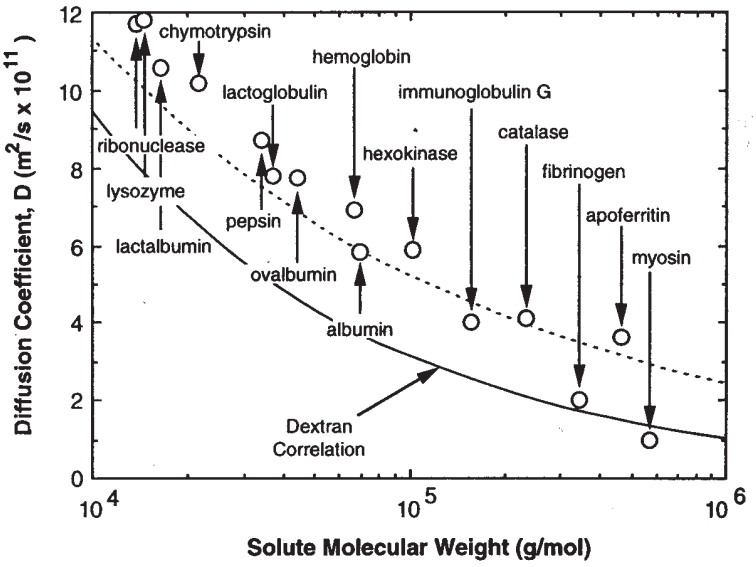

Figure 4.8: Diffusion coefficients of different proteins. The dashed line is the model of equation (4.3) and the solid line of equation (4.5). [9]

The difference of MW-Stokes radius relation is in accordance with the results of figure 4.7 and emphasizes the fact that the selectivity of a membrane is more likely to be compared by the Stokes radius of the molecule when dealing with proteins and/or dextrans.

4.5 Selection of nanoporous membranes

The choice of the suitable membrane for the IGLUS is based on its requirements (section 4.2), the basic chemistry and physics of membranes (section 4.3) and the properties of the involved macromolecules (section 4.4). The membrane requirements for the IGLUS can be summarized as follows:

1. Selective to ConA and dextran
2. Rigid (to sustain osmotic pressure)
3. Asymmetric (to optimize glucose diffusion)
4. High porosity (to optimize glucose diffusion)
5. Low tortuosity (to optimize glucose diffusion)
6. Chemically inert (for long term chemical stability of membrane and SF)

7. Low protein adsorption (for chemical stability of SF and fouling prevention)

8. Coating possibilities (to improve selectivity and prevent biofouling)

Considering these requirements, we reviewed the existing membranes and made a selection.

There are several kinds of membranes with nano-sized pores. In fact, there are thousands of commercially available membranes in the ultrafiltration range [121]. Each manufacturer has his own recipe for membrane fabrication, modification and also characterization. As discussed previously in section 4.3.4, there is no standardization for determination of the MWCO or pore size of a membrane. The end-users of ultrafiltration membranes have to face an enormous difficulty in comparing membrane products provided by different manufacturers and made of different polymeric or ceramic materials. In the industry, the ultrafiltration membranes are mainly employed for filtration in production processes. And since polymer and ceramic membranes are adapted for this use, they are the most present membranes on the market. Nevertheless many other types of membranes exist and need to be considered. We grouped the reviewed membranes in classes as follows:

- Porous polymer membranes
- Track-etched polymer membranes
- Sol-gel ceramic membranes
- Anodic alumina membranes
- Structures obtained by nano-imprint lithography (NIL) of various materials
- Silicon-based membranes

4.5.1 Porous polymer membranes

Porous polymer flat sheet ultrafiltration membranes exist out of various materials such as polysulfone (PS), polyethersulfone (PES), polyethylene (PE), polyvinylidene fluoride (PVDF), polytetrafluoroethylene (PTFE), regenerated cellulose (RC) (see figure 4.9 a), cellulose acetate (CA) or cellulose ester (CE). These membranes have an asymmetric (skinned) structure, with a thin skin providing the desired selectivity while the substructure with larger pores provides the necessary mechanical support. Some of these synthetic polymers have high thermal stability and chemical resistance, allowing the use of fairly harsh cleaning chemicals. However only the cellulose membranes allow relatively low cut-offs [122] as required by

the IGLUS and recent RC and CE membranes are more hydrophilic, reducing both protein adsorption and fouling. But their chemical resistance is not suitable for a long term implant. We have to point out that suppliers such as Millipore[2] rarely quote rejections above 99%, leaving the potential issue of some pores being much larger than the nominal cut-off. Other drawbacks of the polymer membranes are their non-rigidity and their high tortuosity.

Hollow fibres made of the same polymers exist and are for example used in artificial kidneys for blood dialysis, but their shape is not applicable for the IGLUS.

Recently (2006), nanoporous PE films have been reported by Uehara *et al.* [17] and exhibit promising structural and chemical properties for our application. PE is mechanically and chemically very robust and films can be prepared thinner than 10 μm. These films are flexible and therefore cannot be used on the IGLUS demonstrator presented in this work. However, the flexibility of the PE films is an advantage when considering a non-flat SI for a future version of the IGLUS having a cylindrical shape, nonetheless a rigid supporting structure is required. Taking into account the future of the IGLUS and promising properties of the PE films, we selected this technology as a potential component for the SI.

4.5.2 Track-etched polymer Membranes

Track etching was the first technique to enable fabrication of membranes with straight nanopores of well-defined size [10]. Fabrication procedure consists of a sequence of two operations: irradiation of a thin polymer foil with suitable high-energy particles, followed by a chemical etching of the tracks the particles left in the foil.

From figure 4.9.b), one can see the pores are straight, have a narrow size distribution and a filling factor which could be acceptable, although still relatively low. Common track etched materials include polyethylene terephtalate (PET), which is hydrophilic and biologically inert, and polycarbonate [10].

Commercially, track-etched membranes are available down to 10 nm [3] or 15 nm [4] nominal pore size, which would fit our requirements. However, combining small pore size and high pore filling factor is not possible, because there is an increasing probability of overlapping pores when increasing the pore density. For instance, the aforementioned commercial membranes are limited at $6 \cdot 10^8$ $pores/cm^2$, which corresponds to 6 $pores/\mu m^2$ and therefore yields very low filling factors of 0.4% for 30 nm, 0.1% for

[2] http://www.millipore.com
[3] http://www.spi.com
[4] http://www.whatman.com

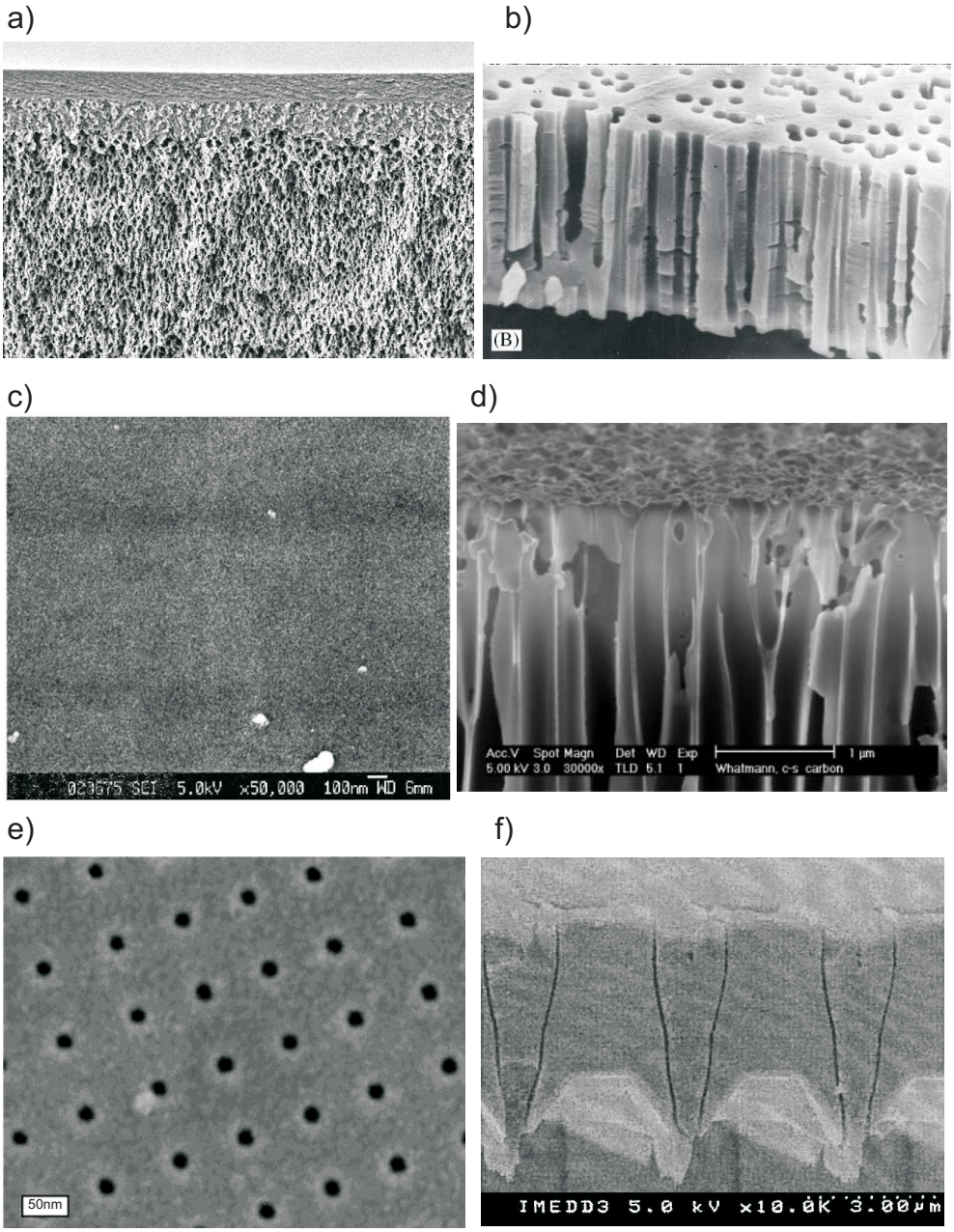

Figure 4.9: SEM images of the different types of membranes; a) regenerated cellulose (RC) polymer membrane [6], b) polycarbonate track-etched membrane [10], c) TiO_2 ceramic membrane [11], d) anodic aluminium oxide membrane, e) nano-imprinted membrane [12], f) silicon dioxide membrane [13].

15 nm, and 0.05% for 10 nm. Moreover, the membranes are relatively thick, *ca.* 6 μm. Considering the very low porosity of such membranes, it is clear that they don't meet the IGLUS requirements. The response time of the sensor would be much too long.

4.5.3 Sol-gel ceramic membranes

Sol-gel / colloïd techniques can be used to form in-situ membranes with a very small pore size (down to < 1 nm). Usually, a liquid containing suitable precursor is applied onto a porous ceramic support by spin casting, dipping or spraying, followed by a drying and a firing step, during which calcination / pyrolysis and partial sintering occur, resulting in a very fine-grained oxide film. By selecting the correct firing temperature, the film may exhibit good cohesion whilst remaining porous. This process inherently yields a large porosity (up to 30%), which however exhibits some tortuosity. The porous ceramic support is easily obtained by classical powder technology.

Many materials may be used, such as TiO_2 (titania / anatase), ZrO_2 (zirconia), SiO_2 (silica), aluminosilicates, $SiO_2 - ZrO_2$, HfO_2 (hafnia) and $\gamma - Al_2O_3$ (alumina) [106, 123, 124, 11, 125, 126]. They may exhibit excellent corrosion resistance [11], which means corrosion is not a critical issue at all in animal body conditions.

Due to the very small achievable pore sizes, cut-off may be achieved just above the size of glucose, for instance between glucose (0.86 nm) and glucitol (0.97 nm) [106]. However, the loss incurred in terms of glucose diffusivity is very high in this case: a factor of *ca.* 4'000. In comparison, the same type of membranes with *ca.* 11 nm pores achieve a quite acceptable decrease of diffusivity compared to free glucose diffusion: only a factor of *ca.* 7, which is quite promising for the IGLUS system. Pore size distribution lies within a factor of *ca.* 2 [123].

There are however three drawbacks to this technology: 1) the theoretical possibility of cracks if the process is not well controlled; 2) the lack of commercial availability of standard sheets of membrane material; 3) an important lower diffusivity due to the tortuous nature of the pores. These are only relatively small difficulties, however, compared with the relative simplicity of the fabrication process and the very fine structures (figure 4.9.c) that can be achieved.

4.5.4 Anodic alumina membranes

Anodic aluminum oxide (AAO) or anodic alumina membranes is a peculiar technology that shares common features with both the track-etched membranes and the ceramic membranes. AAO membranes exhibit arrays

of straight parallel pores of quasi-uniform shape and have the chemical properties of a ceramic, i.e. alumina. Initially developed by Anotec Ltd., the technology was sold to Whatman Ltd.[5] The pore size ranges from $>$ 200 nm down to $<$ 10 nm and the thickness from 100 μm down to 15 μm. The smallest pore size has been reported by Zhang *et al.* [64] at 6.8 nm and the smallest pore size commercially available is 5-7 nm from Synkera Technologies Inc.[6] The pore size is regulated by the choice of the acid electrolyte and the anodization voltage employed during preparation. More details about the fabrication are given in section 4.6. The porosity of such membranes can go up to 50% and they exhibit a low protein adhesion [9]. Alumina is rigid and the straight pores (minimum tortuosity) allow an optimum diffusion of small solutes such as glucose.

Anodic oxide films and membranes also can be made from sputtered or evaporated aluminum thin films, which means they may be applied on practically any substrate [127, 128, 129, 130]. The natural hexagonal ordering of the pores may be improved by nano-imprinting the aluminum with spheres, provided that the pattern is close to the natural one [131]. Finally, the surface of nanoporous alumina can be modified and various coatings can be added especially for biomedical applications [20]. This makes the AAO membranes a good candidate for the IGLUS.

4.5.5 Structures obtained by nano-imprint lithography of various materials

Nano-imprint lithography (NIL) involves fabrication of a mould, which is then repeatedly imprinted onto a soft material. This may then be followed by various etching steps to obtain the desired structure. NIL is potentially a relatively inexpensive fabrication technology [132]. While fabrication of molds is usually a tedious and expensive process, the mold may then be replicated a large number of times. Additionally, there are techniques to produce "daughter-molds" from the original one at a fraction of the cost of initial fabrication: wear is not a severe problem. There is a wide choice of materials, as NIL may be used to pattern several photolithographic resins. The resulting pattern can then be transferred to many materials using standard etch methods. For example, pores of anodic alumina membranes can be patterned by NIL to create organized porous alumina membrane [131].

The method have the following drawbacks. A compromise must be made between membrane thickness and pattern size. The mold features should not have a too high aspect ratio as they would become fragile. Therefore, if one wishes to have a large open cross section of very small pores, for example 25 nm pores with 100 nm spacing, the nanoimprinted

[5] http://www.whatman.com
[6] http://www.synkera.com

layer has to be as thin as 10 nm [12]. However, one should not forget that the nano-imprinted layer can then be used as a mask for etch techniques which allows a much larger aspect ratio, such as reactive ion etching. The problem of pore density may be ameliorated if one chooses another pore geometry such as slits instead of circular holes. However, at present stage of development, NIL produces very low porosity membranes and the pore size remains too large. The method is still young and future development must be followed.

4.5.6 Silicon-based membranes

Membranes based on silicon structuring should a priori be available, given the wide knowledge and industrial base of this technology. However, existing photolithographic techniques still do not allow the desired feature size, especially if the cost factor is taken into account. However, we do not need to confine ourselves to cylindrical pores, and slit-based geometries, where the width of the slit is defined by the thickness of a thin film, may easily be defined in the 10 nm range [133].

The open area fraction of silicon structured membranes is around 1% at 20 nm [13], which is roughly 1 order of magnitude higher than that achievable by track etched membranes, and they are available commercially [7]. The low porosity is a major drawback for the IGLUS.

A newer technology (2007) has recently been described by Striemer *et al.* [134, 135], where a nanoporous membrane of crystallin silicon is obtained by self-organization. They presented a 5-17 nm pores membrane with a thickness of 15 nm which bears a pressure of 1 bar. The achievement of thinner membranes down to 5 nm with a surface of up to 2×2 mm^2 is also described. The technology is promising but too recent to be investigated in the present work.

4.5.7 Conclusion on membrane selection

Among the presented technologies summarized in table 4.2, two types of membranes were selected to constitute a base for the SI: the anodic alumina membranes and the polyethylene films. For the IGLUS demonstrator presented in this work, anodic alumina membranes are clearly the most mature nanoporous membrane technology, because of their good availability and performance. However, their diffusion performance were not yet sufficiently characterized. It remains to be seen whether they can achieve the necessary molecular selectivity. In order to fully satisfy the requirements for the IGLUS (see section 4.2), the PPEGMA coating was selected to improve the performances of the anodic alumina membranes (see section 3.5).

[7] http://www.imeddinc.com

Table 4.2: Summary and comparison of membrane technologies.

Membrane technology	Advantages	Disadvantages
Porous polymers	small pore size, availability	chemical resistance excepted for PE, high tortuosity, support required
Track-etched polymers	narrow pore size distribution	very low porosity, support required
Sol-gel ceramics	high chemical resistance, small pore size	high tortuosity, defects
Anodic alumina	High porosity, narrow pore size distribution, rigid, chemical resistance	limited shape availability (flat), brittle
NIL structured	narrow pore size distribution	very low porosity, pores too large
Silicon based	thickness, small pore size	availability

Selectivity results of a nanoporous alumina membrane coated by PPEGMA are presented in chapter 5. The details of structure and fabrication of the anodic alumina membranes and polyethylene films are presented in sections 4.6 and 4.7 respectively.

Other alternative technologies may be available in the future such as nanograin oxide ceramics, NIL and silicon technologies since they also have the potential for fabrication of nanosieving membranes with sufficient open area. Alternatively, RC with a coating to prevent biodegradation could be possible. Unfortunately, at their current stage of development, they are not suitable for the IGLUS.

4.6 Anodic alumina membrane

4.6.1 Structure

Anodic aluminum oxide (AAO) membranes (or anodic alumina membranes) have symmetrical morphology with high density cylindrical pores that are aligned perpendicular to the membrane plane. The fabrication process, described in section 4.6.2, is intrinsically selfhealing and yields defect-free nanoporous membranes.

An electrochemical process involving anodic oxidation of high purity aluminum sheets can be used to form porous oxide films. In certain acid

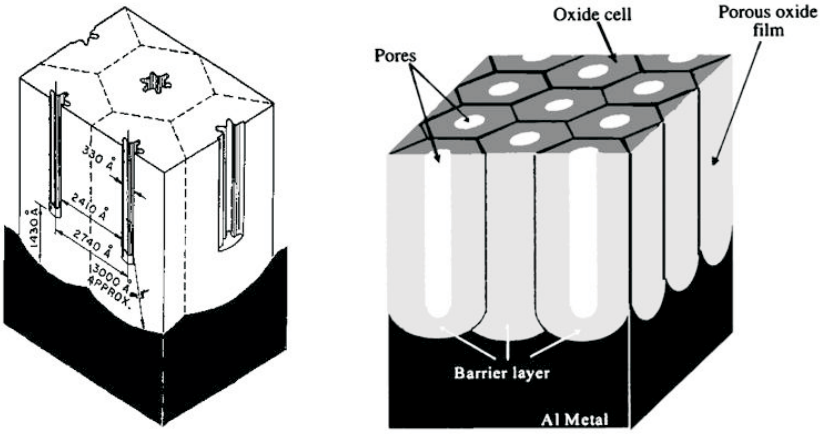

Figure 4.10: Anodic aluminium oxide structure. [14, 15]

electrolytes, this oxidation process results in a film comprised of a uniform columnar array of parallel-sided, closely packed, hexagonal alumina cells, each containing a circular pore. This film is in intimate contact with a thin nonporous alumina layer adjacent to the aluminum substrate, as shown in figure 4.10. By appropriate selection of the process conditions, pore diameter is controlled with great precision and reproducibility in a wide range, from $<$10 to $>$200 nm. The corresponding pore density is from 10^{12} to 10^{8} cm^{-2}. The porosity varies from 8 to 50%, depending on other specifications. The standard deviation of pore diameters is typically $<$10% and as low as 5% for optimized conditions. No other type of membrane can match such pore uniformity.

4.6.2 Fabrication process

Anodic alumina membranes are formed by an electrochemical process involving the oxidation of high purity aluminum sheets. In this process, an electrical circuit is established between a carbon cathode and a thin film of aluminum which serves as the anode, resulting in the oxidation of the aluminum to form alumina.

In appropriate electrolyte solutions, the film that is formed has a uniform columnar array of hexagonally close packed alumina cells, each containing a circular pore. This film is in intimate contact with a thin nonporous alumina layer, called the barrier layer, which is adjacent to the aluminum anode. Pores form in the oxide film because of field assisted dissolution of the alumina from the base of each pore. As the alumina and the pores penetrate the aluminum film, chemical dissolution of alumina from the pore walls also occurs, yielding pores which are slightly larger at the exterior film surface than at the base. With appropriate process conditions,

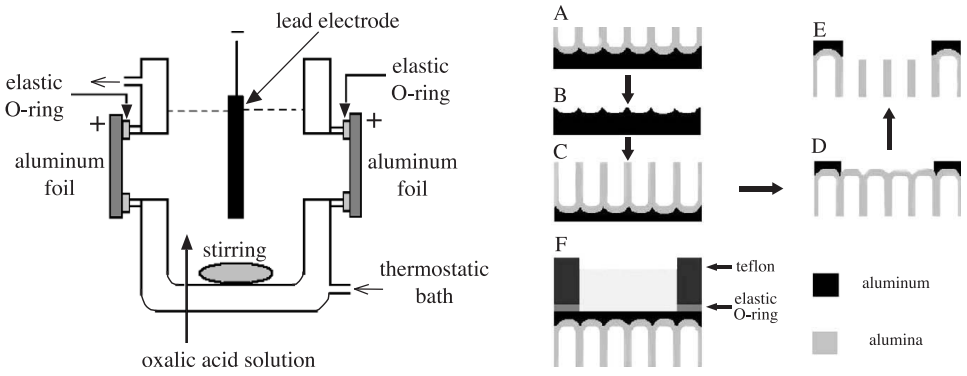

Figure 4.11: Example of anodization equipment and corresponding membrane fabrication steps. A) pre-anodisation step; B) removal of pre-anodisation oxide; C) final anodisation; D) removal of Al; E) removal of barrier oxide. [16]

Table 4.3: Detailed geometric parameters of Whatman Anopore 20 nm alumina membranes [20].

Layer	Mean pore diameter [nm]	Pore density [m^{-2}]	Pore area fraction
Active	26	6.5×10^{14}	0.37
Support	207	1.0×10^{14}	0.37

films can be formed with pore diameters between 10 and 300 nm, pore densities between 10^8 to 10^{12} cm^{-2} and film thicknesses up to 200 μm [136]. Porous membranes can be prepared from these films by removing the barrier layer and the unoxidized aluminum from the porous oxide layer. An example of an anodization equipment and the corresponding membrane fabrication steps are depicted in figure 4.11.

Anodic alumina membrane can also be prepared with a bilayer structure. These are called asymmetrical as each layer has a different pore size. The most common commercial membranes having this structure are the Anopore membranes from Whatman. In this work we used the product with 20 nm pores. As described by the manufacturer, they have a thin active layer of 1 μm thick with 20 nm pores and a support layer of 59 μm thick with 200 nm pores. More precise values are given by Lee *et al.* [20] and detailed in table 4.3. In order to assess the structure of the 20 nm asymmetric membrane that we purchased from Whatman, we performed Scanning Electron Microscopy (SEM) and Transmission Electron Microscopy (TEM) on a sample. The obtained images are shown in figure 4.12 and correspond to the ones found in literature [20, 137]

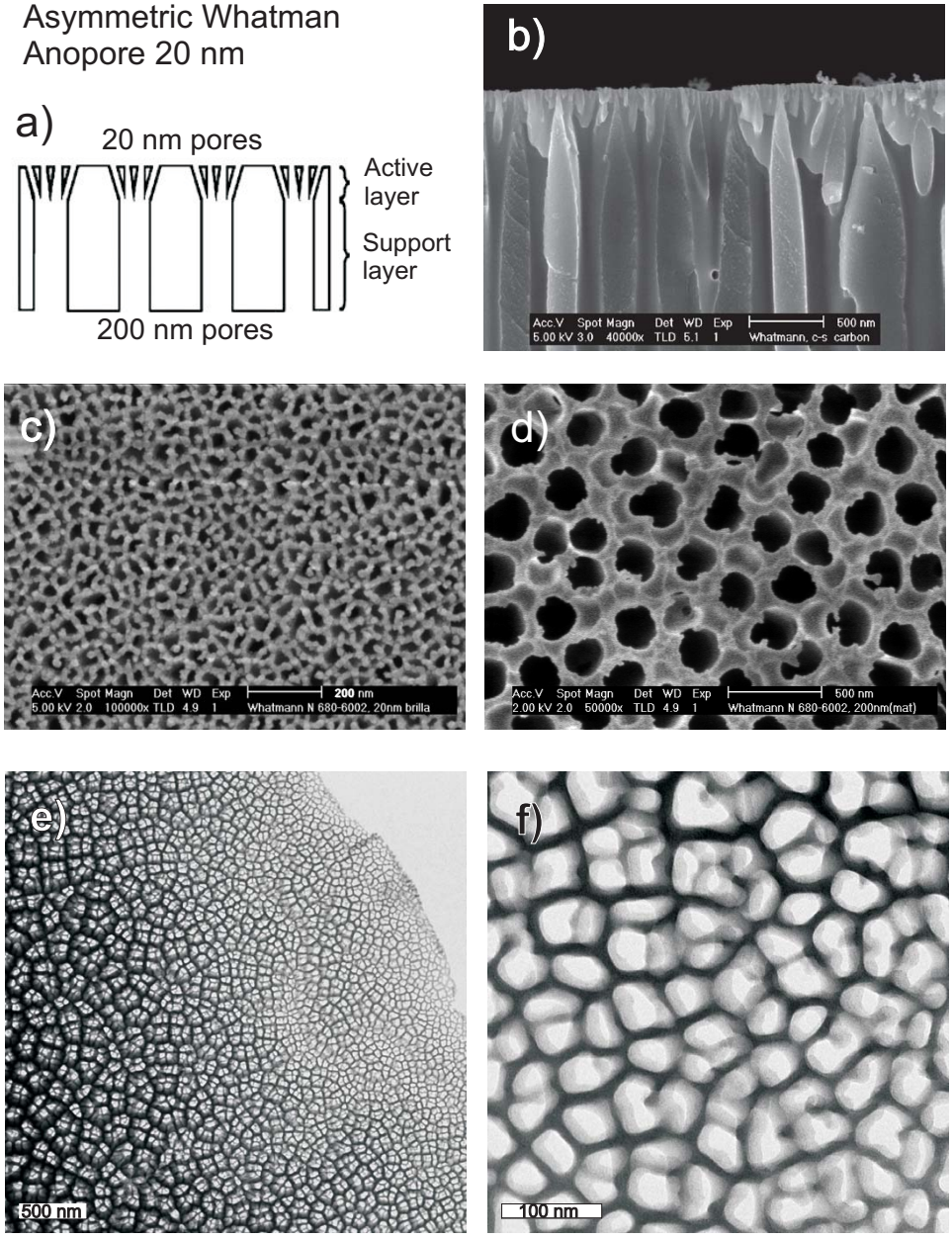

Figure 4.12: Electronic micrographs of a Whatman Anopore 20 nm asymmetric alumina membrane. a) illustration of the asymmetric structure, b) SEM image in cross-sectional view, c) SEM image of the active layer, d) SEM image of the support layer, e) and f) TEM micrographs of the active layer in different magnification.

4.6.3 Chemical properties

As-prepared amorphous AAO can be converted by annealing into polycrystalline γ- and α-alumina that retain nanoporous morphology. Such membranes have excellent chemical resistance and long-term stability in aqueous solution. Their upper operating temperature is up to 1000˚C for γ-alumina and up to 1100˚C for α-alumina membranes. AAO membranes are mechanically robust and exhibit good flexibility, hardness, and fracture toughness. The Whatman Anopore membranes are out of γ-alumina and their pI has been reported to be pI = 4.4 [9, 138] (see table 4.1).

4.6.4 The PPEGMA coating and antifouling mechanism

The polymer used to coat and pore-fill the alumina membrane is poly(poly-(ethylene glycol) methacrylate) brushes (PPEGMA) grown on the surface by surface-initiated polymerization. An illustration is shown in figure 4.13. The PPEGMA brushes have also shown to have non-fouling properties [139, 108, 140] which is essential for long-term permeability of the membrane.

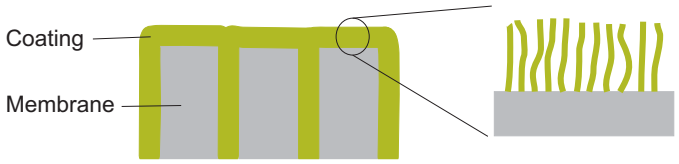

Figure 4.13: PPEGMA brushes coat the surface of the alumina membrane and partially fill the pores.

As discussed previously in section 3.5, it is the nonspecific adhesion of proteins on the surface of the implant that creates an immune response, followed by a tissue encapsulation. The mechanisms for prevention of adhesion of proteins have been suggested [140]. It has been found that poly(ethylene glycol) (PEG), a water soluble, nontoxic, and nonimmunogenic polymer, serves as an excellent coating material [139]. It is compatible with biological systems and has been shown to reduce protein adsorption and cell adhesion on synthetic surfaces [141]. The protein repulsive nature of PEG is mainly attributed to its hydrophilicity, steric stabilization force, and chain mobility effect. The two main contributions to this repulsive force are the excluded volume component and the mixing interaction component. When protein molecules approach the PEG-coupled surfaces, the available volume for each polymer segment is reduced, and consequently a repulsive force is developed due to loss of conformational entropy of the PEG chains. Also, the number of available conformations of the PEG segments is reduced owing to their compression or interpenetration of the pro-

tein chains generating an osmotic repulsive force. We made the choice of a neutral polymer as a coating because a charged surface like alumina at physiological pH can promote protein adsorption. Finally, we can summarize the PPEGMA properties as follows:
- Neutral polymer to screen the charges of the substrate (alumina)
- Prevent non-specific adhesion of proteins

4.7 The polyethylene membrane

4.7.1 Structure

The polyethylene membranes have been kindly provided by Prof. Dr. Hiroki Uehara from Gumna University, Japan. In a publication [17], he describes the structure and fabrication procedure in detail. The provided PE films are 15 or 30 μm thick and have pores of about 10-30 nm. The fabrication process is limited to ultrathin films and the pore size is linked to the film thickness, i.e. the thinner the film, the smaller the pores. This property is an advantage to create a selective and diffusion efficient interface. At the end of the fabrication process, an etching step creates the pores and the pore size can be somewhat tuned by the time length of etching. The nanoporous structure of the PE film is depicted in figure 4.14. The films exhibit a continuous cylinders porous structure which comes from the structure of the crystalline component (PE). The crystallinity of the PE component was estimated by density measurement as 45%.

The nanoporous PE films prepared by Uehara *et al.* are very flexible and mechanically very resistant. Moreover PE is very stable over time, since it is chemically inert. Such superior characteristics make the PE nanoporous film an excellent candidate for a SI if coupled to a rigid support.

4.7.2 Fabrication process

The PE films are prepared from a polyethylene (PE)/polystyrene (PS) diblock copolymer. The average MW of each component was 5.4×10^4 for PS and 6.7×10^4 for PE, with a MW distribution of 1.04. The PE block is semicrystalline, but the PS block is always amorphous. Thus, their crystalline/amorphous phase separations are controlled by processing conditions, including isothermal crystallization temperature and time after the melt. The amorphous component (PS) is selectively removed by wet etching with fuming nitric acid. With increased etching time, the pores gradually develop and interconnect with each other.

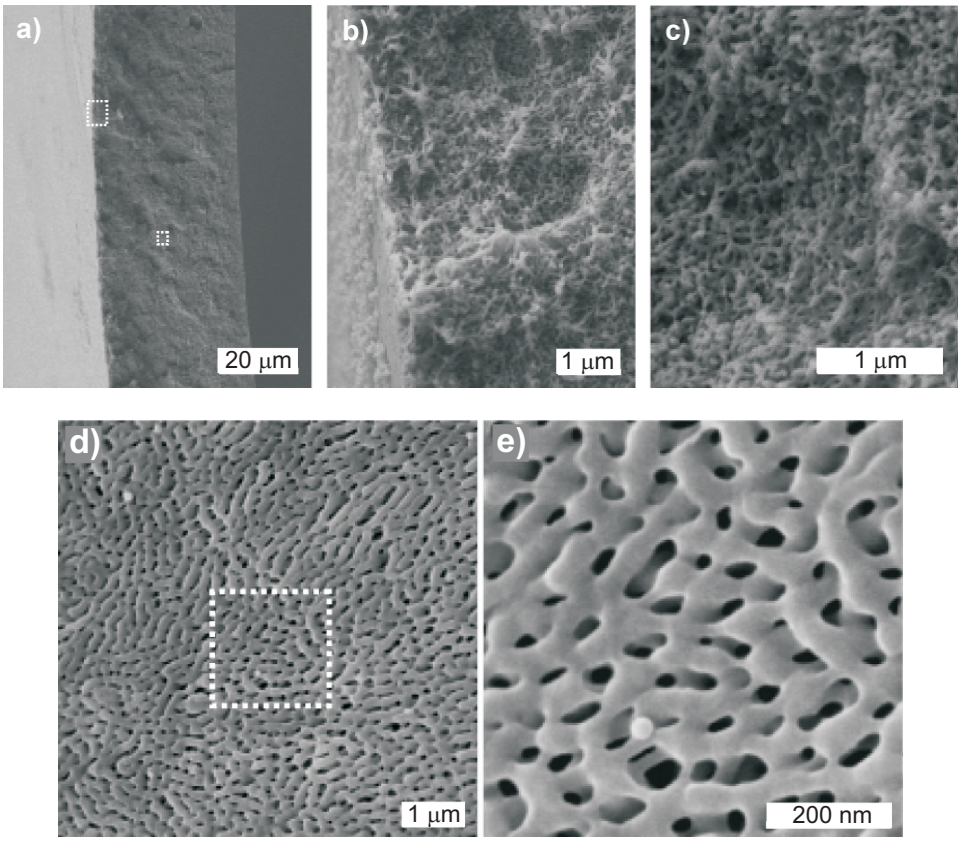

Figure 4.14: (a-c) SEM images of the edge of the film etched for 30 min. The film was freshly cleft in liquid nitrogen. (a) Whole image with a scale bar of 20 μm. The surface and internal regions that are marked by the dotted line are enlarged in (b) and (c) with each scale bar of 1 μm. SEM image with a scale bar of 1 μm. (d-e) surface view of PE film, (e) enlarged image of the area marked by the dotted line in (d) [17].

4.8 Diffusion theory in membranes

4.8.1 Situation

Different membranes have been characterized in diffusion cells and we propose a theoretical model to understand the experimental results presented further in chapters 5 and 6. In the cases of a membrane in the diffusion cell or on the IGLUS demonstrator in the *in vitro* setup, we face similar situations where a membrane is separating two volumes and the solute (glucose) can go from one volume to the other by pure diffusion through the membrane.

We present here a general model inspired from the work of Hoogervorst *et al.* [142] which will allow us to compare different situations. The model describes the transient diffusion through a membrane separating two unequal volumes of well-stirred solutions. The treatment is restricted to one-dimensional flow, the volume flow being zero at every point in the membrane. We consider the membrane to be homogeneous.

4.8.2 General solution

As shown in figure 4.15, the system is composed of three zones, the two volumes V_a and V_b, and the membrane. The latter is of cross sectional area S and thickness l. Outside the membrane, the solute is present in concentration $c_a(t)$ and $c_b(t)$, whereas the solute concentration inside the membrane at coordinate x and time t is defined as $c(x,t)$.

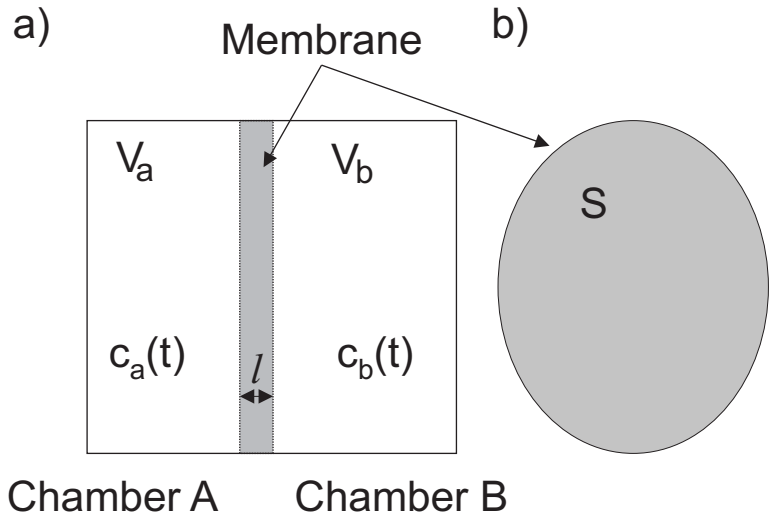

Figure 4.15: Schematic of the model situation; a) cross-sectional view, b) top view.

At the interfaces ($x = 0$ and $x = l$) a coefficient k describes the partitioning of the solute

$$k = \frac{c(0,t)}{c_a(t)} = \frac{c(l,t)}{c_b(t)} \tag{4.6}$$

This coefficient k can be developed as

$$k = K\phi\frac{v_0}{v} \tag{4.7}$$

where K is the partition coefficient, ϕ the porosity of the membrane and v_0 and v are the molar volumes of the solute outside and inside the membrane respectively. K is defined for two solvents at their interface at equilibrium as

$$K = \frac{[solute_1]}{[solute_2]} \tag{4.8}$$

k is thus a partitioning coefficient which takes into account the volume occupied by the membrane and the molar volumes changes at the interface.

The diffusion process is described by the diffusion equation

$$D\frac{\partial^2 c}{\partial x^2} = \frac{\partial c}{\partial t} \tag{4.9}$$

and by the boundary conditions

$$\begin{aligned} Al\frac{\partial c(0,t)}{\partial t} &= D\left(\frac{\partial c}{\partial x}\right)_{x=0} \\ Bl\frac{\partial c(l,t)}{\partial t} &= -D\left(\frac{\partial c}{\partial x}\right)_{x=l} \end{aligned} \tag{4.10}$$

with the abbreviations

$$A = \frac{V_a}{kSl}, \quad B = \frac{V_b}{kSl} \tag{4.11}$$

and by the initial conditions

$$\begin{aligned} c_a(0) &= a \\ c_b(b) &= b \\ c(x,0) &= k[(q - p\frac{x}{l})(a-b) + b] \end{aligned} \tag{4.12}$$

Where D is the diffusion coefficient and p and q represent adjustable parameters which can describe any linear solute concentration profile. The boundary conditions (eq. (4.10)) relate the change in the solute concentration in the external volumes to the rate at which the solute penetrates or leaves the interfaces. In fact they express the continuity of fluxes together with the solute partition equilibrium at the interfaces.

The system of equations 4.9-4.12 can be solved using the Laplace transformation method (see [142]). The solution can be expressed as

$$c(x,t) = k\left(C_\infty + \sum_{n=1}^{\infty} C_n(x)\exp(-\frac{t}{\tau_n})\right) \tag{4.13}$$

where C_∞, $C_n(x)$ and τ_n represent

$$C_\infty = \frac{(A+q-\frac{1}{2}P)a + (B+1-q+\frac{1}{2}p)b}{A+B+1} \tag{4.14}$$

$$\begin{aligned} C_n(x) = [(a-b)(E+F)]/([\frac{1}{2}(A+B)Q_n^2 + ABQ_n^2]\frac{\sin Q_n}{Q_n} \\ -[\frac{1}{2}(A+B) + \frac{1}{2}(1-ABQ_n^2)]\cos Q_n) \\ E = \left\{(1-q)A + \frac{P}{Q_n^2}\right\}[BQ_n \sin\left\{Q_n(1-\frac{x}{l})\right\} \\ -\cos\left\{Q_n(1-\frac{x}{l})\right\}] \\ F = \left\{(q-p)A + \frac{P}{Q_n^2}\right\}[\cos\left\{(\frac{Q_n x}{l})\right\} \\ -AQ_n \sin\left\{(\frac{Q_n x}{l})\right\}] \end{aligned} \tag{4.15}$$

$$\tau_n = \frac{l^2}{Q_n^2 D} \tag{4.16}$$

and where the Q_n are the nonzero, positive roots of the transcendental equation

$$(ABQ^2 - 1)\tan Q = Q(A+B) \tag{4.17}$$

We notice that the local concentration c(x, t) changes with time until a uniform limiting value $k \cdot C_\infty$ has been reached. One can also note that the coefficients C_n are dependent of the initial condition parameters (eq. (4.12)) imposed on the membrane, while the characteristic times τ_n is not but rather depends on the geometric parameters.

Equations for the measurable concentrations $c_a(t)$ and $c_b(t)$ can be derived by substituting the expression for k (eq. (4.6)) into the general solution (eq. (4.13)) of the diffusion equation. We have

$$\begin{aligned} c_a(t) &= C_\infty + \sum_{n=1}^{\infty} C_n(0)exp(-\frac{t}{\tau_n}) \\ c_b(t) &= C_\infty + \sum_{n=1}^{\infty} C_n(l)\exp(-\frac{t}{\tau_n}) \end{aligned} \tag{4.18}$$

4.8.3 Case p=0 and q=0

The initial conditions (eq. (4.12)) have been established as a function of coefficients p and q with the aim to be as general as possible. In the literature [142], three cases are discussed: I. $p = 0$ and $q = 0$, II. $p = 0$ and $q = 1$, and III. $p = 1$ and $q = 1$. Cases I and II represent the situation where the membrane is first equilibrated by the solutions of volume b and a respectively. The case III represents an initial linear concentration profile within the membrane with equilibrium at the interfaces. These cases are accessible experimentally and cases I and II are equivalent. Our experimental situation corresponds to case I and therefore we now propose to detail the solution for this specific case.

Considering $p = 0$ and $q = 0$, we substitute these values into eq. (4.18) and rearrange with the use of eq. (4.17), and we find for the difference of the solute concentrations in the bathing solutions

$$\Delta c(t) = \Delta c(0) + \sum_{n=1}^{\infty} A_n \exp(-\frac{Q_n^2 Dt}{l^2}) \tag{4.19}$$

in which

$$A_n = \frac{A\{(1 + B^2Q_n^2) \pm [(1 + A^2Q_n^2)(1 + B^2Q_n^2)]^{\frac{1}{2}}\}}{\frac{1}{2}\{(1 + A^2Q_n^2)(1 + B^2Q_n^2) + (A + B)(1 + ABQ_n^2)\}} \tag{4.20}$$

The plus sign in the equation for A_n applies if the Q_n lie in the first and the second quadrant, whereas the minus sign applies if the Q_n lie in the third and the fourth quadrants. A great simplification is obtained if the volumes of the bathing solutions are equal $(A = B)$. In that case eq. (4.17) and A_n in eq. (4.19) reduce respectively to

$$\begin{aligned} AQ \tan^{\frac{1}{2}} Q &= 1 \\ A_n &= \frac{4A}{1 + A^2Q_n^2 + 2A} \end{aligned} \tag{4.21}$$

4.8.4 The quasistationary case

Generally the sum in eq. (4.13) represents a rapidly converging series to which all terms contribute in early stages of the diffusion process. However, after a certain period only the leading term $(n = 1)$ is of importance and the diffusion process is said to be quasistationary. Under this condition eq. (4.13) and (4.19) reduce with eq. (4.16) to

$$\begin{aligned} c(x,t) &= k\left(C_\infty + C_1 \exp(-\frac{t}{\tau_1})\right) \\ \Delta c(t) &= \Delta c(0) \exp\left(-\frac{t-\theta}{\tau_1}\right) \end{aligned} \tag{4.22}$$

in which θ is

$$\theta = \tau_1 \ln A_1 = \frac{lnA_1}{Q_1^2}\frac{l^2}{D} \tag{4.23}$$

and represents the time lag with which a region of simple exponential decay sets in.

Explicit expressions for Q_1 and τ_1 can be formulated in the case where the quantities A and B are very large compared to unity. This corresponds to the case where volumes V_a and V_b are much larger than the volume of the membrane given by Sl. And so the approximation $\tan Q_l = Q_l$ applied to eq. (4.17) yields with eq. (4.11)

$$Q_1^2 = kSl\frac{V_a + V_b}{V_a V_b} \tag{4.24}$$

Substitution of this equation into eq. (4.16) leads to

$$\tau_1 = \frac{V_a V_b l}{kS(V_a + V_b)D} \tag{4.25}$$

This expression for the relaxation time of the solute diffusion can be applied to compare the measurements of glucose diffusion with the diffusion cell and in the case of *in vitro* testing of the IGLUS demonstrator. The difference between these two cases is the geometry since in both cases the volumes are stirred.

4.8.5 Model extension

The present model can be extended to unstirred and/or semi-infinite volumes [143, 144]. The complexity of the transport of the solute at the interface solvent-membrane and inside the membrane can be increased by developing in more details the partition coefficient k [142]. The non-equilibrium thermodynamics in membranes is detailed by Staverman [145]. It is also possible to integrate the dynamic of the chemical reaction inside the sensor as done by Clark *et al.* [146].

4.9 Conclusion

In this chapter, we have presented the chemical and physical basis necessary to understand the use of a membrane, and exposed the requirements of the IGLUS for a SI. From this basis, we reviewed the different membrane technologies and selected two potential candidates for the IGLUS, the anodic alumina membranes and the polyethylene films. The properties and

structure of these two types of membranes were subsequently detailed. Finally, we presented a theoretical model for the transient diffusion of a solute through a membrane, which will be validated through experiments in the coming chapter (see section 5.3.2.A).

Chapter 5

Selective interface characterization

5.1 Introduction

As discussed in the main introduction (section 1.5), the purpose of characterizing membranes is to select the appropriate membrane for the IGLUS. We aim to provide simple tools to measure the important parameters necessary for the well functioning of the sensor. Following this thread, the first experiment performed was to measure the diffusivity of glucose. Next comes to measure the retention capabilities of each membrane for concanavalin A (ConA) and dextran. Dextran being much larger than ConA (see table 3.1), the retention of ConA is a priority and a tool was built for this purpose.

In order to measure the diffusivity of glucose through a membrane, we fabricated a diffusion cell which consists of two chambers separated by a membrane. The setup is detailed in section 5.3. The idea is to fill the two chambers with water, set glucose in one of the chambers and monitor the glucose concentration over time in the other one. The measurement of glucose concentration is an issue when dealing in the range of body concentrations (2-30 mM). Among different techniques, such as infrared spectroscopy, polarimetry, viscosity, density and reagent assay, refractometry turned out to be the most accurate (1.5 mM sensitivity, see section 5.2.1) and accessible. Refractometry is limited to determine the concentration variations of one species at a time, but on the other hand, the concentration variations of several species can be monitored. Therefore we also used this technique to measure dextran leakage.

The concentration measurement of proteins requires a more sensitive technique in order to detect small leakage through a membrane. We chose the UV absorption spectrometry as it is a simple and accessible technique. An enzymatic technique such as ELISA (Enzyme-Linked ImmunoSorbent

Assay) would be more sensitive but we have not found the specific procedure for ConA. We found a possible antibody, the anti-canavalia ensiformis lectin[1], but the process still needs to be established by specialists. Moreover the UV absorption spectroscopy is sufficient for a quick "yes or no" test for leakage of a protein and therefore we used it for retention measurements of ConA as well as bovine serum albumin.

ConA presents some solubility issues and the commercially available ConA is not pure. Therefore we used a test protein, the bovine serum albumin (BSA), because it is a standard for testing membrane selectivity in literature. BSA also presents the advantage to be stable over days and is commercially available with a high purity. The size of BSA is similar to the ConA dimers and smaller than the ConA tetramers, therefore its retention is representative of dimers and tetramers of ConA.

In the previous chapter, the reasons of the choice of an alumina membrane with a poly((polyethylene glycol) methacrylate) (PPEGMA) coating as a selective interface for the IGLUS (see section 4.5) have been revealed. Anodic alumina membranes with 20 nm pores have been purchased from Whatman and coated with PPEGMA. The selectivity (glucose diffusivity vs. protein retention capability) of these membranes has been studied and presented in this chapter. In order to compare this choice of interface with another technology, we characterized the selectivity of polyethylene (PE) membranes as they show the same coating ability and high chemical resistance. The PE membranes are not suited for the IGLUS sensor presented in this work but are envisioned for a future version with a tubular shape membrane.

5.2 Experimental techniques

5.2.1 Refractometry

Refractometry is the method of measuring the refractive index (rI) of a substance. The rI measurement is commonly used for the measurements of sugars concentrations in the food industry. The rI of a substance is strongly influenced by temperature and the wavelength of light used for measurement. Therefore rI measurements are reported at the reference temperature of 20°C and at the reference wavelength of 589.3 nm (the sodium D line). To perform the rI measurements, we used the high precision refractometer Bellingham+Stanley[2] RFM 342. This apparatus is shown in figure 5.1 and has a resolution of five digits and an accuracy of ± 0.00004, which corresponds to an accuracy of 1.5 mM of D-glucose. For high accuracy measurements, a drop as small as 60 μl is sufficient and placed on the refractometer

[1] http://www.sigmaaldrich.com/catalog/search/ProductDetail/SIGMA/C7401
[2] http://www.bs-ltd.com

Figure 5.1: Refractometer with five digits precision.

crystal for acquisition. In figure 5.2, the calibration curve for D-glucose is presented.

5.2.2 UV absorption spectrometry

Ultraviolet (UV) absorbance spectrometry is used to quantify the concentration of a protein. The UV light absorbance of proteins come from 3 sources: peptide bonds (190-220 nm), aromatic amino acids (250-295 nm) and prosthetic groups (Ca^{2+} and Mn^{2+} ions for ConA). Hence the nature of the protein cannot be determined but for a single protein solution the quantity can be determined. Our system allows measurements from 220 nm and above and therefore we detect the tyrosine (274 nm) and tryptophan (280 nm) aromatic amino acids because they are the most absorbing component of proteins[3].

We used an ultraviolet-visible (UV-Vis) light spectrometer and its configuration is shown in figure 5.3. The light source is a DT-MINI-2-GS with a deuterium bulb from Ocean Optics[4] and the spectrometer is a USB4000-UV-VIS from the same company. The UV light is transported via optical fibers in order to minimize losses and is collimated by quartz lenses through a UV micro-cuvette. We used the UV-Cuvette micro from Brand[5] with a ca-

[3]http://www.sci.sdsu.edu/TFrey/Bio750/UV-VisSpectroscopy.html
[4]http://www.oceanoptics.com
[5]http://www.brand.de

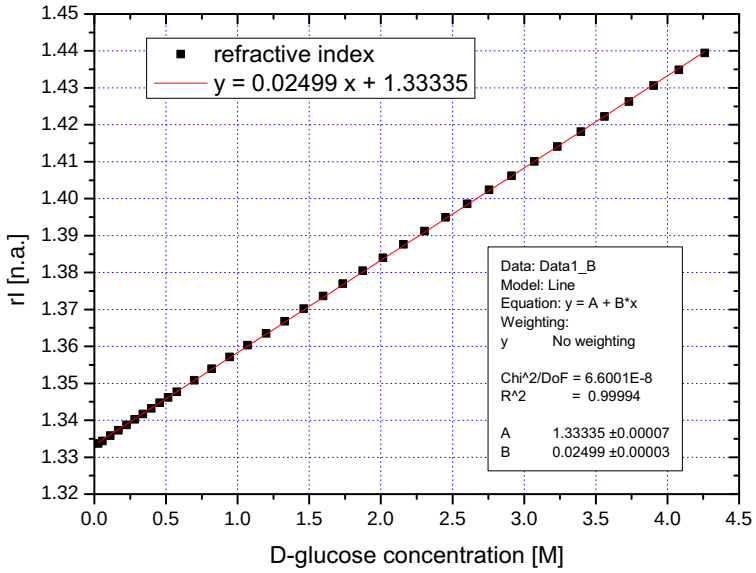

Figure 5.2: Calibration curve of the refractive index of D-glucose in deionized water, measured at the standard reference of 20°C and 589.3 nm wavelength.

pacity of 70 μl and a path length l_a of 10 mm, and the cuvette holder is home-made. The liquid to be measured is set in the cuvette and the spectrometer measures the intensity of the transmitted UV light. The technique requires a reference in order to measure the relative absorption. For all measurements, the reference has the same ionic and buffer solution as the one containing the protein.

The absorbance is measured as a function of the wavelength and is defined as

$$A(\lambda) = -\log_{10} \frac{I(\lambda)}{I_0(\lambda)} \tag{5.1}$$

where I is the transmitted intensity, I_0 the reference transmitted intensity and λ the wavelength.

The concentration of the protein or solute to be detected is calculated using the Beer-Lambert law

$$A = \epsilon C l_a \tag{5.2}$$

where ϵ is the molar absorptivity or molar extinction coefficient of the solute, C the concentration and l_a the path length. Another measure of the extinction coefficient is $E^{1\%}$ which gives the mass extinction coefficient. $E^{1\%}$ is the absorbance of a 1% solution by mass and has the units $\frac{l}{g \cdot cm}$. The conversion between ϵ and $E^{1\%}$ is $\epsilon = E^{1\%} \times MW$, MW being the molecular weight.

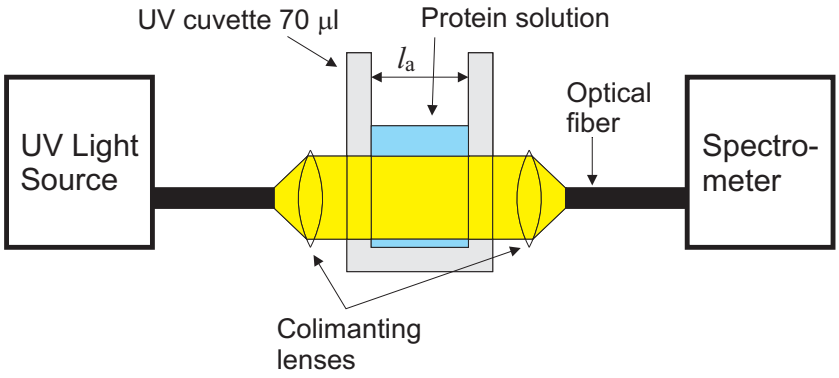

Figure 5.3: UV absorption spectrometry setup.

Figures 5.4 and 5.5 contain the calibration spectra and absorbance at 280 nm employed to determine the BSA and ConA concentrations respectively. The BSA was purchased from Sigma-Aldrich and the product number is A7906. The ConA was purchased from Sigma-Aldrich and the product number is Type IV C2010.

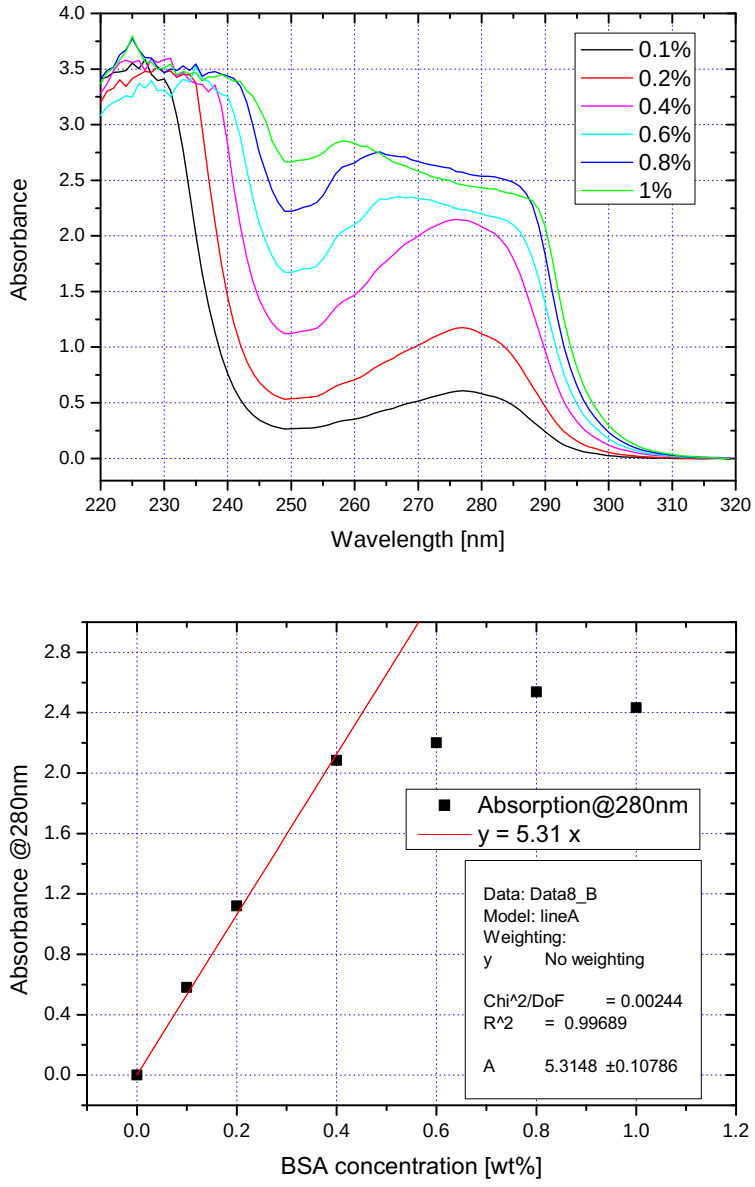

Figure 5.4: Calibration spectra of UV absorption and absorbance at 280 nm of BSA in 150 mM NaCl pH=7.0 at 25°C.

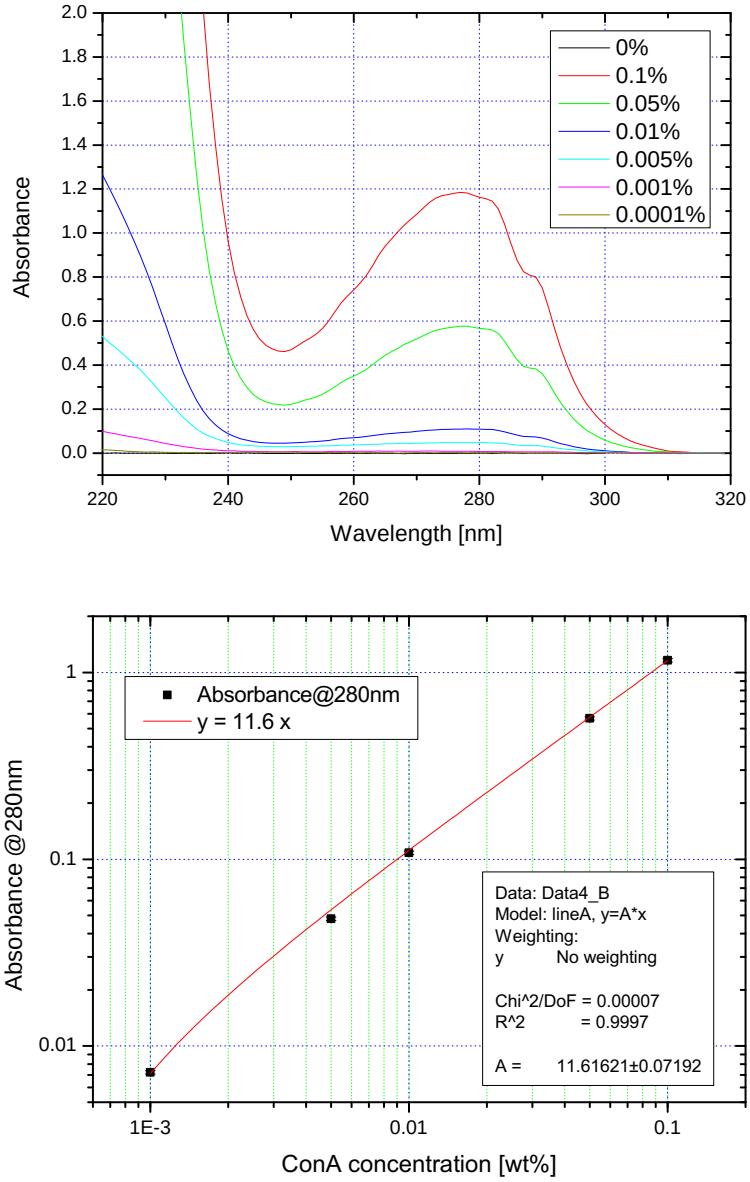

Figure 5.5: Calibration spectra of UV absorption and absorbance at 280 nm of ConA in 50 mM TrisHCl buffer pH=7.0 at 25°C.

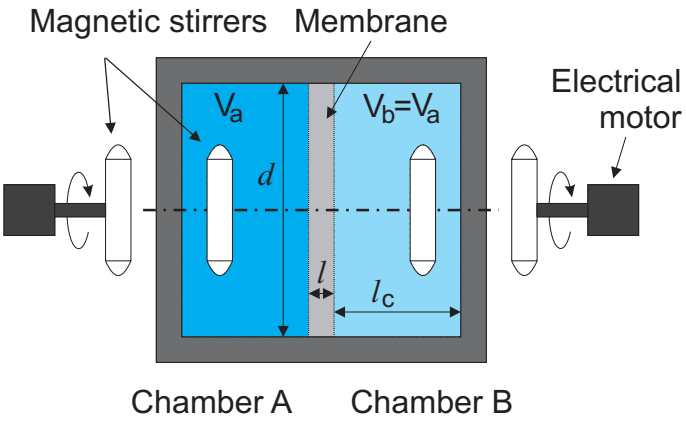

Figure 5.6: Diffusion cell configuration.

5.2.3 Diffusion cell

For diffusion measurements of D-glucose and retention tests of dextran, BSA and ConA, we used home-made diffusion cells. The setup configuration is shown in figure 5.6. The test cell has two compartments which are separated by the porous membrane to be characterized. A solution with a given concentration of the solute is set in chamber A and pure solvent in chamber B at the beginning of the experiment. Both chambers are well stirred by standard PTFE magnetic stirrers, and solute diffusion is monitored in the low concentration chamber by taking samples and measuring the solute concentration by either refractometry or UV absorption spectrometry.

We designed and fabricated three different types of cells with two equal volume chambers ($V_a = V_b$) of 393 μl, 785 μl and 1178 μl. They have been designed for 13 mm diameter disk membranes and all the chambers have an inner diameter of 10 mm but different length l_c of 5 mm, 10 mm and 15 mm respectively. Hereafter the cells are call by their chamber length, e.g. "15 mm cell". All cells are made of poly(methyl methacrylate) (PMMA) and the sealing between the chambers and the membrane is ensured by a silicone rubber ring of 50 Shore A.

5.3 Glucose diffusion

5.3.1 Experimental conditions

The glucose diffusion measurements were conducted in the diffusion cells described in section 5.2.3. A 100 mM D-glucose (in ultrapure water) solution and ultrapure water are put in the chambers A and B, respectively, at the beginning of each experiment. Both chambers are well stirred dur-

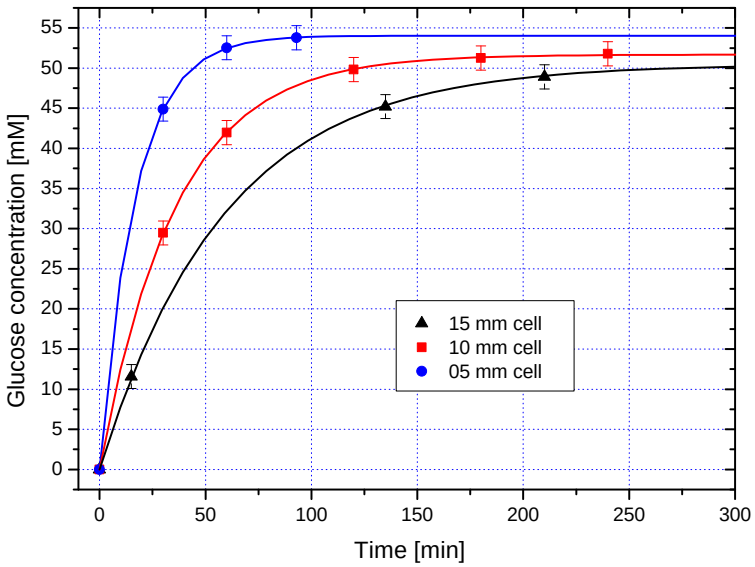

Figure 5.7: Comparison of glucose diffusion kinetics in three different cell sizes: l_c = 5 mm, 10 mm and 15 mm. A Whatman alumina 20 nm pores membrane was employed and the measurements were performed at 25°C.

ing the whole experiment. The glucose concentration of the liquid in the chamber B is measured by refractometry from time to time as described in section 5.2.1. The rI values are converted to glucose concentration values using the calibration curve of figure 5.2. We obtain a curve of the glucose concentration variation in chamber B as a function of time. The glucose diffusion measurements were performed at 25°C because it is a standard in literature and the diffusion coefficient can be easily extrapolated to the desired temperature using the Stokes-Einstein relation (see eq. (4.2)).

5.3.2 Results

5.3.2.A Assessment of the glucose diffusion setup

As the IGLUS requires, the glucose needs to diffuse through the membrane and this diffusivity has to be as fast as possible in order to minimize the response time of the sensor. It is thus important to understand the glucose diffusive properties of the selected membranes. We started by measuring the diffusivity on a non-coated Whatman anodic alumina 20 nm pores membrane and compared the results obtained in the three diffusion cell sizes, as shown in figure 5.7. This experiment was a validation of our method in relation with the diffusion theory exposed in section 4.8.

From the resulting curves of the diffusion measurements, we can extract

Table 5.1: Effective diffusivities D_e of glucose in a Whatman alumina 20 nm non-coated membrane measured in 5 mm, 10 mm and 15 mm diffusion cells at 25°C.

Diffusion cell	$\tau_1\ [min]$	$D_e\ [\frac{mm^2}{s}]$
05 mm cell	16.9 ± 0.1	$1.25 \pm 0.04 \times 10^{-04}$
10 mm cell	35.7 ± 0.2	$1.29 \pm 0.08 \times 10^{-04}$
15 mm cell	59.0 ± 0.8	$1.21 \pm 0.17 \times 10^{-04}$

the relaxation time τ_1 by fitting the data with the relation

$$\Delta c(t) = \Delta c(0) \exp\left(-\frac{t}{\tau_1}\right) \tag{5.3}$$

which corresponds to eq. (4.22) without the transition term θ which is negligible. In the case of our diffusion cell, eq. (4.25) is adapted with the following simplifications

$$\begin{aligned} V_a = V_b &= V \\ V &= Sl_c \end{aligned} \tag{5.4}$$

and becomes

$$\tau_1 = \frac{Vl}{2SD_e} = \frac{l_c l}{2D_e} \tag{5.5}$$

where l_c is the length of diffusion cell chambers, l the membrane thickness and D_e is the parameter commonly used in the literature to express the effective diffusivity of a solute in a membrane [109]. From eq. (5.5), we can express D_e as a function of the geometric parameters

$$D_e = \frac{l_c l}{2\tau_1} \tag{5.6}$$

The effective diffusivity D_e is nothing more than the contraction of $k \cdot D$ and therefore includes the interaction processes between the solute and the membrane and the porosity of the membrane.

The results of processing the measurements from figure 5.7 are given in table 5.1. We observe that the effective diffusivity of glucose is the same when measured in the three different cell sizes. D_e being an intrinsic parameter of the membrane, it must be independent on the cell geometry. This result demonstrate the validity of the experimental setup and the accordance of the results with the theory.

The obtained effective diffusivity D_e of glucose can be compared to its diffusion coefficient in water $D = 6.8 \cdot 10^{-4} \frac{mm^2}{s}$ [147] knowing that the porosity of the membrane is $\phi = 0.37$ [20]. By combination of eq. (4.7) and the definition of D_e, we get

$$D_e = K\phi \frac{v_0}{v} D \tag{5.7}$$

Table 5.2: Effective diffusivities D_e of glucose through PPEGMA coated Whatman alumina 20 nm with different thicknesses of coating expressed in polymerization time. Measurements performed in a 15 mm diffusion cell at 25°C.

Membrane	Coating	$\tau_1\ [min]$	$D_e\ [\frac{mm^2}{s}]$
WA20-NC	non-coated	59.4 ± 1.8	$1.20 \pm 0.36 \times 10^{-04}$
WA20-10-1	coated 10 min	41.9 ± 1.4	$1.70 \pm 0.57 \times 10^{-04}$
WA20-20-1	coated 20 min	57.4 ± 1.8	$1.24 \pm 0.39 \times 10^{-04}$
WA20-30-1	coated 30 min	61.3 ± 2.3	$1.16 \pm 0.43 \times 10^{-04}$
WA20-40-1	coated 40 min	76.2 ± 2.2	$0.93 \pm 0.26 \times 10^{-04}$
WA20-60-1	coated 60 min	133.0 ± 3.1	$0.54 \pm 0.13 \times 10^{-04}$

We can extract the unknown factor coming from the chemical interactions between the non-coated membrane (alumina), the solvent (water) and glucose

$$K\frac{v_0}{v} = \frac{1}{2} \tag{5.8}$$

which expresses the reduction of the diffusion coefficient in the membrane pores compared to bulk water. We can then calculate D_m the modified diffusion coefficient of glucose in the non-coated membrane

$$D_m = K\frac{v_0}{v}D = \frac{D_e}{\phi} = 3.4 \times 10^{-04}\,\frac{mm^2}{s} \tag{5.9}$$

5.3.2.B Diffusivity through PPEGMA coated alumina membranes

We now present the results obtained for Whatman 20 nm alumina membranes coated with different thicknesses of PPEGMA. The diffusion curves are shown in figure 5.8 and the calculated effective diffusivities are given in table 5.2. The different coated membranes are compared using the effective diffusivity D_e because the porosity and chemical interactions are modified by the PPEGMA coating and only D_e is important for the IGLUS response time. The thickness of the coating is expressed with the polymerization time as we have not been able to establish a direct link between thickness and polymerization time. The current issues are the non reproducible coating process and the impossibility to measure the coating thickness by ellipsometry.

The nomenclature of the alumina coated membranes has the form WA20-XX-Y, where WA20 stands for Whatman alumina 20 nm, XX for the coating polymerization time in minutes and Y for the version number. Refer to appendix B for alternative nomenclature.

We observe that the effective diffusivity is increased with a very thin coating (10 min) and then decreases as the thickness increases. This was

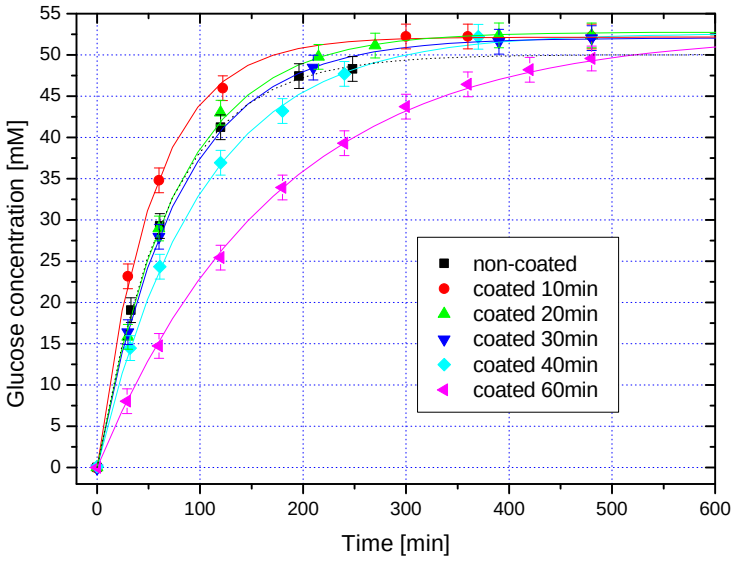

Figure 5.8: Diffusion curves of glucose through PPEGMA coated Whatman alumina 20 nm with different thicknesses of coating expressed in polymerization time. Measurements performed in a 15 mm cell at 25°C.

expected since the coating fills the pores as it grows. The explanation for the increase of diffusivity with a thin coating is the modification of the factor $K\frac{v_0}{v}$ as we can expect that the chemical interaction between the glucose and the coating are different than between glucose and alumina.

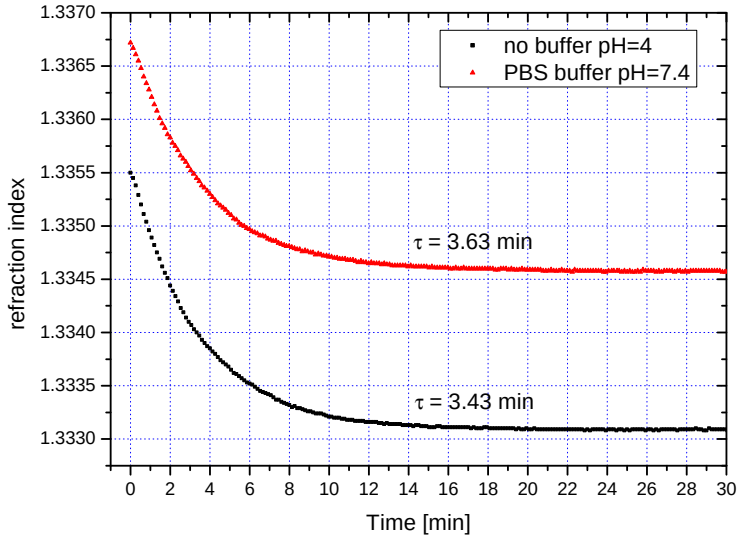

Figure 5.9: Diffusion curves of glucose through PPEGMA coated Whatman alumina 20 nm at pH = 4 and 7.4. The pH has no influence on the diffusion speed. This measurement was performed using an automated measurement of the rI.

5.3.2.C Neutrality of the PPEGMA coating

The PPEGMA coating is supposed to be neutral because PEG, which is at the surface of PPEGMA, is known to be neutral [148, 149]. The non-neutrality can have an effect on the swelling of the coating. In order to check the neutrality of the coating and to verify that the effective diffusivity of glucose is not modified, we performed diffusion measurements at pH=4 and 7.4, the first value being the pH of 100 mM D-glucose in ultrapure water, and the second value being the physiological pH. The curves are shown in figure 5.9 and the result is that the glucose diffusivity is not influenced by the pH. We conclude that the coating is neutral and its swelling by water absorption is not affected by the pH. Hence, the solutions used in the diffusion cells for glucose diffusion measurements do not always need to be buffered at pH=7.4, and a simple solution of D-glucose in ultrapure water can be used.

5.3.2.D Diffusivity in PE membranes

As discussed in the beginning of the chapter (see section 5.1), we also characterized polyethylene (PE) membranes as an alternative technology and as a comparison to the alumina membranes. The nomenclature of the PE films has the form PE-XX-YY, where PE stands for polyethylene, XX for the thickness in μm and YY for the etching time. Refer to appendix B for alter-

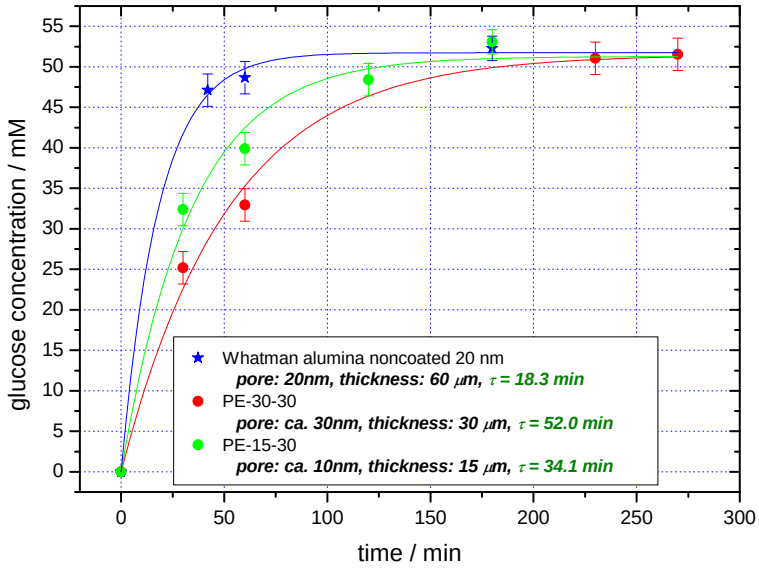

Figure 5.10: Comparison of Whatman alumina non-coated 20 nm pores and PE 30 nm pores membranes. Glucose diffusion measurement were performed in a 5 mm cell at 25°C.

Table 5.3: Comparison of effective diffusivities D_e of glucose in Whatman alumina non-coated 20 nm pores and PE 30 nm pores membranes. Measurements performed in a 5 mm diffusion cell at 25°C.

Membrane	$\tau_1\ [min]$	$D_e\ [\frac{mm^2}{s}]$
WA20-NC	18.3 ± 2.0	$1.16 \pm 0.13 \times 10^{-04}$
PE-30-30	52.0 ± 5.2	$0.102 \pm 0.010 \times 10^{-04}$
PE-15-30	34.1 ± 4.8	$0.311 \pm 0.044 \times 10^{-04}$

native nomenclature. The glucose diffusion curves are shown in figure 5.10 and the calculated effective diffusivities are given in table 5.3. The two PE membranes exhibit low diffusivities of glucose and the reason comes from their structure. The PE membranes are symmetrical (one layer) and have 30 nm pores through the whole thickness of 30 μm. The alumina membrane has the advantage of being asymmetrical and the layer with 20 nm pores is only 1 μm thick. Moreover the high tortuosity of the PE membrane compared to the alumina membrane contributes to its low glucose effective diffusivity.

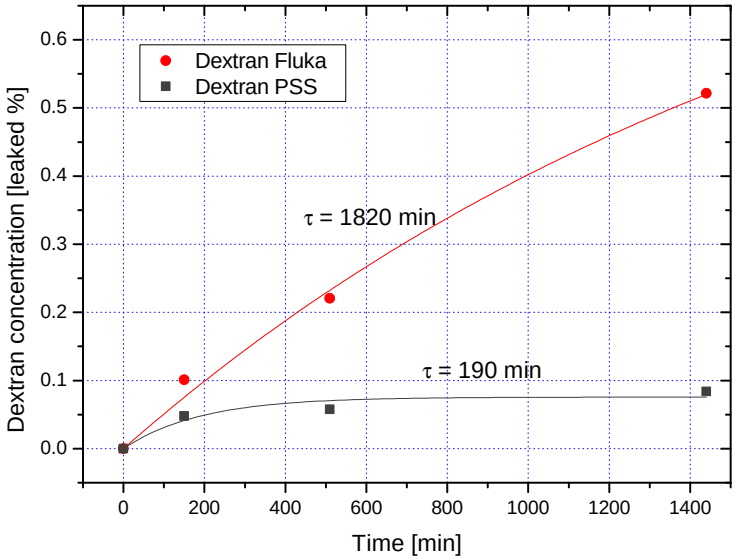

Figure 5.11: Leakage comparison of dextrans from Fluka and PSS through a Whatman alumina non-coated 20 nm pores membrane. Diffusion measurements were performed in a 5 mm cell at 25°C and dextran concentrations were monitored by refractometry.

5.4 Dextran retention

The hydrodynamic radius of 2000 kDa dextran (27 nm) is bigger than the pore radius (10 nm) of the non-coated alumina membranes. Therefore it is expected to be retained by the membrane. The dextran sold by Fluka is however polydisperse in size and contains a lot of smaller fractions. The leakage of the smaller molecules of dextran out of the membrane will result in an instability of the SF viscosity in the IGLUS. We measured the partial leakage of the Fluka dextran through a non-coated Whatman alumina membrane and compared with the purified dextran 3200 kDa obtained from PSS (see section 3.4.2.B). The results shown in figure 5.11 demonstrate a clear leakage of the Fluka dextran whilst the dextran from PSS exhibit a limited leakage. The dextran from PSS is retained by the non-coated alumina membrane and therefore is the appropriate candidate for the sensitive fluid in order to obtain a long term stability of the sensor. In the next chapter, we demonstrate the efficiency of the PSS dextran in the IGLUS demonstrator.

5.5 Albumin retention

5.5.1 Experimental description

The basic concept of the test cell is the same as the one for the glucose diffusion test. A 1%-BSA solution with 150 mM NaCl (pH=7) and 150 mM NaCl solution are put in the chambers A and B, respectively. The liquid in the chamber B is measured with UV spectroscopy, as described in section 5.2.2, in order to quantify the leakage of BSA. Both chambers of the cell are well stirred and the test is conducted over 48 hours. As a reminder, the BSA has a MW of 66 kDa, a size of $4 \times 4 \times 14$ nm^3 and was purchased from Sigma-Aldrich (product No. A7906). The measurements were performed at 25°C for convenience since the temperature only modifies the diffusion coefficient of the protein but not the total retention capability of the selective interface.

5.5.2 Results

We measured the BSA retention ability of the PPEGMA coated alumina membranes that were previously tested for glucose diffusivity. In figure 5.12 we show diffusion curves of BSA through a non-coated alumina membrane and two PPEGMA coated membranes, one with a thin coating and one with a thicker coating. The 60 min coated membrane exhibited a complete retention of BSA over 48h. The BSA diffusivity in the membrane with the thin coating is also higher than in the non-coated membrane as observed for glucose, and this can be attributed to the same reason, i.e. a modification of the factor $K\frac{v_0}{v}$.

We conducted BSA retention test on alumina membranes with different PPEGMA coating thicknesses and compared with their effective glucose diffusivity presented previously. The results of the BSA retention compared to the glucose diffusivity are given in table 5.4 and we observed that there is a relation between the effective diffusivity D_e of glucose and the retention ability of BSA.

The link between the glucose diffusivity and the BSA retention for PPEGMA coated alumina membranes was further investigated by conducting tests on other coated membranes with the aim to find the optimal coating thickness. Knowing that the transition from non-retention to retention occurs around 40 min of polymerization time, a series of membranes with this polymerization time were prepared, the WA20-40-Y series. The first observation was that, for this series of 13 membranes coated in the same conditions and polymerization time, the measured glucose diffusivities are very different from one membrane to the other. This clearly showed the non-reproducibility of the coating process and therefore we decided to set

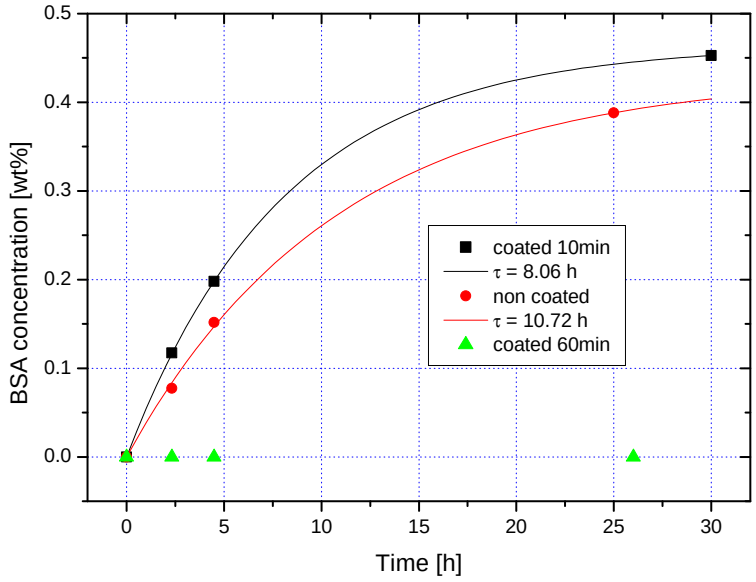

Figure 5.12: Retention of BSA by increasing the PPEGMA coating thickness on a Whatman alumina membrane with 20nm pores.

Table 5.4: Comparison of BSA retention and diffusivity of glucose through Whatman 20 nm membranes coated with different PPEGMA thicknesses.

Polymerization time [min]	Albumin retention	D_e glucose $[\frac{mm^2}{s}]$
0	leaks	$1.20 \pm 0.36 \times 10^{-04}$
10	leaks	$1.70 \pm 0.57 \times 10^{-04}$
20	leaks	$1.24 \pm 0.39 \times 10^{-04}$
30	leaks	$1.16 \pm 0.43 \times 10^{-04}$
40	retained	$0.93 \pm 0.26 \times 10^{-04}$
60	retained	$0.54 \pm 0.13 \times 10^{-04}$
180	retained	retained

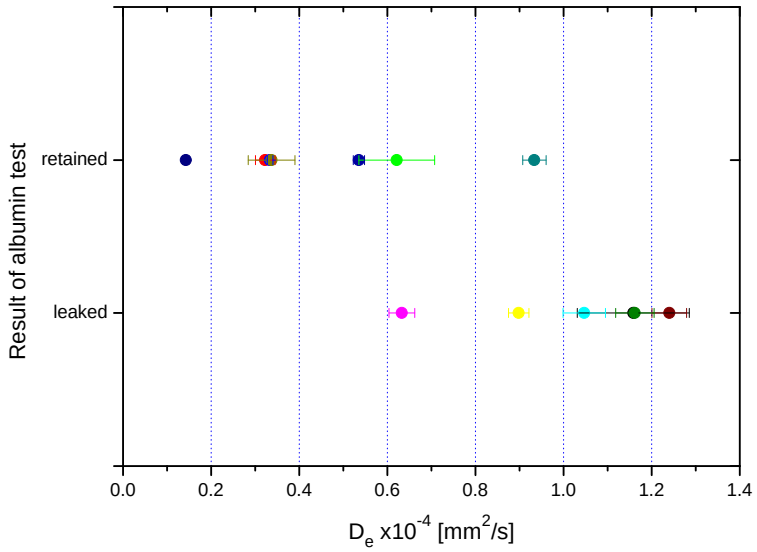

Figure 5.13: Retention of BSA as a function of glucose effective diffusivity. The albumin retention of PPEGMA coated Whatman 20 nm alumina membrane can thus be determined by glucose diffusion kinetics.

the glucose effective diffusivity value as the measure for the coating thickness, and also the protein retention capability. The result obtained with the WA20-40-Y series are presented in figure 5.13 and table 5.5. The first outcome is the confirmation of the results obtained with the first coated membrane series where a transition from non-retention to retention of BSA is observed when the glucose effective diffusivity D_e decreases. More specifically, the transition occurs for D_e values between 0.6 and $1 \cdot 10^{-4}$ $\frac{mm^2}{s}$.

The PE films (membranes), described in section 4.7, have also been tested for BSA retention and the results are presented in table 5.6. We observed that BSA retention is obtained with 15 μm thick films, but at the cost of very low effective diffusivity of glucose. The two films that retained BSA, PE-15-05 and PE-15-10, have short etching time of 5 and 10 min respectively, and therefore exhibit a low porosity. This is a promising result knowing that thinner film with smaller pores and greater porosity can be prepared. The last PE film in table 5.6, PE-15-60, has been etched for 60 min, and neither glucose nor BSA could diffuse through the film. In fact the inner structure of the film collapsed because of the excess of etching.

Table 5.5: Comparison of BSA retention and diffusivity of glucose through Whatman 20 nm membranes PPEGMA coated, 40 min polymerization time. The effective coating thickness varies for the same preparation conditions.

Name	D_e glucose $\times 10^{-4}$ $[\frac{mm^2}{s}]$	albumin test
WA20-40-2	1.70 ± 0.06	leaked
WA20-40-3	1.24 ± 0.04	leaked
WA20-40-4	1.16 ± 0.04	leaked
non-coated	1.16 ± 0.13	leaked
WA20-40-5	1.05 ± 0.05	leaked
WA20-40-1	0.934 ± 0.026	retained
WA20-40-7	0.898 ± 0.023	leaked
WA20-40-8	0.633 ± 0.029	leaked
WA20-40-9	0.621 ± 0.086	retained
WA20-40-10	0.535 ± 0.013	retained
WA20-40-11	0.337 ± 0.053	retained
WA20-40-12	0.334 ± 0.007	retained
WA20-40-13	0.323 ± 0.022	retained
WA20-40-14	0.143 ± 0.006	retained

Table 5.6: Comparison of BSA retention and glucose diffusivity through PE membranes with different pore size and thickness.

Film name	Pore size [nm]	Thickness [μm]	D_e glucose $\times 10^{-4}$ $[\frac{mm^2}{s}]$	Albumin test
PE-30-20	<30	30	0.113 ± 0.021	leaked
PE-30-30	*ca.* 30	30	0.204 ± 0.020	leaked
PE-30-40	>30	30	0.357 ± 0.033	leaked
PE-15-05	<10	15	0.0263 ± 0.0013	retained
PE-15-10	*ca.* 10	15	0.0270 ± 0.0005	retained
PE-15-30	>10	15	0.311 ± 0.044	leaked
PE-15-60	collapsed	15	retained	retained

5.6 ConA retention

5.6.1 Experimental description

For ConA retention tests, we used the same test bench as for albumin retention, i.e. diffusion cells and UV absorption spectrometry. ConA presents the disadvantage to be unstable without the presence of dextran. In fact we observed its precipitation after a few hours at room temperature in a solution with the same ionic composition as the SF. The presence of dextran or PEG [150] increases the solubility of ConA. The purpose being to evaluate the ability of a membrane to retain ConA in similar conditions to the IGLUS, we conducted the ConA retention tests with the sensitive fluid SF36F. Hence the diffusion cell was filled with SF36F in chamber A and filled with reference solution (RS) in chamber B. A 15 mm cell was employed and the operating temperature was 37°C.

5.6.2 Results

Knowing that PPEGMA coated alumina membranes retain BSA for effective diffusivities of glucose below $0.6 \cdot 10^{-4}\ \frac{mm^2}{s}$, we conducted the ConA retention tests on two membranes (WA20-80-1 and WA20-160-1) with D_e values about $0.4 \cdot 10^{-4}\ \frac{mm^2}{s}$. At pH = 7.4, as it is the case for SF36F, the ConA is mainly in tetramer form (104 kDa) and a small portion in dimer form (52 kDa) as detailed in section 3.4. The MW of BSA being 67 kDa and both proteins being globular, we expected the two selected membranes to retain ConA. In figure 5.14 we show the diffusion comparison at 37°C of BSA and ConA through a non-coated membrane and the coated WA20-80-1.

The reduced diffusivity of ConA compared to BSA through the non-coated alumina membrane is caused by three reasons: the ConA tetramers are bigger than BSA, the higher viscosity of SF36F reduces the diffusion coefficient of ConA, and at low glucose concentration the ConA is bound to dextran. In order to minimize the two last effects, we also conducted ConA retention tests with SF36F containing 30 mM glucose where most of ConA is unbound from dextran. The difference of ConA leakage through non-coated alumina membranes with 2 mM and 30 mM glucose is clearly seen in figure 5.14.

The coated membranes WA20-80-1 and WA20-160-1 both exhibit a small leakage of ConA when tested with 30 mM glucose SF36F. The UV absorption spectra are shown in figure 5.15. The spectra are noisy because we are at the limit of the sensitivity of the technique. Considering this small leakage of ConA, we calculated the relaxation time τ_1 of this leakage using eq. (4.22) and extrapolated the results for the geometry of the IGLUS

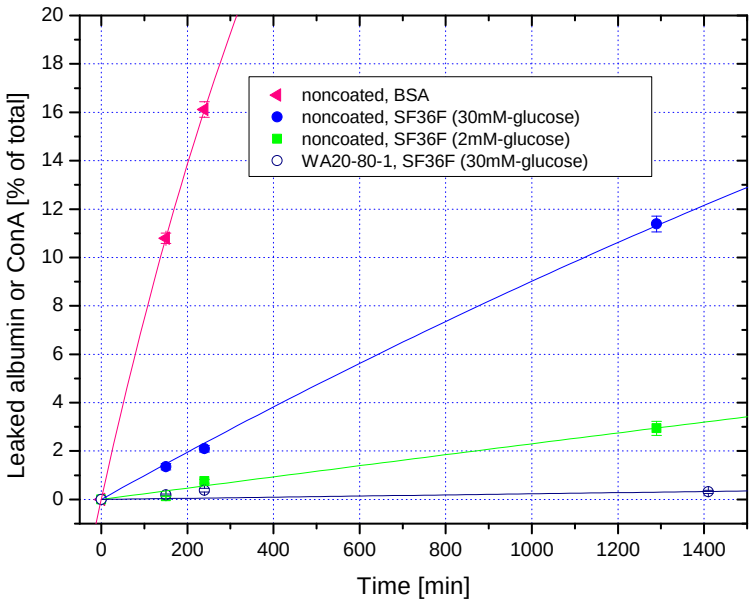

Figure 5.14: Comparison of leakage behaviors of ConA and BSA through a non-coated and a PPEGMA coated 20 nm alumina membrane. The solution containing ConA is SF36F which contains either 2 mM or 30 mM of glucose. The diffusion measurements were conducted in 15 mm diffusion cell at 37°C.

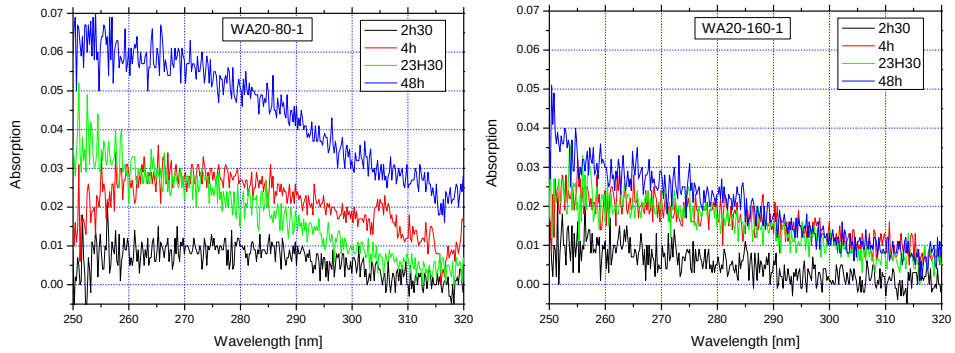

Figure 5.15: UV absorption spectra showing the ConA leakage through PPEGMA coated Whatman 20 nm alumina membranes.

Table 5.7: Relaxation times of ConA leakage for two PPEGMA coated alumina membranes. τ_{cell} is the relaxation time in the diffusion cell and τ_{sensor} is the extrapolated relaxation time for the IGLUS demonstrator.

Name	τ_{cell} [day]	τ_{sensor} [day]	D_e glucose $\times 10^{-4}$ $[\frac{mm^2}{s}]$
WA20-80-1	192 ± 42	34 ± 7	0.439 ± 0.010
WA20-160-1	380 ± 93	67 ± 16	0.395 ± 0.007

demonstrator using eq. (4.25). The results are shown in table 5.7.

The coated alumina membranes showed a good retention over time. The leakage of ConA might be dominated by the leakage of the fragments and some of the fragments may not be detected by UV absorption spectroscopy. This is the case if they do not contain the Tyr amino acid. Tyr is the only amino acid in ConA which absorbs at 280 nm because it is the only amino acid in the ConA sequence to have an aromatic group.

5.7 Fouling

We tested the modification of glucose effective diffusivity through three different PPEGMA coated alumina membranes because a decrease would be the main issue that fouling can cause regarding the functioning of the IGLUS sensor. The coated membrane has been dipped in SF24P for 1 week and no detectable alteration of the effective diffusivity was observed. This result is not further discussed because the study is underway and results will be presented in a later work. Meanwhile no similar experiment using the same hybrid membrane was found in literature. We estimate that the fouling is minimal and that the membrane performance is adapted for a use on the IGLUS demonstrator for at least one week.

5.8 Discussion

5.8.1 PPEGMA coated alumina membranes

Compared to polymer membranes, which are the most widely used membranes for protein separation, the anodic alumina membranes exhibit an ideal structure for fast glucose diffusivity. The straight pores and important porosity (37% for Whatman Anopore 20 nm) are the cause of these performances. It was expected that pores of 20 nm were too big to retain our test protein BSA of 67 kDa. However the strategy of pore-narrowing with the PPEGMA coating, developed in the laboratory of Prof. Dr. Harm-Anton Klok, revealed itself to be efficient, since we demonstrated the completed retention of BSA over 48h in a diffusion cell. We were also able to make a link between the BSA retention ability and the effective diffusivity of glucose. A measure of the PPEGMA coating thickness would be better to control and tune the selectivity of the alumina coated membranes. For this purpose, we would need to master the the polymerization process of the PPEGMA brushes on an alumina membrane in order to prepare membranes with a desired and precise coating thickness. As mentioned previously, a direct measurement of the hydrated thickness of the PPEGMA coating, at least inside the pores, is not achieved at present. At present, reasons for non-reproducibility of the coating thickness with respect to the polymerization time are being investigated but are beyond the scope of this thesis. However one possible reason is the heterogeneity of the surface roughness and chemistry among the purchased alumina membranes, as revealed by a study on anodic alumina [151]. Therefore the measurement of the effective diffusivity of glucose remains the best alternative. Moreover it gives a direct information on the response time of the IGLUS demonstrator functioning with such membranes.

The BSA/glucose selective properties of PPEGMA coated alumina membranes, combined to the low fouling property seem to be a novel result which we have not found in literature. Although we found articles treating either the membrane fouling reduction with a coating, or the tuned selectivity with a coating, but no results were found gathering the both properties in a single membrane. Below, some results of four interesting papers [152, 109, 20, 153] are reviewed, by chronological order, as a comparison to our results.

The first paper is the work of Kapur *et al.* [152]. Their main result is the reduction of protein diffusion (BSA) through a gel-filled pore membrane. They achieved a shut-down of the BSA diffusion by increasing the density of a polyacrylamide (PA) gel in poly(vinylidine fluoride) membrane with 0.22 μm pores. They also showed a diminution of the glucose diffusivity by a factor of 2 when BSA retention is obtained, which is the same ratio obtained in our case. Indeed we measured a glucose effective diffu-

sivity of $0.6 \cdot 10^{-4} \frac{mm^2}{s}$ for BSA retentive membranes whereas we have $1.2 \cdot 10^{-4} \frac{mm^2}{s}$ for the non-coated membrane. The fouling of such membranes has not been studied and the PA gel would not be an appropriate choice for anti-biofouling.

The second comparison is with the study of Praveen *et al.* [109], which showed that glucose can diffuse through a hyaluronic acid (HA) coating with a loss of only 1/3 in diffusivity (i.e. 2/3 of original diffusivity in polyvinyl alcohol (PVA) membrane). The thickness and density of the coating are not controlled and the coating thickness is about 400 μm, which would give rise to a huge response time if applied on a sensor. Nothing about selectivity or protein retention is treated. Nonetheless HA is known to be effective for anti-biofouling and is an alternative to PPEGMA, as discussed in section 3.5.

The third one is the study of Lee *et al.* [20] since the same alumina membrane was used (Whatman 20 nm). They grafted PEG on the surface but their results is limited to a good reduction of BSA adsorption. They also measured a reduction of diffusivity of ovalbumin but no protein retention or selectivity is observed.

The last comparison is to the work of Asatekin *et al.* [153]. An ultrafiltration polyvinylidene fluoride (PVDF) membrane was coated with PEGMA and they observed a reduction of biofouling by BSA, sodium alginate and humic acid by water permeability measurements. Though no information is given on small solutes diffusivity and protein retention, this work clearly shows that PEGMA coating is effective for biofouling reduction.

An ultimate topic to be discussed about our selective interface is the ConA retention. Our results have not concluded with a complete retention of ConA. However we showed that the leakage is very slow (see table 5.7) for membrane with D_e of about $0.4 \cdot 10^{-4} \frac{mm^2}{s}$. Since this value was lower than the one necessary for BSA retention, we expect a successful retention of ConA because the ConA dimers have similar MW to BSA and both are globular proteins. We believe that dimers and tetramers of ConA were retained and that only smaller fragments of the protein leaked through the membrane. Wang *et al.* [83] demonstrated that ConA, obtained with the very same method, contains different fragments. Therefore we performed MALDI (Matrix-Assisted Laser Desorption/Ionization) mass spectrometry of the ConA we used and observed fragments with similar sizes than in the work of Wang. The resulted spectrum is given in figure 5.16. The structure and activity of the fragments are unknown but it is believed that the fragments aggregate to the intact proteins and have a relative activity concerning glucose binding. Therefore we believe that our selective membrane retains the intact units of ConA and that the leakage of the fragments is sufficiently slow in order to use the membrane as an interface on the IGLUS demonstrator with a stable signal over 48h *in vitro*.

As a comparison to ConA, we also performed MALDI mass spectrometry of the BSA used for the retention test, as is shown in figure 5.16. We determined a good purity of the BSA since no fragments were observed. This result confirms the relevancy of BSA as a test protein.

5.8.2 PE films

The studied nanoporous PE films exhibit promising selective properties but the effective diffusivity of glucose is still low compared to coated alumina membranes. BSA retention could be observed with films prepared with a short etching time but at the cost of a very low glucose diffusivity. Nonetheless we have to consider that this technology is new and that it was the first time that such membranes were tested for glucose/BSA selectivity. In order for these films to create a good selective interface for an implantable sensor, an anti-fouling coating needs to be added. Besides, to function in particular on the IGLUS, a rigid support is required.

5.8.3 The ideal selective interface

The ideal selective interface would combine the selective property of small pores (steric) and the anti-non-specific protein adhesion properties of a thin and very dense coating. The necessary selectivity can be obtained by steric and/or electrostatic repulsion, however a charged membrane seems to be efficient only for specific selectivity but not for preventing non-specific adhesion of proteins. Therefore a very thin and dense (high grafting density) coating is effective for preventing non-specific adhesion of proteins [149].

5.9 Conclusion

We have characterized both selected SIs: the hybrid nanoporous alumina-PPEGMA membrane with reduced fouling properties and the nanoporous PE films, with respect to the requirements of the IGLUS. The selectivity of the PPEGMA coated 20 nm pores alumina membrane was shown for the BSA-glucose couple over 48 hours. The ConA from Sigma being not pure, we were not able to prove the complete retention of ConA, though we believe that ConA dimers and tetramers are retained by our membrane with a sufficiently thick coating. As long as we cannot produce a sensitive fluid containing purified ConA, the long term retention of ConA cannot be proved in diffusion cells using UV absorption spectroscopy.

PE films have been studied as an alternative technology with which non flat selective interface could be designed. The BSA retention was shown for small enough pore size but the glucose diffusivity remains too slow.

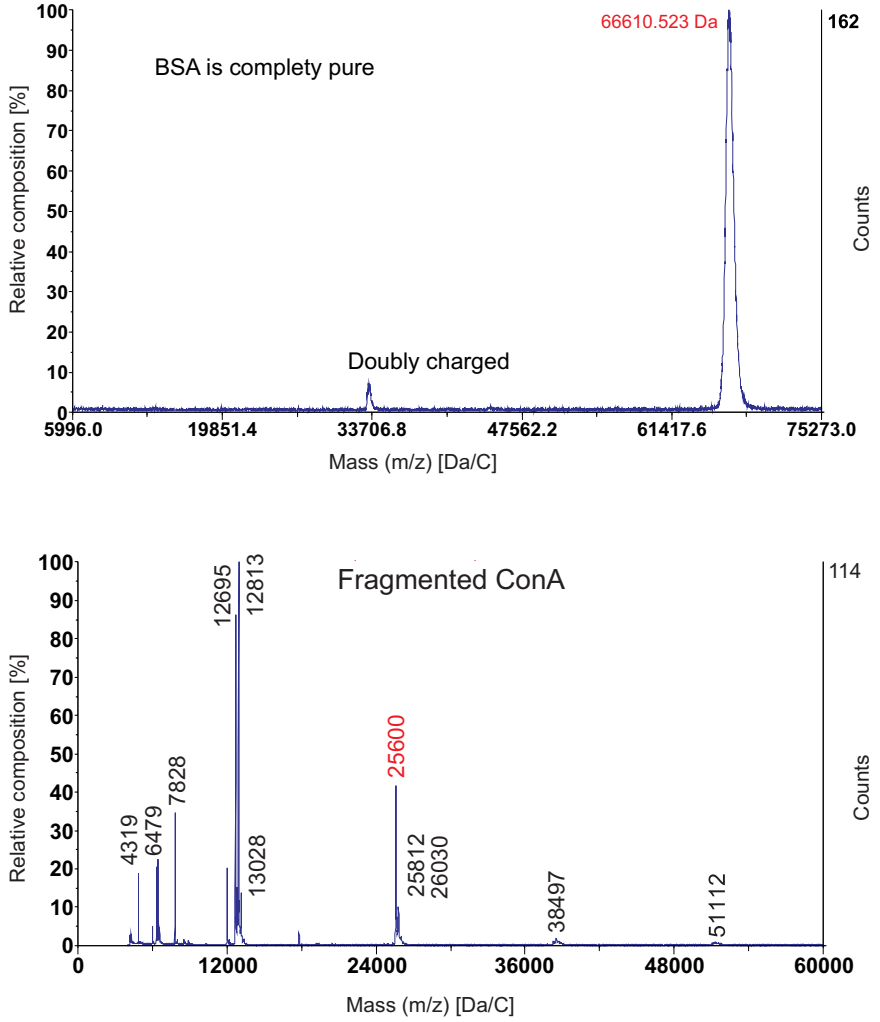

Figure 5.16: MALDI mass spectra, obtained with a ABI 4800 MALDI TOF/TOF Analyzer, of BSA A7906 and ConA C2010 from Sigma. The BSA protein is pure and its MW is 66.6 kDa. The ConA exhibits many frements and the intact units have a MW of 25.6 kDa.

Thinner films coupled to a rigid support should be designed in order to suit the IGLUS. We believe that further developments could lead to a success.

5.10 Outlook

The actual selective interface still needs to be improved. As discussed previously, a better support would be a membrane having a selective layer with smaller pores. A pore size of 3-5 nm and a thin coating would create an efficient selective interface. Recently, alumina membranes with pores down to 5 nm have been achieved. We tested an alumina membrane from Synkera with 5-7 nm pores and BSA was retained. However the quality of these membranes needs to be improved as they are too brittle and exhibit a poor porosity. Nevertheless we can expect further improvement in the near future because of the commercial need for such membranes in other fields.

Chapter 6

Selective interface on the IGLUS

6.1 Introduction

The selective interface (SI), resulting from the combination of an alumina membrane and the PPEGMA coating, gave good results in terms of molecular selectivity in the diffusion cells. In this chapter, we present the integration of the SI on a newer version of an IGLUS demonstrator developed in the scope of this work. The forthcoming experiments allowed us to assess the SI in *in vitro* conditions.

We present the improved version of the IGLUS demonstrator and the preparation and integration of the SI, as well as the setup used for the *in vitro* experimentations. Next, we present and discuss the *in vitro* results obtained using the WA20-80-2 and WA20-80-3 SIs. These interfaces are nanoporous alumina-PPEGMA hybrid membranes (refer to section 5.3.2.B for nomenclature).

6.2 IGLUS demonstrator improvements

As presented in chapter 3.2, the microviscometer and the acquisition system were studied in a previous work [22]. The IGLUS demonstrator used in this work has been redesigned taking into account requirements issued from the implementation of the SI. An exploded and a detailed views of the newer demonstrator are presented in figure 6.1. The complete CAD drawings are in the appendix C.

The exploded view of figure 6.1 shows the different parts of the demonstrator. The housing is made of PMMA and is watertightly sealed with an O-ring. The rotor is based on a Samarium-cobalt ($SmCo_5$) cylindrical magnet, and at both ends a disc of brass is glued which holds the stainless steel

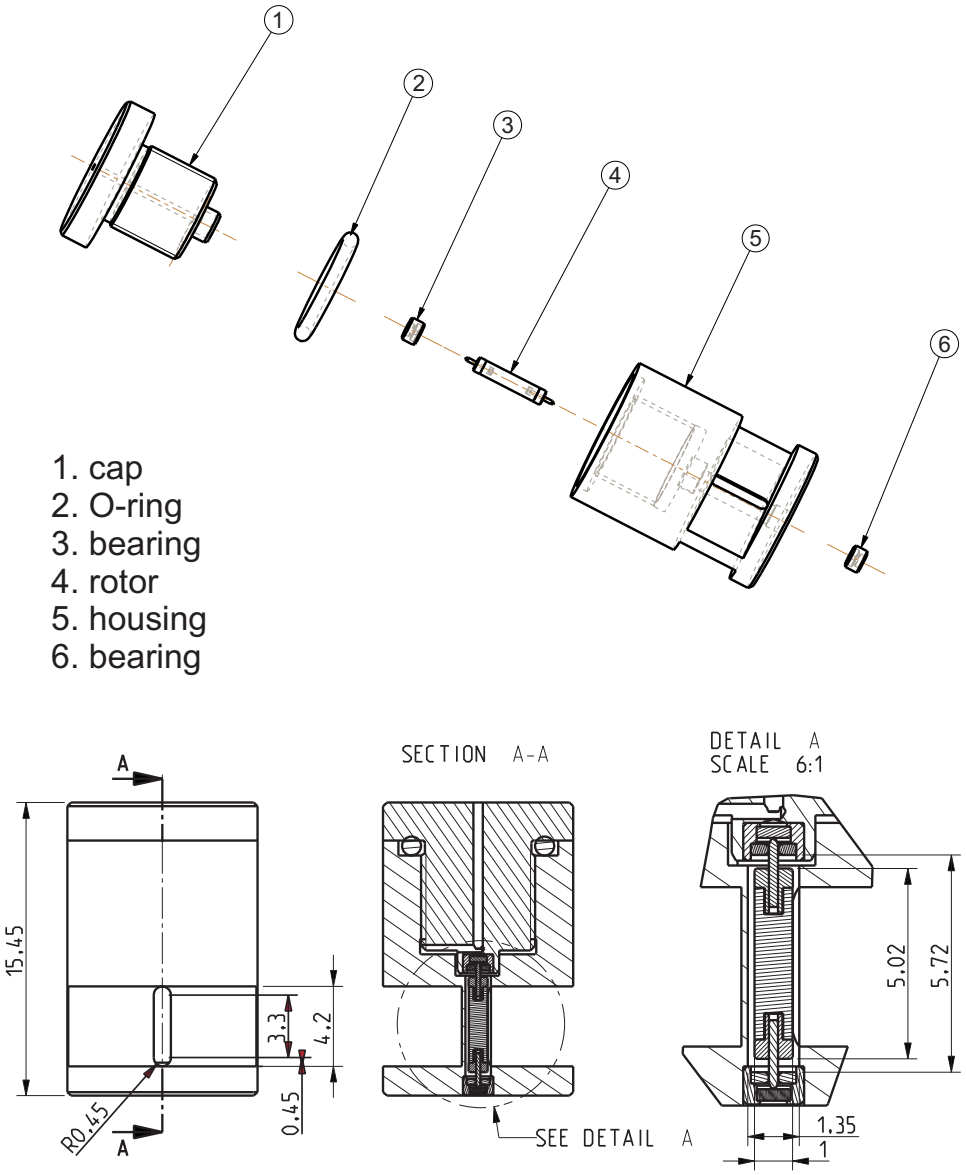

Figure 6.1: IGLUS demonstrator. Exploded and detailed views. Dimensions in mm.

shafts. To prevent any corrosion and water contact, the rotor, excepted for the ends of the shafts, is coated with parylene. The two miniature bearings are made of sapphire and ensure that the mechanical friction is as low as possible.

The newer demonstrator version is optimized for a faster response time since the inner volume (SF volume) has been reduced to 4.1 μl compared to 5.1 μl for the older version, and the open surface for the SI has been increased from 1.7 mm^2 to 3.6 mm^2. This improvement has been achieved by increasing the rotor magnet length by 1 mm and moving the interface closer to the rotor at a distance of 0.175 mm (0.35 mm in the previous version).

The external dimensions of the housing have been enlarged in order to improve the assembly because the previous version necessitated several attempts before the demonstrator was usable. A larger housing led to a 90% successful assembly score and drastically improved two issues which were related to the housing deformation when screwing the cap. The two issues were the cracking of the SI and the jam of the rotor. The necessity of a reproducible and one-step successful assembly procedure becomes essential when considering *in vivo* testing. The assembly in sterile conditions for an implantation does not offer the possibility of reopening the capsule right before the implantation. The external size increase of the demonstrator was thus implemented for practical reasons but does not compromise the future miniaturization of the IGLUS sensor.

In order to assess the SF under repeated shear stress, a closed version (without the opening for the SI) has also been used. In the next section, this slitless version is referred to as the *closed capsule* and the regular version is referred to as the *sensing capsule*.

6.3 Integration of the selective interface

6.3.1 Preparation

The SI is a nanoporous alumina membrane coated with PPEGMA as described in section 4.6 and characterized in chapter 5. The alumina membranes were provided as 13 mm diameter discs and were cut into smaller rectangular pieces of 4.15 $\times$ 2.5 mm^2. The PPEGMA coating was applied prior to cutting.

The small membrane pieces were first pre-cut by laser ablation, leaving 0.4 mm wide bridges connecting to the initial membrane. The individual pieces were then detached by breaking the bridges. The laser ablation was performed using a LS-520G Nd:YAG 1064 nm laser from Laser Systems. The initial porous alumina membrane was placed on a bulk alumina substrate and the laser ablation was operated using the following parameters: power 80%, pulses frequency 3 kHz and speed 1 mm/s.

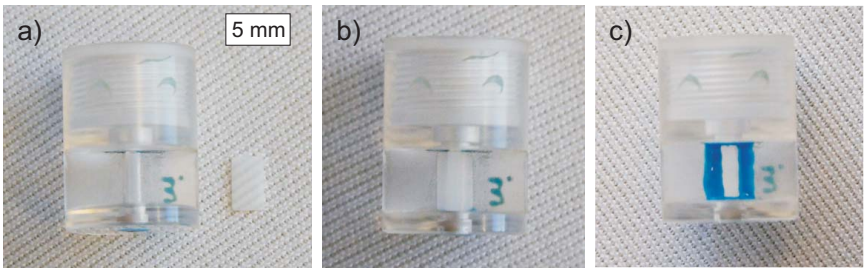

Figure 6.2: Integration of the alumina membrane onto the demonstrator: a) the bare demonstrator and the laser cut membrane, b) the membrane is disposed on the demonstrator opening, c) the membrane is glued onto the demonstrator.

The so-prepared membranes were subsequently integrated onto the IGLUS demonstrator, described in section 6.2, by gluing it on the opening as depicted in figure 6.2. We used the epoxy adhesive Eccobond 268 from Emerson & Cuming because it is adapted to aqueous media, does not release solvents nor ions and has adapted creeping properties to sustain the expansion difference of PMMA and alumina. The glue was polymerized for 8 hours at 37°C.

6.3.2 Filling procedure

In order to avoid the emergence of bubbles and to ensure the watertightness of the demonstrator, we developed a specific filling and assembly procedure. A reproducible and efficient procedure is required to prepare the demonstrator for *in vivo* testing. Indeed the assembly in sterile conditions for an implantation requires the complete sealing of the capsule and eliminates the possibility of reopening the capsule right before the implantation.

After the SI has been glued onto the sensing capsule, the rest of the assembly procedure consists on filling the capsule with the sensitive fluid (SF) and sealing the cap in order to avoid any leakage, mainly due to the osmotic pressure. The concentration difference of a solute on both sides of a selective membrane, in our case dextran and ConA, creates an osmotic pressure which tends to equilibrate the concentrations.

Prior to filling the demonstrator, the housing and the cap are stored for at least one day in the reference solution (RS) because PMMA can absorb a very little amount of water and ions. Shortly before filling, the housing and the cap in their RS bath, as well as 2 ml of SF, are outgassed at 0.05 mPa for 15-30 min at ambient temperature. This step is necessary to avoid the emergence of air bubbles. Next, the housing is filled with the outgassed SF up to the edge, the rotor is inserted and the cap is screwed slowly in order to avoid any excessive overpressure inside the capsule which could cause

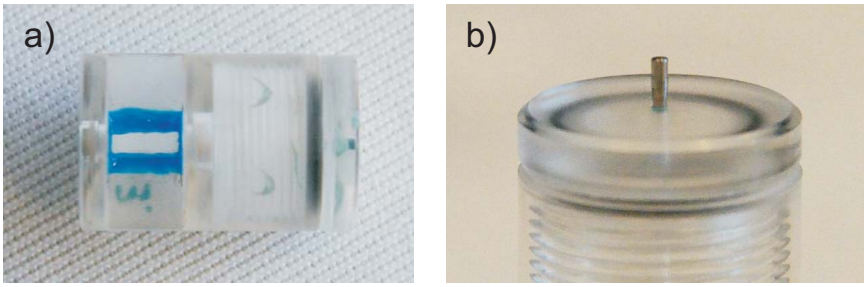

Figure 6.3: IGLUS demonstrator. a) assembled, b) the evacuation channel is sealed with a conically shaped pin.

the burst of the SI. The excess of SF inside the capsule flows out through the overpressure channel in the cap. The last step is to seal the overpressure channel using a conically shaped stainless steel pin, as depicted in figure 6.3.

6.4 *In vitro* test bench

6.4.1 Experimental setup

The experimental setup is composed of the acquisition system, which permits the measurement of the damping factor as described in section 3.3, and the simplified *in vitro* environment model (SITEM), which creates an environment where the ionic physiological conditions are mimicked.

6.4.1.A Acquisition system and thermostatic chamber

The acquisition system is controlled by a multifunction DAQ board PCI-6052E from National Instrument[1]. The sine and cosine waves to accelerate the rotor are generated with the digital-to-analogue converter (DAC) of the board. The setup is depicted in figure 6.4. The board is also used for the acquisition of the two Hall effect sensors signals during the measurement phase. The signals for the coil currents are generated by the DAC and amplified by two current followers based on power operational amplifiers OPA541.

The rotor is accelerated to an angular speed of 210 Hz, and, during the speed decay, the position of the rotor is acquired through two Hall effect sensors, oriented at 90° with respect to each other. The Hall effect sensors used are of the type Honeywell SS94A1F. These sensors are highly integrated and have all necessary electronics and amplification stages on one chip. The output is an analog signal, proportional to the magnetic field

[1] http://www.ni.com/dataacquisition

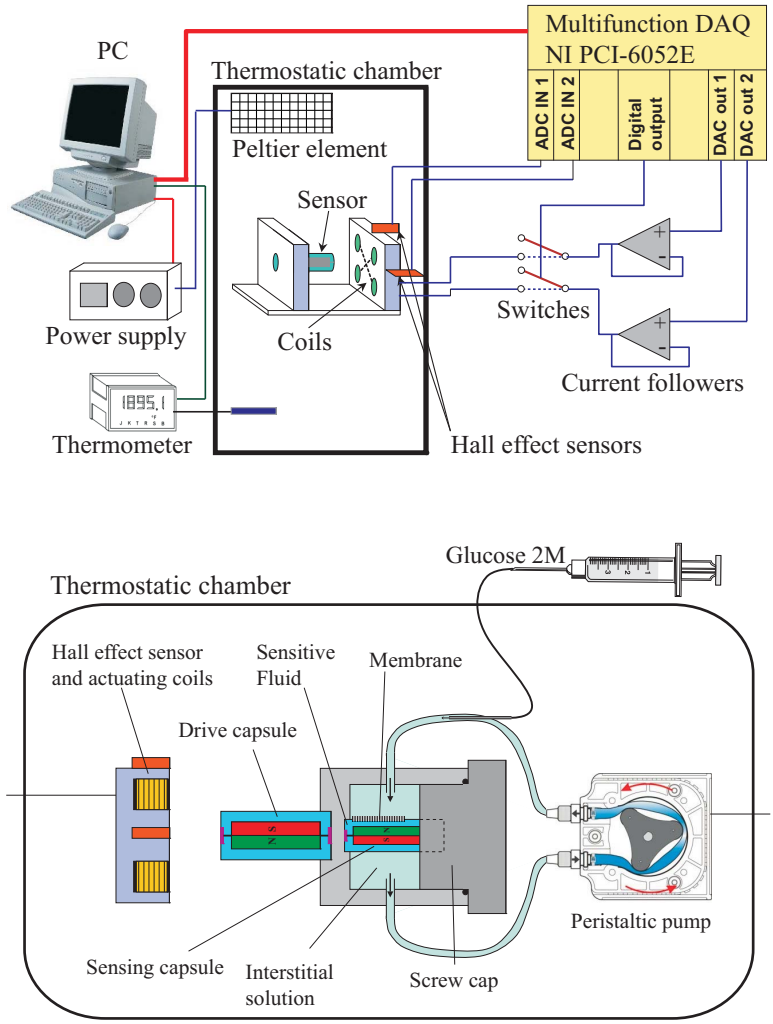

Figure 6.4: Experimental *in vitro* setup.

component perpendicular to the sensor. The acquisition of the signal is done via the DAQ board and Labview[2] is then used to analyze and perform the calculations on the data.

Once the signal has been acquired from the hall effect sensors, the second step is to extract the angular position from which the damping factor is calculated. A previous work [22] determined an accurate and reproducible method for this calculation. The rotor angular position $\theta(t)$ is obtained by computing the arctangent from the sine and cosine signals of the hall effect sensors. For reproducibility issues, the starting and ending values of $\theta(t)$ are discarded. In facts, regarding the angular speed, the rotor is accelerated up to 210 Hz and only the values between 200 and 70 Hz are used to calculate the damping factor λ. The reasons are that the acceleration to 210 Hz is not reproducible and that, for the lower angular speeds, the rotor rotation is influenced by the terrestrial magnetic field.

The temperature of the thermostatic chamber is monitored with a PT100 high-precision thermometer GMH 3710 from Greisinger GmbH[3]. The absolute temperature accuracy is $\pm 0.03°C$ with a reproducibility of $\pm 0.01°C$. The temperature is read via RS-232.

The chamber is heated and cooled by a Peltier element, which is powered with an Array 3645A[4] power supply and controlled via RS-232. A polarity inverter, actuated through the parallel port allows the computer to switch the polarity of the power supply. Thus, only one power source is sufficient for heating and cooling. The temperature control is performed with a PID regulation implemented in Labview. The temperature can be automatically set by the computer and the obtained long term stability is better than $\pm 0.02°C$.

6.4.1.B SITEM setup

As introduced in section 4.2, the SITEM has been deployed in order to assess the IGLUS demonstrator with the SI. The SITEM is a chemical environment where the interstitial fluid (IF) is mimicked by a RS which is an isotonic solution of the SF for all of its constituents but dextran and ConA. See table 6.1 for the detailed composition. In other words, the RS contains equal concentrations of ions and has the same pH and buffer as the SF. The only chemical constituents which differ on both sides of the membrane are dextran and ConA. Using this model, the only constituent whose concentration is varied in and out of the demonstrator should be D-glucose, because ConA and dextran are retained by the SI and all other chemical constituents are already equilibrated on both sides of the interface.

[2] http://www.ni.com/labview
[3] www.greisinger.de
[4] www.array.sh/yq-3600e.htm

Table 6.1: Solutions utilized for the simplified *in vitro* environment model (SITEM). The RS is used to simulate the interstitial fluid and the concentrated glucose solution is injected in the RS in order to modify the glucose concentration.

Solution	Description	Concentration
Reference solution RS	Tris buffer (7.4)	10mM
	NaN_3	0.05%(w/w)
	D-glucose	2 - 30 mM
	$MnCl_2$	1 mM
	$CaCl_2$	1 mM
	$NaCl$	150 mM
	H_2O	-
Glucose solution	D-glucose	2M
	NaN_3	0.05%(w/w)
	$NaCl$	150 mM
	$MnCl_2$	1 mM
	$CaCl_2$	1 mM
	H_2O	-

The setup used to apply the SITEM is represented in the lower part of figure 6.4. The sensing capsule is enclosed in a housing containing the RS. The RS, which thus surrounds the sensing capsule, circulates with the aid of a peristaltic pump in order to mix the RS. This allows us to have a situation were both fluids, inside and outside the sensing capsule, are well stirred and is therefore comparable to the diffusion cell situation. The SF is mixed by the viscosity measurements since the rotor is actuated every 25 seconds.

The whole setup is disposed in the thermally regulated chamber so that the system can be set to the required temperature. In order to be as close as possible to the conditions of the human body, all the measurements are performed at 37°C.

The glucose concentrations were applied to the RS, either by injecting small amounts of a concentrated (2 M) D-glucose solution with a microliter syringe in order to increase stepwise the concentration, or by flushing the RS and replacing it with another RS having the appropriate glucose concentration when a decrease is desired. The chemical composition of the glucose concentrated solution is detailed in table 6.1.

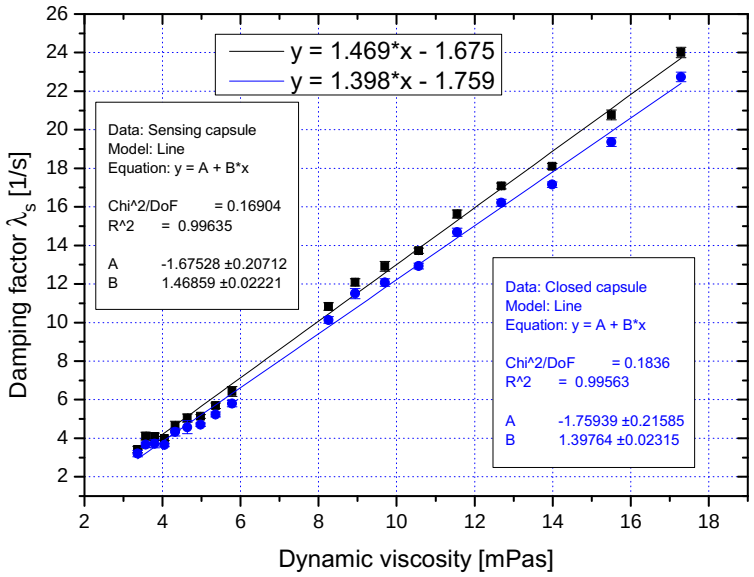

Figure 6.5: Calibration of the sensing capsule (black curve) and closed capsule (blue curve). The damping factor is calibrated as a function of the viscosity using calibration oils (D5 and N10) whose viscosity is varied by adjusting the temperature.

6.4.2 Microviscometer calibration

The IGLUS demonstrator being a microviscometer, we calibrated the measured damping factor using calibration oils from Paragon Scientific Ltd[5]. The viscosity of the calibration oils, being dependent on the temperature, can be adjusted by varying the temperature. The drive capsule was filled with the D5 oil and the damping factor λ_d was determined from 20 to 40°C with an increment of 2.5°C. Subsequently the sensing capsule was filled with the N10 and D5 oils in order to cover a broader viscosity range. The total damping factor λ_t was measured for the same temperatures as previously and the damping factor of the sensing capsule λ_s was calculated using the relation $\lambda_s = \lambda_t - \lambda_d$. The viscosity of the calibration oils as a function of the temperature is given by the manufacturer and thus the damping factor of the sensing capsule can be plotted as a function of the viscosity. The results are shown in figure 6.5. The viscosity range of 3-6 mPas is covered by the D5 oil and the 8-18 mPas range is covered by the N10 oil.

Figure 6.5 also shows a calibration curve for the closed capsule since this latter was used to assess our system as presented in the next section.

[5]http://www.paragon-sci.com

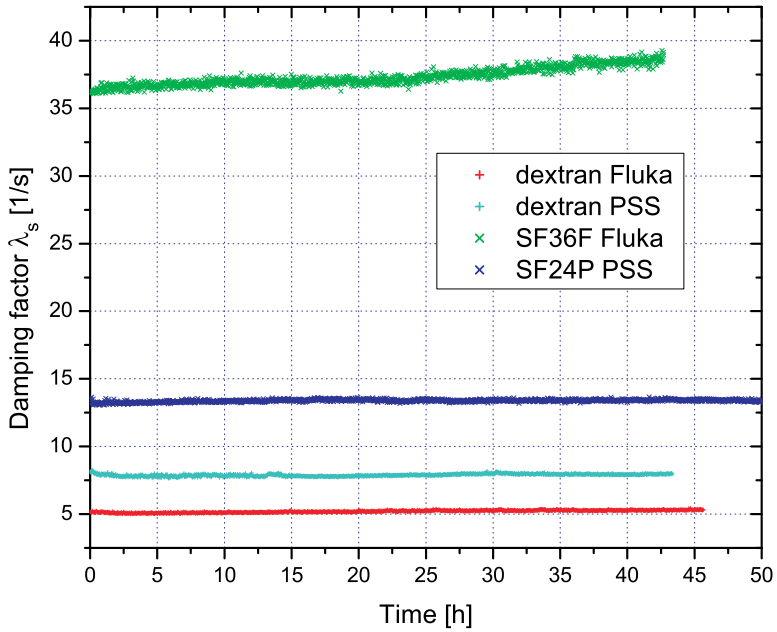

Figure 6.6: Stability measurements of dextran solutions and SFs in the closed capsule at 37°C.

6.5 *In vitro* results

The results obtained with the IGLUS demonstrator are presented in three sections. First we present stability measurement obtained with a closed capsule. This study was required in order to verify the viscosity stability of the SF over time when repeated measurements, i.e repeated shear stress, are applied to the SF. In a second part, we studied the viscosity stability of a dextran solution in the demonstrator with the SI (sensing capsule). The third section deals with the response of the IGLUS demonstrator to glucose concentration variations using the SITEM.

6.5.1 Stability in closed capsule

In order to evaluate the SI on the IGLUS demonstrator, the first step was to determine whether the repeated viscosity measurements are supported by the SF. Hence we measured the viscosity stability over time in a closed capsule with four different fluids at 37°C. A measurement was taken every 25 s. We tested two SFs, the SF36F and the SF24P, and two dextran 3 wt% solutions prepared with Fluka and PSS dextrans respectively. The dextran solutions were prepared by dissolving the dextran in the RS. The damping factors as a function of the time are plotted in figure 6.6.

The viscosity remained constant for more than 40 hours for almost ev-

Table 6.2: Effective diffusivity of the two selected SIs for the IGLUS demonstrator.

Name	D_e glucose $[\frac{mm^2}{s}]$
WA20-80-3	$0.0501 \pm 0.0019 \times 10^{-4}$
WA20-80-2	$0.0628 \pm 0.0006 \times 10^{-4}$

ery solutions, only the SF36F showed a slight increase. The reason for this increase is unknown but was observed in many experiments. As a comparison, the SF24P, prepared with purified PSS dextran, exhibited a much better stability, since the viscosity remained the same for more than 50 hours. This observation lead us to use the SF prepared with the PSS dextran for the assessment of the IGLUS demonstrator with the SI.

None of the two dextran types showed any weakness during the experiment. Both dextran solutions had a very stable viscosity. We therefore conclude that the repeated shear stress applied to the tested fluids does not alter nor break the molecules of dextran or ConA. The slight increase of viscosity of the SF36F is thought to be a reorganization of the dextran-ConA network.

6.5.2 Stability in sensing capsule with SI

In the previous section, we demonstrated that the SF and the dextran solutions have a stable viscosity over time in a closed capsule. The next step was to assess the SI on the sensing capsule, both parts assembled together creating the IGLUS demonstrator. Two SIs were selected, the WA20-80-3 and WA20-80-2, because they exhibited an effective diffusivity of glucose close to $0.06 \cdot 10^{-4}\ \frac{mm^2}{s}$, which is much below the maximum value of $0.6 \cdot 10^{-4}\ \frac{mm^2}{s}$ for BSA retention. The detailed values are given in table 6.2. Given the low values of D_e, the coating was relatively thick and this is required in order to retain the fragments of ConA as well as possible.

Prior to using a SF, we tested the demonstrator with the SI WA20-80-3 using a dextran solution in the SITEM setup. This interface had the thicker coating (since D_e is smaller). In figure 6.7, we show the viscosity evolution of a dextran solution in the demonstrator and we compared it to a non-coated SI. The main outcome of this experiment is that the WA20-80-3 SI retained the dextran over 24 hours (green curve), whereas the non-coated version did not (red curve). The two jumps in the green curve are due to the presence of a bubble.

This experiment taught us other things. Regarding the measurement with the non-coated SI, the black curve was obtained without sealing the sensing capsule with the pin and the red curve was obtained with the pin. We observe that without a good sealing, the viscosity stabilizes faster but

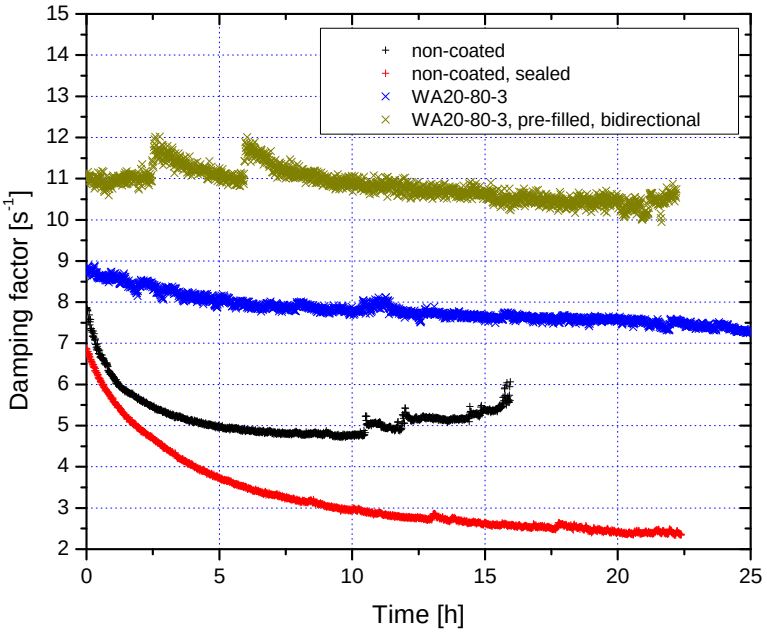

Figure 6.7: Stability measurements of dextran PSS 3% solutions in the IGLUS demonstrator. Two Whatman 20nm membranes were tested, a non-coated and a PPEGMA coated (WA20-80-3).

air bubbles appear after a few hours. After 10 hours, we clearly see on the black curve the discontinuity of the signal due to the bubbles. We believe that the faster stabilization of the viscosity was either due to the air bubbles preventing the dextran to leak out, or due to the very slow water flux entering the demonstrator through the membrane, because of the osmotic pressure, which slows down the leakage of dextran.

We also observed that pre-filling the sensing capsule with the dextran solution gave rise to a better viscosity stability. The pre-filling means that we filled the capsule with the dextran solution for 24 hours prior to performing the measurements. Just before the measurements, the dextran solution was renewed with a fresh and outgassed solution. It is known that PMMA adsorbs certain solutes, especially proteins, and hence we expected that dextran would also be adsorbed. By pre-filling the sensing capsule, we created a layer of adsorbed dextran on the inside walls of the capsule which prevents further adsorption. This is the difference between the blue curve and the green curve in figure 6.7, where the latter curve was obtained after pre-filling and we observed a better stability of the viscosity over 24 hours. What happens with the blue curve is that the capsule was rinsed with ultrapure water before the measurement and we observe a slight decrease of the viscosity, due to the slow adsorption of dextran on the walls.

While studying the viscosity stability of the dextran solution in the sensing capsule, we discovered that we could obtain a better stability by changing the rotating direction of the rotor for every measurement. This operation is named bidirectional mode and was used for the measurement of the green curve in figure 6.7. The reason for the improved viscosity stability by using the bidirectional mode is not yet determined. However we suspect a rearrangement of the dextran molecules when the shear stress is repeatedly applied in the same direction, which creates a variation of the viscosity over time, as it has been evidenced by Beyer *et al.* [154]. It is important to note that we only observed this phenomenon with PSS dextran and in the sensing capsule. It was not observed in the closed capsule. The reason for this phenomenon is not understood yet. The bidirectional measurements were adopted for the later experiments using the SF.

6.5.3 Demonstrator response to glucose variations

The ultimate step of the validation of the SI on the IGLUS demonstrator was to implement the SF and test the response of the complete system to glucose variations using the SITEM. The experiment was repeated only a limited number of times because we only achieved to prepare two SIs with a sufficient coating thickness, the WA20-80-2 and the WA20-80-3. Their properties were detailed in section 6.5.2. In addition, we will see that their use with the SF on the sensing capsule is limited in time.

The SI was glued on the sensing capsule as described in section 6.3.1 and the capsule was filled with the SF24P following the procedure detailed in section 6.3.2. The capsule was pre-filled with the SF36P 48 h before the measurements, as we also observed that it leads to a better viscosity stability. All measurements were performed using the bidirectional mode.

6.5.3.A Experiment A

In figure 6.8, we present the result of a typical experiment with the SI WA20-80-3. The system was first tested with a dextran solution in order to verify the assembly and sealing of the capsule. The blue curve shows the good stability. Subsequently, we used the SF, and during the first 24 h the black curve shows a good stability of the viscosity at 2 mM of glucose (region B). The region A corresponds to the signal stabilization which occurs every time the demonstrator is started with a fresh SF. We remind that the damping factor accuracy is increased for lower values since the rotor speed decay takes place on more turns for lower viscosities. Therefore we have a higher noise in region B.

At the start of region C, we set the sensing capsule environment at 4 mM glucose. A viscosity decrease followed by stabilization is expected, but

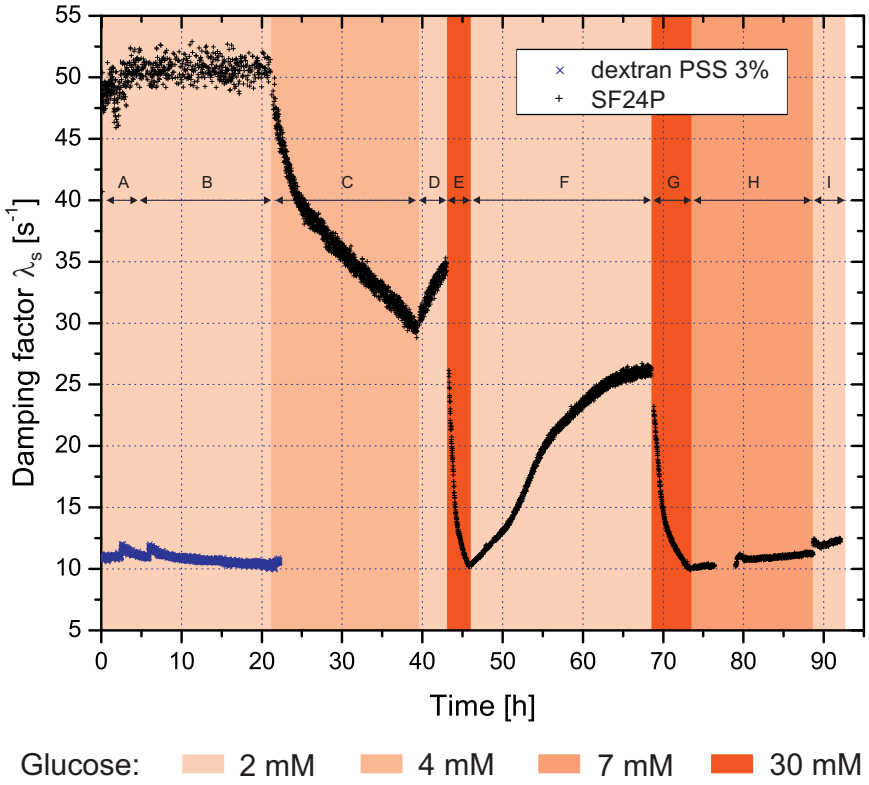

Figure 6.8: *In vitro* measurements of the IGLUS demonstrator with the PPEGMA coated alumina membrane WA20-80-3 in the SITEM. The system was first tested for stability with a dextran solution (blue curve). Subsequently, the SF24P was used and the external glucose concentration was varied: A. stabilization, B. 2 mM, C. 4 mM, D. 2 mM, E. 30 mM, F. 2 mM, G. 30 mM, H. 7 mM and I. 2 mM.

instead of stabilizing, the viscosity keeps decreasing linearly. This phenomenon is not clearly understood but we suppose that the SF is subjected to a molecular reorganization due to the increase of the glucose concentration. Indeed the viscosity of the SF at the beginning was unexpectedly high at 36 mPas, refereing to the calibration of figure 6.5, whereas we measured 9.4 mPas for another preparation of the SF24P in section 3.4.3. This highlights the non-reproducibility of the nominal viscosity at the preparation. In order to verify whether the SF was still chemically active, the glucose was set back to 2 mM in region D. From region E to region I the glucose concentration was varied two times up to 30 mM and back down to 2 mM in order to assess the reversibility. For both regions with 30 mM glucose (E and G), the same damping factor value was reached when stabilizing. Whereas the stabilized damping factor values were different with a decreasing tendency over time for every region at 2 mM (B, D, F and I). The reversibility was thus not complete, but a partial reversibility was observed.

The possible reasons for the incomplete reversibility of the viscosity measurements under glucose concentration variations are various. The ConA leakage is favored at higher glucose concentrations. At 2 mM glucose, the network constituted by the dextran and ConA is highly linked and, as a consequence, the ConA cannot leak through the SI. At higher glucose concentration, i.e. at 30 mM, the network is untied and the ConA is free to diffuse out of the sensing capsule through the SI. As previously discussed in section 5.8.1, the ConA contains fragments which can possibly leak out of the SI. Another reason is the unstability of the SF upon glucose variations. The SF24P was assessed in a closed capsule and the result, presented in section 6.5.1, demonstrated the viscosity stability over 50 hours, but this experiment was operated at constant glucose concentration (2 mM) and no data exists about the resistance of the SF under glucose variations. In fact, the SF is not completely understood and many questions remain, especially when the glucose concentration is varied. Investigations in a different system should be undertaken in order to give answers to these questions, because it is difficult to validate the SI and the SF simultaneously.

During this experiment, we observed that the response time of the demonstrator was higher for every supplementary glucose variation. At the end of the experiment, regions H and I, the sensor showed only a very slow response to the glucose concentration change. After 92 hours of run, the demonstrator was rinsed and the SF replaced, but the sensor did not respond to glucose variations anymore. The SI was fouled, because impermeable to glucose. We believe that dextran and/or ConA fragments clog the pores. An investigation of this hypothesis is underway and results will be presented in a later work. The decay of the sensor response time throughout glucose variations is studied in details in experiment B.

We have to emphasize an important achievement. The SITEM setup

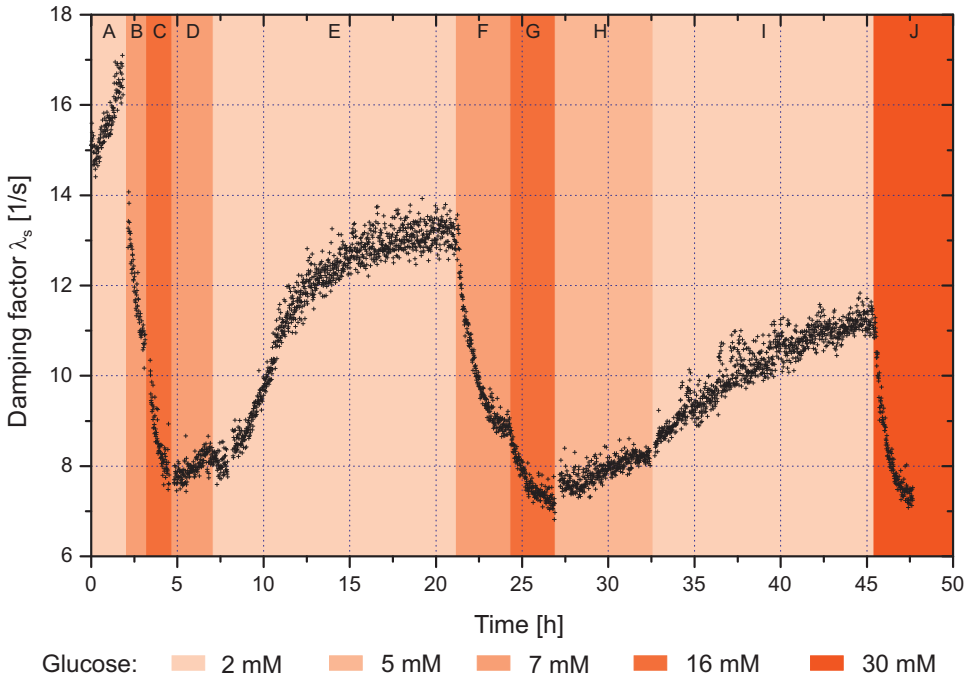

Figure 6.9: *in vitro* measurements of the IGLUS demonstrator with the PPEGMA coated alumina membrane WA20-80-2. The SF24P was used and the external glucose concentration was varied: A. stabilization at 2 mM, B. 7 mM, C. 16 mM, D. 7 mM, E. 2 mM, F. 7 mM, G. 16 mM, H. 5 mM, I. 2 mM. and J. 30 mM.

and IGLUS demonstrator completed a 92 hours run without the appearance of a bubble, which shows the capability of the system to run over 4 days. This achievement is the result of the improvement of the preparation and filling procedures described in sections 6.3.1 and 6.3.2.

6.5.3.B Experiment B

Experiment B is similar to experiment A. We replaced the SI by the WA20-80-2 version which has very similar properties, as seen in table 6.2. The experimental and preparation conditions were identical. In this experiment, we applied glucose concentration variations by renewing the RS around the sensing capsule with a defined glucose concentration. Renewing the RS is more precise regarding the glucose concentration than adding shots of concentrated glucose. Hence, for every time region, named from A to J in figure 6.9, the glucose concentration was precise and constant. Two cycles of glucose concentration variation were applied by starting at 2 mM up to 16 mM with an intermediate step at 7 mM. The purpose of the cycles was to test the viscosity reversibility. The result is presented in figure 6.9.

As a result, the sensor followed the glucose variations, however the complete reversibility was not observed. Indeed, the stabilized damping factor values are not identical in regions A, E and I. We observed the similar decreasing tendency when going back to 2 mM in the previous experiment.

The stabilized damping factor values for the high glucose concentration are very close, see regions C, G and J. The stabilized value of region G is a little lower than in region C, which is in accordance with the global viscosity decrease over the entire experiment. The viscosity difference at 16 mM is smaller (between regions C and G) than at 2 mM (between regions A, E and I) simply because the viscosity sensitivity to glucose is much higher at lower concentrations, see viscosity variations of the SF24P in figure 3.12. The last glucose variation to 30 mM (region J) was applied to verify the non-fouling of the SI, and to show the poor sensitivity of the SF24P at higher glucose concentration, above 16 mM.

After 48 hours of use, we stopped the experiment to preserve the demonstrator in order to use it for the *in vivo* experiment presented in the next chapter.

The response of the IGLUS demonstrator to the glucose variations was analyzed and the response time for each time region was fitted using the following equation

$$y = A(1 - e^{-\frac{t}{\tau}}) + B \tag{6.1}$$

which is derived from eq. (5.3) and where τ is the relaxation time. It is common for sensors to give the $\tau_{90\%}$ value, which is the response time of the sensor to reach 90% of the variation amplitude. The calculated values are given in table 6.3. In addition, we calculated the extrapolated response time $\tau_{90\%}$* for the situation where the SI would totally surround the sensor. The demonstrator presented in this work only has a partial opening for a flat SI, as illustrated in figure 6.2, and a future version could integrate a tubular-shaped SI which would surround the rotor. This situation would reduce the response time since the surface is increased whilst the inner volume (SF volume) remains equal. $\tau_{90\%}$* is calculated using eq. (4.25).

In the results of table 6.3, we observe that the response time is higher when the glucose concentration is decreased (regions D, E, H and I) than when it is increased (regions B, C, F, G and J). Furthermore the response time is lower when the glucose variation is in a higher concentration range, i.e. τ is smaller when passing from 7 mM to 16 mM (regions C and G) than from 2 mM to 7 mM (regions B and F). This observation is also valid for the case of decreasing concentrations. The reason is that, at higher glucose concentration, the SF viscosity is lower and thus the diffusion of glucose is higher. The SF is supposed to be stirred by the rotor rotation, but we suspect that a thin layer region on the inside face of the SI is not correctly mixed and, in this region, the glucose is transported by pure diffusion. And we know from the Stokes-Einstein relation (eq. (4.2)) that the diffusion

Table 6.3: Response time of the IGLUS demonstrator according to the time regions of figure 6.9. τ is the response time obtained by fitting with eq. (6.1), $\tau_{90\%}$ is the time to reach 90% of the variation and $\tau_{90\%}$* is the extrapolated time for a surrounding SI.

Region	Glucose variation	τ [min]	$\tau_{90\%}$ [min]	$\tau_{90\%}$* [min]
B	2 to 7 mM	48	110	18
C	7 to 16 mM	26	60	10
D	16 to 7 mM	156	359	59
E	7 to 2 mM	202	465	76
F	2 to 7 mM	64	147	24
G	7 to 16 mM	57	131	22
H	16 to 5 mM	227	522	86
I	5 to 2 mM	466	1072	176
J	2 to 30mM	37	85	14

coefficient of a solute is proportional to the viscosity of the medium.

As also observed in experiment A, the response time of the demonstrator increases progressively throughout the experiment. As in experiment A (section 6.5.3.A), the SI is progressively fouled when glucose variations are applied.

The extrapolated response time $\tau_{90\%}$* (assuming a cylindrical shaped SI) is rapid, when increasing the glucose concentration, compared to the 20 min which is the required lag time from the medical point of view. The response time remains important for decreasing glucose concentrations, but the actual IGLUS demonstrator can be further optimized through various modifications.

6.6 Discussion

The intrinsic performance of the SI on the demonstrator is difficult to assess because many questions remain open concerning the SF. However the SI showed good results since we could observe the glucose concentration variations with the IGLUS demonstrator and the response time is promising. The only negative point is the incomplete reversibility of the SF viscosity. At present, it is difficult to distinguish between a lack of performance of the SI or the SF.

As previously discussed in section 5.8.1, ConA contains fragments which could leak out of the SI, and would induce a progressive decrease of the SF viscosity. The quantification of this effect is not in the scope of this work and a further investigation on the SF could distinguish the performance of the SI and SF. For instance, a SF should be prepared with purified ConA and

the stability of the fluid be assessed. Another possibility would be the modification of ConA by pegylation since it increases its solubility. This modification consists of grafting PEG molecules to the protein. In fact, ConA has a limited solubility in water which can be the cause of a slow precipitation over time. In addition, the ConA pegylation increases its affinity to D-glucose [150].

During the experimentation with the SF and the IGLUS demonstrator, we observed a non-reproducibility from batch to batch and instability of the nominal viscosity of the SF during storage, and this remains an important source of unexplained behaviors of the demonstrator.

Regarding the SI, we previously discussed the progressive fouling. In fact, the SI that were tested on the demonstrator showed a tendency to improve their retention capability when used for a series of experiments. We believe that a partial fouling of the membrane ameliorates the retention capabilities, while the glucose diffusion is altered. This conclusion is highlighted by the fact that several SI got fouled after 4 to 6 days of use. At present, we have not studied the details of the fouling process, but both dextran and ConA can be the cause. Regarding dextran, we know that both PEG (from PPEGMA) and dextran are very hydrophilic and polar molecules. This makes them rather miscible and there is a possibility for dextran to partially penetrate the PPEGMA coating. The possibility of a simple adsorption of the dextran on the coating is minimum, if we refer to the work of Singh *et al.* [155]. And, as discussed previously, the fragments of ConA are also susceptible to foul the SI.

6.7 Conclusion and outlook

In this chapter, we demonstrated the promising performance of the SI composed of an alumina membrane and a PPEGMA coating. We showed the partial reversibility of the chemical process of the SF over two cycles of glucose variations and demonstrated the use of the sensor over 92 hours. The assessment of the SI on the IGLUS demonstrator is currently limited by the SF performance.

At the present state of research, the IGLUS still needs improvements to precisely monitor the glucose concentration. Nevertheless glucose variations can be clearly observed and the situation is very encouraging for a proof of concept. Since the demonstrator presented in experiment B (see section 6.5.3.B) showed a sufficient response to glucose variations, we used it for an *in vivo* experiment which is presented in the next chapter.

Another way to assess our SI could be to use a different system than the IGLUS since the performances of the SF, containing dextran and ConA, are questioned. For example, a sensor recently developed by Lei *et al.* [63] uses a phenylboronic acid based hydrogel to sense glucose. Alternatively, a

possibility is to synthesize a stable and biocompatible SF based on phenylboronic acid as proposed by Siqi *et al.* [156].

In 1994, Ballerstädt and Ehwald wrote in a scientific article [66] that the SF is suitable and that "The technical challenge lies in miniaturization by microengineering and microelectronics." At this point of our research, we believe the microengineering and electronics not to be a challenge anymore. For the IGLUS, the new challenge lies on the chemistry of the relation between the SF and the SI and their long-term stability.

Chapter 7

IGLUS *in vivo* investigation

7.1 Introduction

As the IGLUS demonstrator showed promising results *in vitro*, we investigated its sensing performance *in vivo*, since there are various differences in the environmental conditions. The step from *in vitro* to *in vivo* experimentation being a complex work, we did not intend to validate the functioning of the sensor *in vivo*, but we investigated and established the necessary basis for further *in vivo* assessment of the IGLUS, with the aim to observe glycemia variations of the animal. Prior to the sensor *in vivo* validation, which is beyond the scope of this work, the new environment needs to be investigated. Following this thread, we present the developed procedure and the experiment in which an IGLUS demonstrator was implanted in an animal over a period of five days. A Zucker Diabetic Fatty (ZDF) Type 2 diabetic rat was selected for the implantation. The ZDF rat model is appropriate since it is possible to control its glycemia either to hyper-, normo-, or hypo-glycemia depending on the test requirements.

The implanted part of the demonstrator is a single capsule without electronics. It contains the sensitive fluid (SF) prepared with purified dextran 3200 kDa, ConA and phenol as an antiseptic. The demonstrator, used in this experiment, is the version presented and tested in section 6.5.3.B, with the selective interface (SI) WA20-80-2, i.e. an alumina membrane with 20 nm pores with a PPEGMA coating. We used a in-house developed hand-held reader to measure the signal of the sensor through the skin. The body temperature of the rat was measured with a transponder located beneath the skin right next to the sensor. The blood glycemia was monitored by commercially available blood glucose meters, for which blood drop samples were taken by pricking the tail, ear or tongue of the animal.

In this chapter, we present the assessment of the preparation and implantation procedures of a working sensor device in a living animal. In addition, we present and discuss the measurements obtained with the im-

planted sensor. This experimentation was done in collaboration with the Swiss Institute for Experimental Cancer Research (ISREC) and the Centre d'Application du Vivant at EPFL.

7.2 Experimental description

7.2.1 Protocol

As the *in vivo* experimentation is a complex procedure. A protocol has been written by our team and the main features are presented in the followings.

Objectives

• To validate the IGLUS demonstrator in-vivo, with semi-permeable membrane

• To quantify the glucose variability of a ZDF rat and compare it to the sensor response time

• To investigate the blood glucose behavior upon skipping an insulin bolus

Material

• 1 male rats of 8 weeks, ZDF

• 1 glucose sensor demonstrator, filled with SF with PSS dextran and phenol, with semi-permeable membrane (WA20-80-2)

• One Plexx temperature transponder and reader

• One glucose meter for follow-up on glycemia

• Insulin Lantus Sanofi-Aventis®, ultra-slow insulin, 100U / mL, injection at 27U/kg

Sterilization

• Sensor capsule: γ radiation with ^{60}Co, 29 kGy

• Sensitive fluid: contains 0.2% phenol

• Sterile assembly: in sterile laminar flow bench

ZDF rat glycemia regulation test. This series of experiments performed prior to sensor implantation must help us understand how the rat glycemia behaves when an insulin bolus is skipped.

Day 1:

• Evening: measure blood glycemia, insulin bolus injection, feed overnight

Day 2:

• Morning: remove food, measure rat blood glucose

• Evening: measure blood glycemia, skip insulin bolus, feed overnight

Day 3:

• Morning: remove food, measure blood glycemia

• Evening: measure blood glycemia, insulin bolus injection, feed ZDF rat overnight

Implantation (see figure 7.7):

• Duration: 5 days, prolonged if successful

• Anesthesia: isoflurane, induction 4%, maintenance 2%

• Analgesia: injectable buprenorphine, Temgésic® SC, 0.0005 mg/ kg body weight (BW) then Acetaminophen in drinking water, 300 mg/ kg BW
• Anti-infectious prophylaxis: Amoxicillin in drinking water, 100 mg/ kg BW
• For surgery: skin disinfection with Betadine®
• Location: on the flank
• Suture: with vicryl 4.0
• Temperature measurement: Shearing and disinfection with Betadine®

Rats identification:
• Rat #1: ZDF rat, grey and white fur and obese
• Rat #2: anti-depressive companion rat, white fur

Measurements with implant:
Day 1:
• Morning: sensor implantation, 2-3 measurements with implanted glucose sensor to check its integrity
• Afternoon: measure blood glycemia (BG) and temperature (T), 10 measurements under anesthetic with implanted glucose sensor, 1 min. interval for checking coupling and sensor integrity
• Wait 1 hr: measure BG and temperature, 10 measurements with sensor
• Evening: slow-acting insulin bolus, feed
Day 2:
• Morning: 8:00 measure BG and T, 20 measurements with sensor; wait 2 h; 10:00 measure BG and T, 20 measurements with sensor
• Afternoon: 14:00 measure BG and T, 20 measurements with sensor; wait 2 h; 16:00 measure BG and T, 20 measurements with sensor
• Evening: skip insulin bolus (should be done as early as possible in the experimental planning in case of sensor stability issues), feed
Day 3: With previous insulin delivery more than 36 hr before, the ZDF rat should be reaching hyperglycemia
• Same as Day 2, however with insulin administration at 8:00
Day 4:
• Same as Day 3, however with insulin administration at 16:00
Day 5:
• Same as Day 3, i.e., with insulin administration at 8:00
From Day 6: Only if previous measurement campaign was successful
• Measure the blood glucose prior to insulin bolus and 3-4 h later, perform a few measurements for statistics
Explantation:
• Keep the rat alive

7.2.2 Implant and acquisition system

The IGLUS demonstrator was chosen for implantation after *in vitro* tests. The demonstrator, detailed in chapter 6, with the SI WA20-80-2 showed the best results *in vitro* (see section 6.5.3) in terms of reversibility and time stability, and was therefore appointed for the in-vivo experimentation. The SF used for this experiment was obtained from SF36P prepared with purified dextran 3200 kDa from PSS, 0.2 wt% phenol, 2 mM glucose, and from RS prepared with same concentrations of phenol and glucose. The mixing ratio was 2:1 (SF:RS) in order to obtain an SF24P.

The acquisition system used to measure the damping factor is an in-house developed system named "Glucorat System". It is a portable version of the acquisition system presented in section 6.4.1.A. The hand-held reader measures the damping factor of the implanted sensor through the skin and sends the data wirelessly. The Glucorat is an electronic system which consists of two parts: a hand-held electronic reader (Glucorat Reader) capable of measuring the damping factor of the implanted sensor through the skin and a remote base station (Glucorat Base Station) that, when connected to a PC, gathers data from the reader for further analysis. The Glucorat has been developed by Sadasing Kowlessur and Julien Chassot. The global system is depicted in figure 7.1 and the hand-held reader is detailed in figure 7.2. The main gathered data are the damping factor and the temperature of the drive. Contrary to *in vitro* measurements, the drive capsule has a different temperature than the sensor capsule, which means that we need to collect the damping factor and temperature for each capsule. For every measurement we get the coupled damping factor of the two capsule λ_t and, right after, the damping factor of the drive alone λ_d. Knowing that $\lambda_t = \lambda_d + \lambda_s$ [22], we can extract the damping factor of the implanted sensor λ_s. The temperatures T_d and T_s are acquired from the Glucorat Reader and an implanted transponder respectively.

In order to monitor the rat body temperature we placed a IPTT-300 Programmable Temperature Transponder from PLEXX[1] beneath the skin next to the glucose sensor. The temperature acquisition was done with a DAS-6007 Handheld Scanner also from PLEXX. The data acquisition with the Glucorat Reader and the DAS-6007 Scanner are shown in figure 7.3. This system allows temperature reading wirelessly and the transponder is correctly located for measuring the temperature of the implant. Rectal temperature measurement is a standard for body temperature, but the temperature beneath the skin is slightly lower ($\sim -1^{\circ}C$).

[1] www.plexx.eu

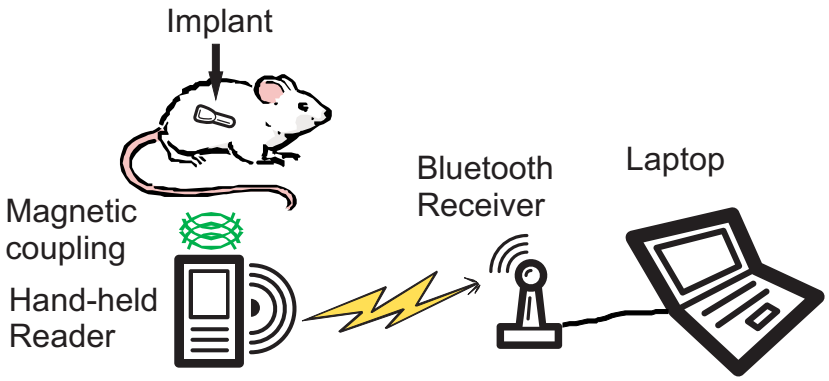

Figure 7.1: Data acquisition from implanted sensor with the Glucorat System.

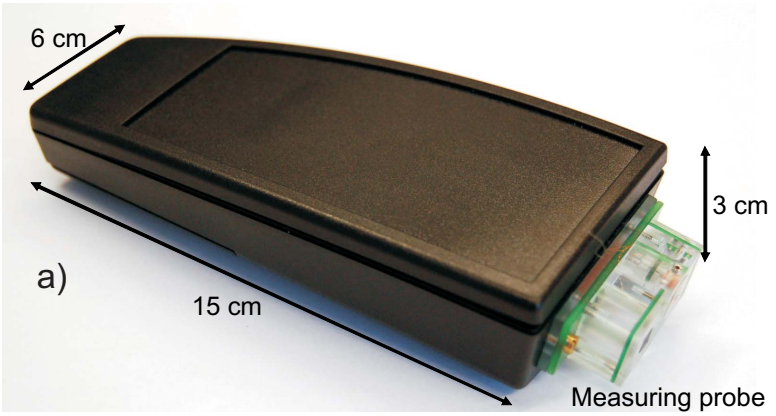

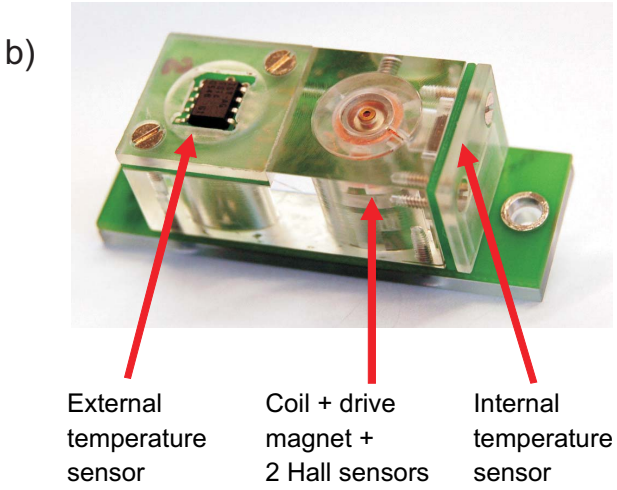

Figure 7.2: Hand-held reader (Glucorat Reader) the *in vivo* data acquisition. a) the hand-held reader, b) the measuring probe.

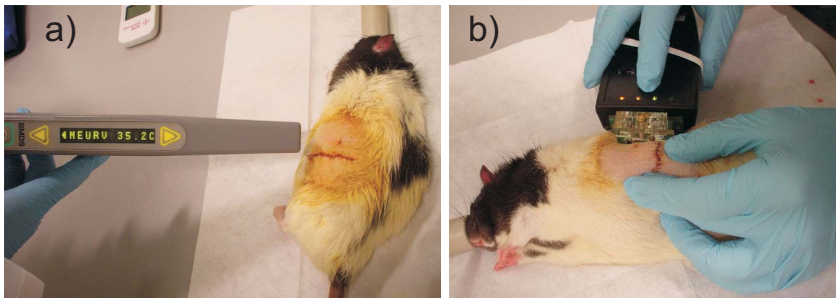

Figure 7.3: Data acquisition on implant. a) temperature acquisition from the subcutaneous transponder, b) damping factor acquisition through the skin.

7.2.3 *In vivo* data acquisition assessment

The data acquisition with the implanted sensor and the Glucorat System can suffer from misalignment when in-vivo. Therefore we studied the errors caused by misalignment on the damping factor measurement in a prior experiment. To this end, we implanted a closed capsule in a non-diabetic rat and measured its damping factor with the Glucorat System, once varying the distance between the capsule and the reader l_A (axial displacement), and once shifting the reader perpendicularly to the alignment axis l_L (lateral displacement). The results are shown in figure 7.4 and are necessary for *in vivo* measurement when a swelling appears around the implant and makes the alignment difficult. The results shows that the axial displacement must be $>$4 mm to affect the measurement, and the lateral displacement $>$2 mm. The skin of the rat being only 1-2 mm thick, the axial displacement is not an issue, but the lateral displacement is an error caused by the practitioner and needs a guiding system to be avoided. Therefore a series of guides has been designed and adapted to the Glucorat reader head. The series of guides ranges from 10 mm to 19 mm inner diameter and are shown in figure 7.5.

7.2.4 The ZDF rat

The ZDF (Zucker Diabetic Fatty) rat is an inbred rat model that, through genetic mutation and a managed diet of Purina 5008, will closely mimic human adult onset diabetes (Type 2) and related complications. When fed with a diet of Purina 5008, homozygote recessive males (fa/fa) develop obesity, hyperlipidemia, fasting hyperglycemia, and Type 2 diabetes. The ZDF rat is an accurate model for Type 2 diabetes based on impaired glucose tolerance caused by the inherited obesity gene mutation which leads to

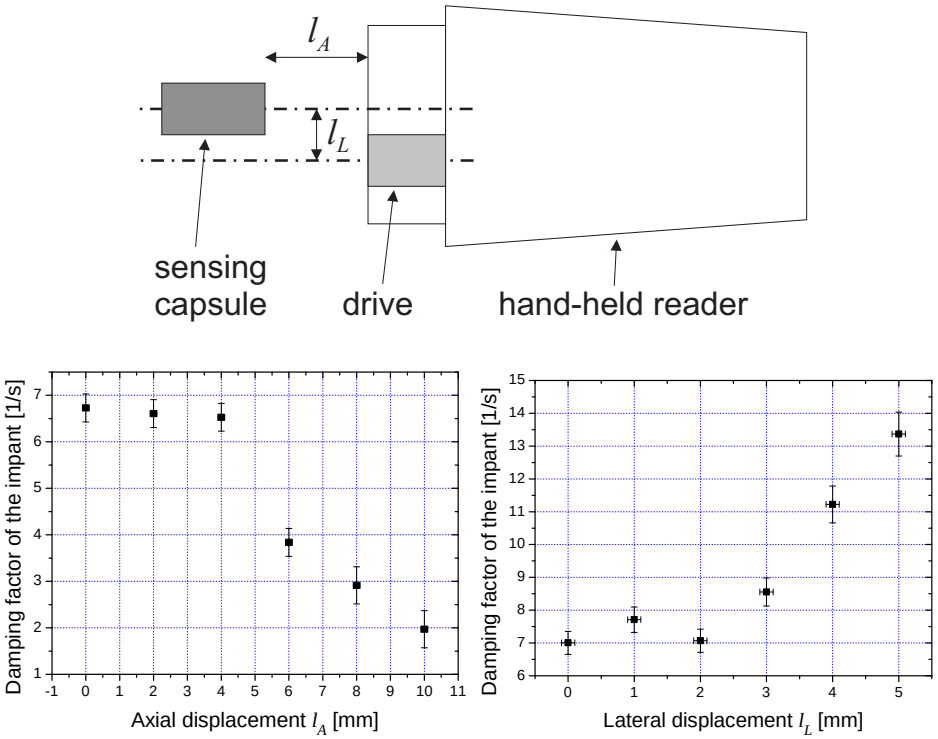

Figure 7.4: Misalignment effect on damping factor reading.

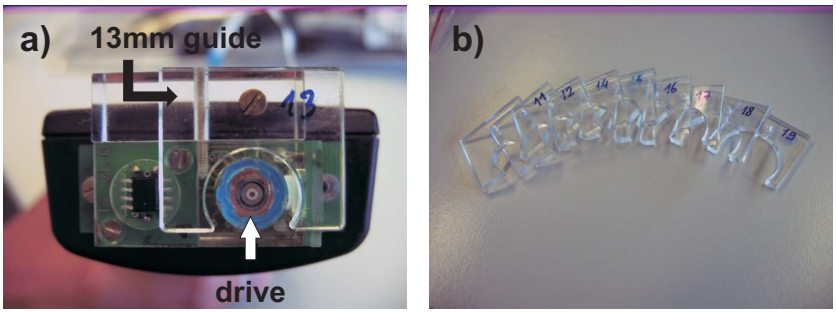

Figure 7.5: a) Glucorat Reader head with 13 mm alignment guide. b) 10 mm to 19 mm inner diameter guides.

insulin resistance[2]. We acquired the ZDF rat at the age of 4 weeks and fed it with a diet of Formulab Diet 5008 (Purina 5008 equivalent) from PMI Feeds Inc.. Formulab Diet is a high-energy and high-protein formulation diet.

The rat followup of its weight, blood glycemia, insulin injections and nutrition evolution before implantation is presented in table 7.1. As expected, the rat developed obesity and a Type 2 diabetes at the age of 8 weeks. It also showed an insulino-resistance to the injected insulin. On day 33 in table 7.1, we started the glycemia regulation test described in section 7.2.1. We tried to control the blood glycemia of the rat, but the regulation remains difficult.

7.2.5 Procedures for sensor preparation and implantation

Every step for sterilizing, assembling the sensor and implanting are listed hereafter. The following procedure are essential for the well functioning of the experiment.

Sterilization protocol:

• Demonstrator core with glued membrane in reference solution (RS) with phenol, sterilized by γ-radiation 29 kGy
• Demonstrator cap in RS with phenol, sterilized by γ-radiation 29 kGy
• Rotor, sterilized with ethanol/water (70%/30%)
• Sensitive fluid, contains 0.2 wt% phenol
• Reference solution, contains 0.2 wt% phenol
• Physiological solution 0.9% NaCl and 2 mM glucose, filtration with 0.22 μm filter

The sterilization choices have been tested and compared with other techniques. For example the sterilization by ethylene oxide vapor has been discarded because it affects the membrane coating though it is easier to deploy. And the SF cannot be sterilized by γ-radiation because both dextran and ConA are destroyed. The γ-radiation dose is given by the sterilization standard as a minimum of 25 kGy[3] according to the International Atomic Energy Agency [157]. After irradiation of the demonstrator core, the membrane had a brown coloration, see figure 7.6. It is due to the partial degradation of the phenol during the γ-radiation exposure.

Assembly protocol:

1. Fill demonstrator core with degassed SF
2. Insert rotor
3. Screw cap, slowly to avoid overpressure, keep membrane wet with degassed RS
4. Check if rotor spins without resistance with a magnetic object, if not ad-

[2]Charles River Laboratories specification sheet.
[3]The gray (symbol: Gy) is the SI unit of absorbed radiation dose.

Table 7.1: ZDF rat evolution of weight, blood glycemia (BG), injections of insulin units (IU) and periods without food (Diet).
Insulin unit definition: The activity contained in 1/22 mg of the international standard of zinc-insulin crystals.

Date	Day	Time	Weight g	BG mM	BG mg/dl	IU	Diet
13.03.2008	1	09:00	198	7.9	142.2		
17.03.2008	5	09:00	227	3.2	57.6		
20.03.2008	8	09:00	247	5.3	95.4		
25.03.2008	13	09:00	285	7.7	138.6		
27.03.2008	15	09:00	300	7.6	136.8		
01.04.2008	19	09:00	326	17.3	311.4		
04.04.2008	22	09:00	337	16.2	291.6		
06.04.2008	24	09:00	341	19	342		
07.04.2008	25	09:00	346	17	306	9	
08.04.2008	26	09:00		17.3	311.4	9	
09.04.2008	27	09:00	354	17.8	320.4	12	
10.04.2008	28	09:00	365	5.8	104.4	11	
11.04.2008	29	09:00	371	14.9	268.2	12	
12.04.2008	30	09:00	374	4.4	79.2	11	
13.04.2008	31	09:00	380	6.7	120.6	10	
14.04.2008	32	09:00	382	16.3	293.4	11	
15.04.2008	33	09:00	398	15	270		
		16:00		14	252	12	
16.04.2008	34	09:00	393	6.1	109.8		start
		10:30		5.4	97.2		at 9:30
		13:30		6.5	117		
		14:30		11.1	199.8		
		15:30		9.8	176.4		
		16:30		7.9	142.2	11	end
17.04.2008	35	09:00	402	4.8	86.4		start
17.04.2008		11:00		3.9	70.2		end
17.04.2008		16:00		10.8	194.4	12	
18.04.2008	36	09:00	416	7.5	135	12	
19.04.2008	37	16:00	397	2.6	46.8	9	
20.04.2008	38	16:00	371	2.9	52.2	8	
21.04.2008	39	10:00	371	3.4	61.2		

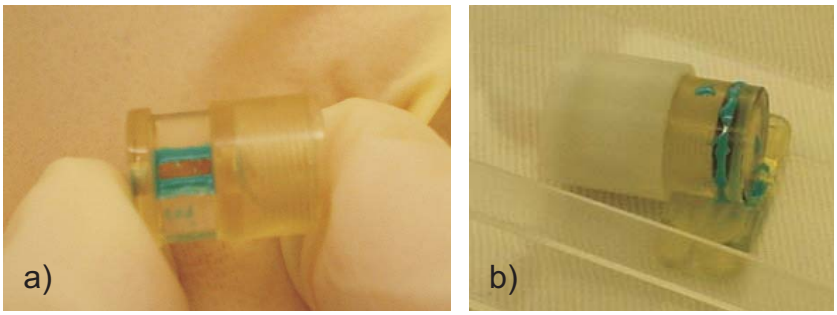

Figure 7.6: Sensor assembly. a) the body of the sensor before assembly, b) the assembled sensor right before implantation.

just cap tightening
5. Place PTFE sleeve over the demonstrator on the other side of the cap and cover the membrane opening of the core, the membrane opening is filled with degassed RS
6. Glue (Ecobond) the cap with the core and the cap overpressure hole in order to seal the demonstrator
7. Glue (Ecobond) the support onto the demonstrator
8. Wait 3h at ambient temperature for the glue to polymerize
9. Check functioning of demonstrator with reader (repeat 2-3 acquisitions)
10. Rinse the demonstrator with degassed NaCl-glucose solution just before implantation

The assembly procedure is essential to avoid drying of the membrane, and thus air bubbles formation in the sensor. The assembled sensor is shown in figure 7.6.

Implantation procedure (see figure 7.7):
11. Shave and disinfect implantation site (flank)
12. Open of the skin and fat layer in order to see the abdominal muscle of the flank
13. Stitch demonstrator onto the muscle and inject physiological solution with 2mM glucose so that the membrane remains wet
14. Stitch the opening
15. Inject subcutaneously some more physiological solution with 2mM glucose

7.3 Results and discussion

The results of the *in vivo* experiment are presented in two parts. The first part deals with the preparation, the implantation procedure of the sensor and the surgical observations. In the second part, we expose and discuss the measurements obtained with the implanted demonstrator while the

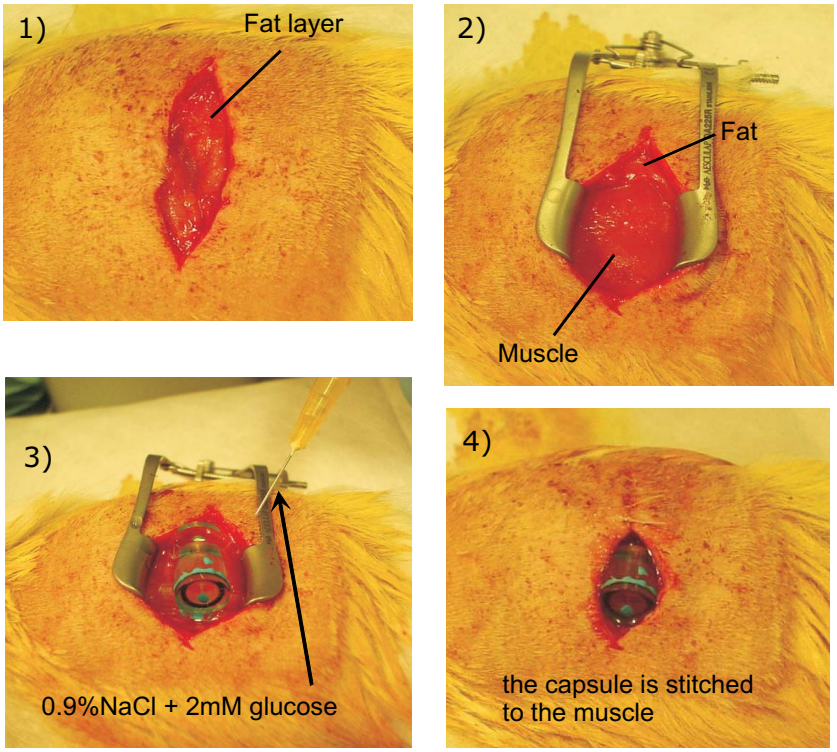

Figure 7.7: Implantation of the sensor demonstrator.

rat's glycemia evolves.

7.3.1 Preparation and implantation procedure

An important outcome of the in-vivo experimentation was to validate the preparation and implantation procedure of the sensing device. In order to prepare the in-vivo study, we have performed the necessary biocompatibility tests of different materials of which the implanted part of the sensor are composed, i.e. PMMA, the Eccobond adhesive and the SI. The biocompatibility tests implied the implantation of pieces of the materials for several weeks and an histology of surrounding tissues. The tests are still underway and hence the results are not presented in this work, and will be presented in an upcoming study. However the present results show a positive tendency and the PPEGMA coating shows an improved biocompatibility. We have also tested the different sterilization ways for each component of the implant.

The implantation of the sensor did not cause any complication (see figure 7.7). Since the ZDF rat is obese, the important fat layer needs to be spread in order to stitch the sensor to the flank muscles. After implantation, we have observed the evolution of the scar and of the swelling around the implant, as shown in figure 7.8. On day 1, the important swelling is due to the physiological solution around the implant which was injected to avoid drying the membrane as well as any air bubble appearance in the implant. We used the 14 mm guide for the measurement (see 7.2.2). On day 2, the swelling became more important. The injected physiological solution was not completely resorbed and apparently there was some inflammation due to the surgery. The handling of the sensor was thus more difficult but achievable with a 15 mm guide. It was difficult to hold the implant in such conditions, but we were able to align the reader with the sensor. With good alignment, the distance between the sensor and the reader is not an issue. Day 3, the swelling started to reduce so the sensor handling became more precise. Day 4, the swelling kept reducing so that the sensor shape under the skin started to be visible and we used the 14 mm guide. Day 5, the swelling disappeared and one sees distinctly the sensor shape under the skin. We could even use the 13 mm guide.

In addition to the body reaction to the implant, the influence of the implant on the ZDF rat was also an important point to be observed. As described above, the sensor shape became visible through the skin after three days of implantation. As long as we observed, the rat did not seem to be bothered by the implant, thus didn't eat its stitches either. Even though the size of the implant was rather large compared to the ZDF rat, it was not a disturbance for the rat. Indeed the implant was of the same thickness as the fat layer, and the protuberance it created didn't disturb the animal.

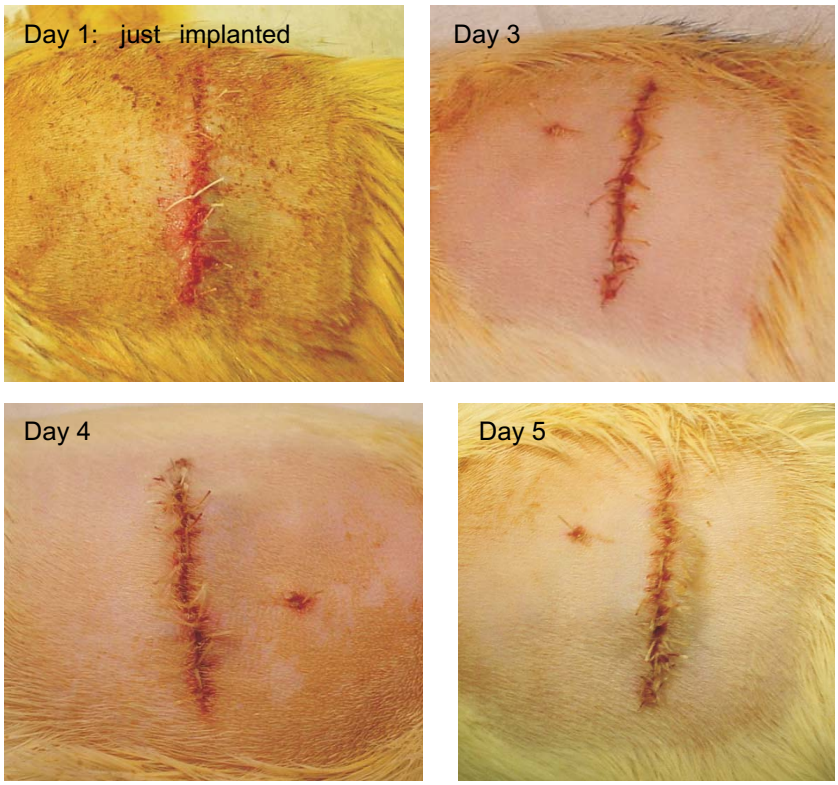

Figure 7.8: Evolution of the scar. On day 1 the important swelling was due to injection of physiological solution. Day 3, the swelling reduced so the sensor handling became more precise. Day 4, the swelling kept reducing so that one sees the sensor under the skin. Day 5, the swelling disappeared and one sees distinctly the sensor.

Finally, the implantation site did not reveal any infection or important inflammation at explantation, as depicted in figure 7.9. After explantation, we did not observe any damage of the sensor. The most fragile part of the demonstrator, the SI, was unimpaired. Finally, as shown in section 7.2.5, the SI became brownish after gamma irradiation, but this wasn't an issue since no extraordinary inflammation was observed.

7.3.2 Implanted sensor response

While the sensor demonstrator was implanted, the signal that we measured is the damping factor of the implanted capsule. As previously discussed in section 6.6, the glucose concentration cannot be systematically determined, due to the non-reproducibility of the SF characteristics and the difficulty to calibrate the damping factor to the glucose concentration. For these reasons, we plotted the inverse of the damping factor in order to have the

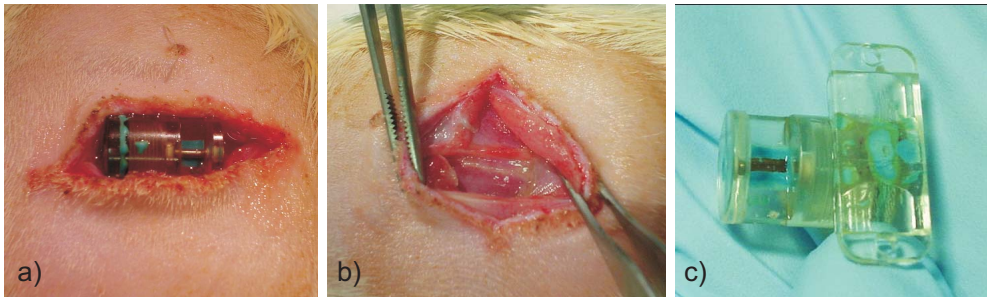

Figure 7.9: Explantation of the sensor demonstrator: a) reopening of the scar, b) there is no infection nor important inflammation, c) the sensor is unimpaired.

same trends as the glucose concentration. The signal variations were compared to blood glycemia measurements and plotted in figure 7.10. Since the measurements with the implant require an operator, and the rat to be anesthetized, the measurements have been planned as 3-4 sessions per day (see protocol in section 7.2.1). In each session, 20 measurements were performed (1 measurement/min). The plot in figure 7.10 shows the average (■) and the standard deviation (error bars) of every session.

The blood samples were taken by pricking the tail, ear or tongue of the animal and glycemia values were analyzed with a commercial blood glucose meter. The results of blood glycemia measurements are presented in figure 7.11. These measurements were not accurate, the reasons are the precision of the glucose meter, which is only of 20%, and the fact that intensive stinging on a skin area created hematomas which significantly alter the blood measurements. We measured the blood glycemia before and after each anesthesia and, in most of the cases, it was lower after the anesthesia. The anesthesia seemed to reduce the glycemia value though the isofluran can cause a temporary increase of the blood glucose[4]. On the contrary, the amoxicillin, which we administrated as anti-infectious, can reduce the glycemia value result as amoxicillin interferes in the chemical process[5]. Therefore it is difficult to determine a systematic reduction of the glycemia because the variations are due to a combination of the following factors: hematomas, drugs, anesthesia, stress, sampling site. We would need a central venous catheter, no anesthesia and no drugs in order to have reliable and comparable measurements. In figure 7.10, we chose as a reference the blood glucose measurements done before the anesthesia with the Pharmacia meter. We usually did 2-3 measurements, thus we plot the mean value and the error.

If one compares the data obtained with the sensor and the blood glu-

[4]Compendium suisse des médicaments, see Isofluran Baxter
[5]Compendium suisse des médicaments, see Amoxicillin-CIMEX

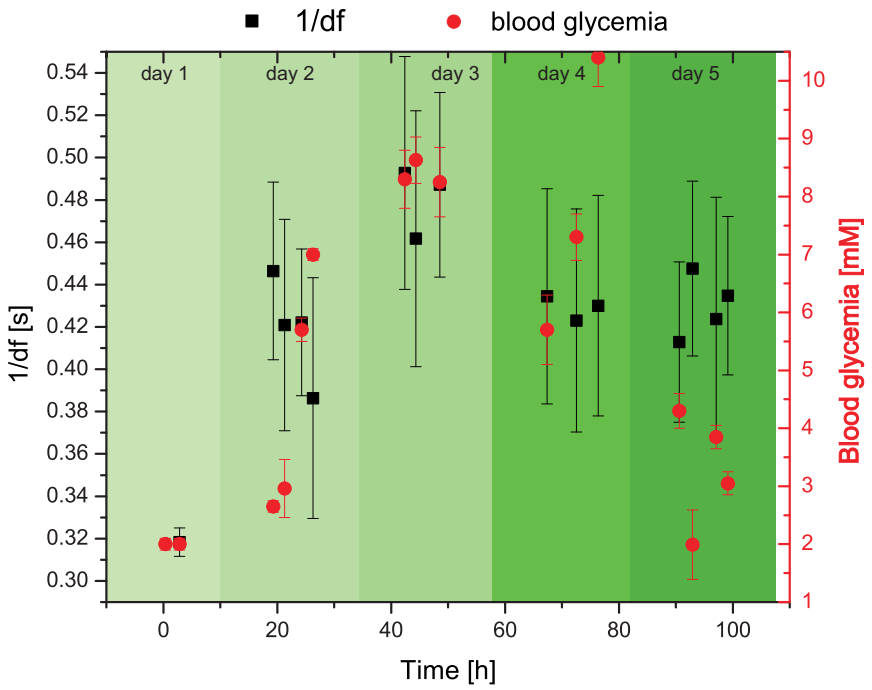

Figure 7.10: Superposition of the sensor measurements and the blood glycemia evolution.

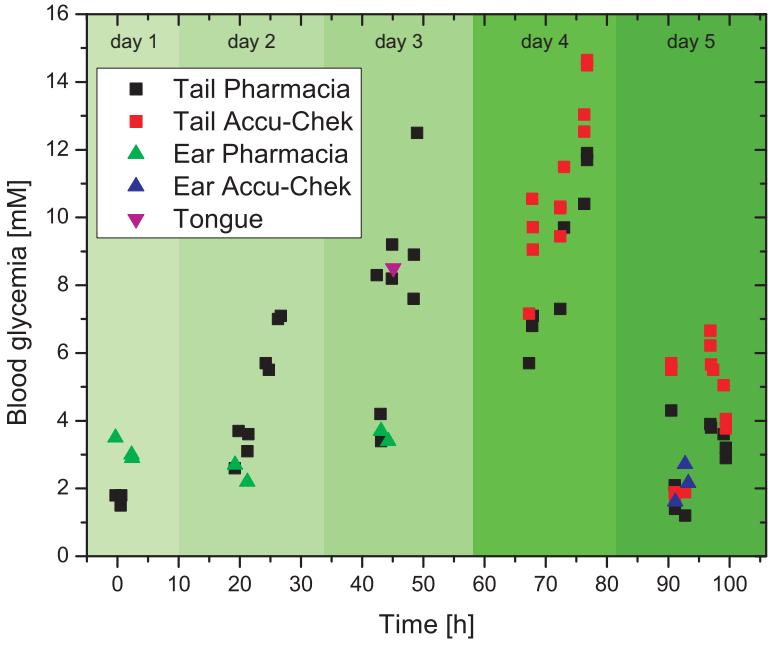

Figure 7.11: Blood glycemia measurements obtained by pricking the tail, ear or tongue. Two commercial blood glucose meters were used: the Pharmacia and the Accu-Chek.

cose measurements, we see a similar trend in the variations, see figure 7.10. These results must be interpreted cautiously. In fact the damping factor values are much lower than expected. This means that the viscosity of the SF inside the sensor is very low. There are different hypothesis to explain this low viscosity. The SF has been prepared with purified dextran and we have noticed that it is an issue regarding the viscosity reproducibility with such a preparation. Furthermore a solution can change its viscosity after a few days when stored, without changing its composition. Another hypothesis is that the ionic composition of the interstitial fluid around the sensor is different from the in-vitro experimentation. For example, the Mn^{2+} concentration is very low in the body [158]. In fact, Mn^{2+} only appears as trace element in the blood, in the order of 30 μg/l [159], but we found no data on the interstitial fluid concentration. Because of the low concentration, there is a chance that the Mn^{2+} ions leave the ConA protein. The site can be replaced by Ca^{2+} without losing the glucose affinity [93], but we don't know the effect on the viscosity of the solution. This could partially explain the drop of viscosity when the sensor was implanted. We also observed a precipitation in the batch of SF prepared for this experiment one week after dilution. It seems to resolubilize when shaken. The batch was prepared 3 days before the sensor assembly and its viscosity was much higher at this moment. There has been a drop of viscosity over 3 days which we can't explain with our current knowledge. We have less experience with the use of purified dextran 3200 kDa (PSS) than non-purified dextran 2000 kDa (Fluka). For this experiment, we wanted a low viscosity in order to make sure to be able to measure the damping factor with the reader, and to maximize the diffusion time of the glucose inside the sensor since the mixing is not continuous as *in vitro*. Right before the implantation, the SF turned out to have a lower viscosity than expected, probably due to a partial loss of activity of ConA. Another observation is that the rotor started rusting after explantation. We cannot tell if the corrosion process already started when implanted. This can also induce a loss of viscosity because it can change the pH and bring new ions in the solution. Corrosion of the rotor can also affect its rotation, but the corrosion was not sufficient at explantation. We cannot explain the deterioration of the rotor parylene coating. With the aim to quantify the decrease of viscosity with respect to a loss of ConA, we qualified a SF23P in the capillary viscometer (see figure 3.11). We observe that a loss of 25% of ConA leads to a viscosity decrease of 25 - 35% at 35°C (rat subcutaneous temperature). This shows that the leakage and/or degradation of ConA have an important impact on the viscosity. Considering all these unknown parameters, it is difficult to ensure that the variations observed with the implanted sensor are solely due to glycemia variations.

The results of day 5 show an important mismatch with the blood glycemia measurements. We know from experiments that the membrane gets fouled

after a few days of use on the sensor (see section 6.5.3). After explantation, we tested the demonstrator *in vitro* again and noticed that the membrane was fouled. This can explain the non-match for day 5.

7.3.3 Statistical analysis

As discussed previously, we cannot ensure that the observed signal variations with the implanted sensor are solely due to glucose variations. Indeed, the damping factor values are <3 and, in this range, the dependence of the damping factor as a function of the viscosity is not linear anymore and is difficult to qualify as it exhibit a high error. Therefore we proposed a statistical analysis to determine whether the signal variations are lost in the noise and to qualify the correlation between the sensor signal and the blood glycemia evolution.

7.3.3.A Correlation Test

In order to qualify the correlation between the two sets of data, one can perform a correlation test [18]. In probability theory and statistics, a correlation (measured as a correlation coefficient) indicates the strength and direction of a linear relationship between two random variables. A number of different coefficients are used for different situations. The best known is the Pearson product-moment correlation coefficient, which is obtained by dividing the covariance of the two variables by the product of their standard deviations:

$$r = \frac{1}{n}\sum_{i=1}^{n}\left(\frac{X_i - \overline{X}}{\sigma_X}\right)\left(\frac{Y_i - \overline{Y}}{\sigma_Y}\right) \tag{7.1}$$

where $\frac{X_i - \overline{X}}{\sigma_X}$, $\overline{X}$, and σ_X are the standard score, population mean, and population standard deviation (calculated using n in the denominator).

The correlation result ranges from 0.1 to 1, 0.1 being the minimum and 1 the maximum (1 indicates that the two variables analyzed are equivalent modulo scaling). When applied to both sets of data, we obtain the following result[6] :

> Pearson's product-moment correlation:
> data: sensor and blood glycemia (day 1 to 4)
> df = 225, p-value = 4.337e-06
> alternative hypothesis: true correlation is not equal to 0
> 95 percent confidence interval: 0.1762 0.4136
> sample estimates: r = 0.2995704

where df is the degree freedom and r the correlation coefficient. This result

[6]This has been done with the program R, www.r-project.org

includes only day 1 to day 4. It is clear from figure 7.10 that the data from day 5 don't match. As the preliminary analysis, we want to qualify only the data showing a correlation. A correlation of 0.3 means a small to medium correlation. The interpretation of these values is arbitrary depending on the context and purposes. Nevertheless we can conclude that we have an existing correlation between the two sets of data, blood glucose and sensor readings.

7.3.3.B Student T-test

Looking at the results on figure 7.10, one notices a grouping of the measurements per day. As described in section 7.2.4, the glycemia of the rat was regulated so that it varies from day to day. As a matter of fact, the sensor had a slow response time as described in section 6. Moreover the regular but not continuous mixing of the SF inside the sensor, as was the case for *in vitro* experiments, leads to an even slower response time. The first day, we started with a very low glycemia which increased continuously until day 3, and then was reduced on day 4. We thus proposed to compare the sensor data grouping them per day, making every day a data set, from which we can analyze the data spreading. The analysis allows us to tell if the variations from day to day are random (lost in the noise) or distinct. We applied the Student T-Test [18] which is a test of the null hypothesis that the means of two normally distributed populations are equal. Given two data sets, each characterized by its mean, standard deviation and number of data points, we can use a t-test to determine whether the means are distinct, provided that the underlying distributions can be assumed to be normal [18]. The equation for unequal sample sizes and equal variance is

$$t = \frac{\overline{X}_1 - \overline{X}_2}{\sqrt{\frac{(N_1-1)\sigma_1^2+(N_2-1)\sigma_2^2}{N_1+N_2-2}\left(\frac{1}{N_1}+\frac{1}{N_2}\right)}} \tag{7.2}$$

where $\overline{X}_i$, σ_i^2 and N_i are the mean, variance and number of participants of the two samples. The statistical significance level associated with the t value calculated in this way is the probability that, under the null hypothesis of equal means, the absolute value of t could be that large or larger just by chance.

The hypothesis required for this test are the following: a) normal distribution of data, b) equality of variances (determined by using a variance test), c) determine if samples are independent or dependent (different equations). The data grouped per day are represented in a box plot in figure 7.12. Prior to the t-tests, we performed a variance test between data sets in order to verify the hypothesis of equal variances. We chose the F-test [18] with the null hypothesis being *the equality between variances*. The p-values

are given in table 7.2. If the p-value is $> 5\%$, the test is accepted, which is the case for all cases of 7.2. The variances being equal, hypothesis b) is fulfilled for the T-tests. Hypothesis a) is also fulfilled because we have enough data to apply the central limit theorem [18], which tells us tha the sum of a large number of independent random variables each with finite mean and variance will be approximately normally distributed. Finally all couples of data sets are independent. We can thus apply the t-tests with the null hypothesis being *the means of the two normally distributed populations are equal* and the p-values are given in table 7.3. If the p-value is $< 5\%$, the test is rejected and this proves the discrimination of the means of the data sets. We can see that the means of day 2 and 3, and day 3 and 4 are distinct, whereas the means of day 2 and 4 are equal. Assuming that the sensor signal variation are coupled glucose variation, the sensor reacts to glucose variations from day 1 to day 4.

Table 7.2: p-values for the variance test (F-test). If the p-value is >5%, one can say that the variances are equal.

	day 2	day 3	day 4
day 2	1	0.4357	0.88
day 3	0.4357	1	0.5579
day 4	0.88	0.5579	1

Table 7.3: p-values for the Student T-test. If the p-value is <5%, this proves the discrimination of means of the data sets.

	day 2	day 3	day 4
day 2	1	2.692e-10	0.2096
day 3	2.692e-10	1	4.898e-07
day 4	0.2096	4.898e-07	1

7.4 Conclusion and Outlooks

The preparation and the implantation procedure of a working sensor device in a living animal were well validated. We successfully implanted the sensor demonstrator in the ZDF rat without any complication such as infection and important inflammation. The sensor shape was visible through the skin after three days of implantation which is a sign of minimal inflammation. After explantation we did not observe any damage of the sensor.

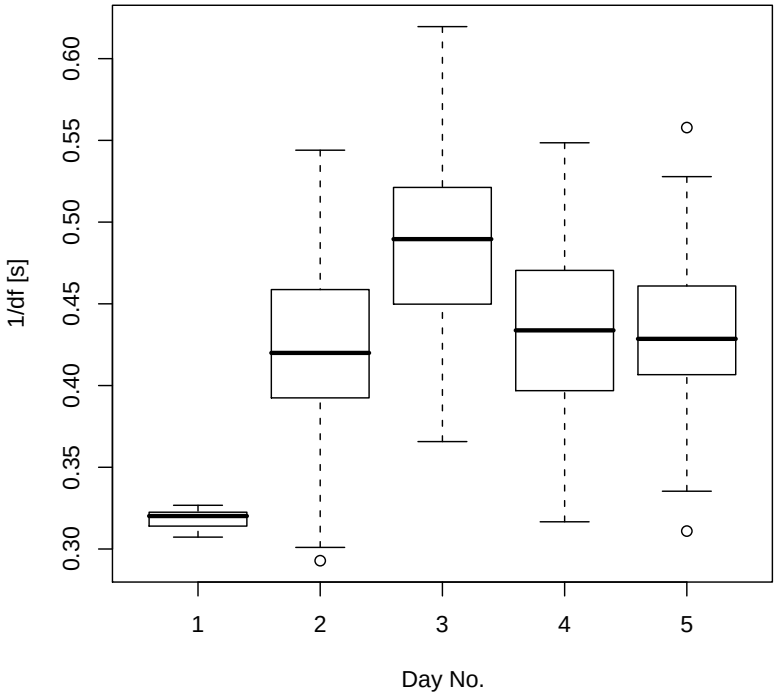

Figure 7.12: Box plot [18] of measured data per day. The center bold line represents the median. The lower and upper limits of the box are the first and third quartile and thus the box contains 50% of the distribution. The "error bar" contains 99.3% of the distribution. The closed dots indicate the outliers. The representation shows the discrimination of the data from day 3 compared to day 2 and 4.

The *in vivo* demonstration of the sensor was also successfully carried out. We could observe variations of the sensor signal corresponding to the glycemia variations, but we cannot ensure that the signal variations are solely due to glycemia variations. Several parameters needs to be better controlled. A full success can be achieved by further *in vivo* experiments.

We need to know more about the ionic variations below the skin and their effect on the SF viscosity. Detailed characterization of the sensitive solution with PSS dextran will be necessary: a) Adjustment of viscosity (by changing composition / dilution). b) Investigate the influence of much less Mn^{2+} in the reference solution.

By means of these advances, we would improve, not only the demonstrator itself, but also the blood glycemia measurements, more continuous

measurements, better knowledge on sensor response time as a function of inner mixing and a better knowledge of the SF behavior. For the next experiments, we would need a rat with a central venous catheter to get reliable blood glycemia measurements. An automated continuous measurement using the demonstrator sensor and an implantable electronics would be a must in order to study the *in vivo* response time. This would also avoid recursive anesthesia and stress to the animals since these factors influence the glycemia.

In order to get a fully working glucose sensor, the research has to be emphasized on the chemistry of the SI and the SF. The actual methods to characterize the SI allow a rough determination of the retention properties. Efforts need to be deployed on analytical chemistry to measure very slow leakage of polypeptides and polysaccharides. The permeate resulting of the leakage needs to be analyzed to determine its nature and molecular weight. The fouling of the membrane is also an issue. The SF still has unknown behaviors and its characterization with purified dextran needs to be studied in details. As a matter of fact, the micro-engineering and electronic parts of the project are sufficiently advanced at this research stage. The implantation protocol meets also the requirements.

For a long term implant, a suitable coating is needed on the entire outer surface in order to prevent an encapsulation. Because the encapsulation tissue have a threefold slower diffusion time for small species like glucose compared to regular subcutis tissue [160], which would drastically increase the lag time of glucose concentration between blood and the implant site.

Chapter 8

Conclusion

After a literature search and theoretical considerations, based on the IGLUS requirements, we selected two selective interfaces among the most actual technologies: hybrid membranes composed of a nanoporous alumina membrane coated with PPEGMA brushes and nanoporous polyethylene films, which have different advantages from each other. The presented theoretical model for the transient diffusion of a solute through membranes permitted us to quantify the membrane performance.

Both selective interfaces were characterized systematically and their selectivity to a test protein was thoroughly demonstrated. Furthermore, we highlighted the link between the diffusion rate of glucose and the protein retention threshold, which enabled us to determine the membrane performance without complex analysis. The optimized hybrid porous alumina-PPEGMA selective interface revealed sufficient retention properties of dextran and ConA in diffusion cells over 48 hours.

In a second step, we integrated the hybrid selective interface to a newer IGLUS demonstrator in order to investigate the performance of the hybrid selective interface under an environment mimicking the real working condition of the sensor. The integrated IGLUS demonstrator showed its good ability to respond to glucose variations *in vitro*, and we transferred all the knowledge obtained from *in vitro* experiments to *in vivo* experimentation. The *in vivo* test was carried out over 5 days in a rat model, and the implantation as well as the transcutaneous data acquisition were successfully demonstrated. On the other hand, there are still many points to be improved. One of the most important hurdle to overcome is the sensitive fluid. The assessment of the selective interface on the IGLUS demonstrator is currently limited by the performance of the sensitive fluid. For realization of a long-term implant, a suitable coating is needed on the entire outer surface in order to prevent any encapsulation, which should be achievable once such materials are available.

The technologies for a selective interface which we investigated are not restricted to the glucose-sensitive fluid composed of dextran and ConA.

Indeed the actual well-known chemicals capable of selectively recognize D-glucose are ConA and boronic acid, and a sensitive fluid containing boronic acid may also be used for our system.

We have developed a characterization procedure of the selective interface for the IGLUS, experimentally and by theoretical analysis, which now offers a solid basis for the realization of a long-term implantable continuous glucose sensor. We believe to have paved an important part of the road to a working device.

Chapter 9

Acronyms and Glossary

AAO	Anodic Aluminium Oxide.
BSA	Bovine Serum Albumin.
CA	Cellulose Acetate.
CE	Cellulose Ester.
CGM	Continuous Glucose Monitoring.
ConA	Concanavalin A.
IF	Interstitial Fluid.
IGLUS	Implantable GLUcose Sensor.
MALDI	Matrix-Assisted Laser Desorption/Ionization.
MW	Molecular Weight.
MWCO	Molecular Weight Cut-Off.
PE	PolyEthylene.
PEG	PolyEthylene Glycol.
PES	PolyEtherSulfone.
PET	PolyEthylene Terephtalate.
PMMA	Poly(Methyl MethAcrylate).
PPEGMA	Poly PolyEthylene Glycol MethAcrylate.
PS	PolySlufone.
PSS	Polymer Standard Service GmbH.
PTFE	PolyTetraFluoroEthylene.
PVDF	PolyVinyliDene Fluoride.
RC	Regenerated Cellulose.
RF	Radio Frequency.
rI	refraction Index.
RS	Reference Solution.
SEC	Size-Exclusion Chromatography.
SEM	Scanning Electron Microscopy.
SF	Sensitive Fluid.
SITEM	Simplified In-viTro Environment Model.
TEM	Transmission Electron Microscopy.
ZDF	Zucker Diabetic Fatty.

$c(x,t)$	Concentration as a function of position and time $[M]$
$\Delta c(t)$	Concentration difference between the two chambers as a function of time $[M]$
D	Bulk diffusion coefficient $[\frac{mm^2}{s}]$
D_e	Effective diffusivity $[\frac{mm^2}{s}]$
D_m	Modified diffusion coefficient $[\frac{mm^2}{s}]$
K	Partition coefficient $[n.u.]$
k	Partitioning coefficient $[n.u.]$
l	Thickness of selective interface $[mm]$
l_c	Chambers depth of the diffusion cell $[mm]$
S	Surface of selective interface $[mm^2]$
V_a	Volume of chamber A $[mm^3]$
V_b	Volume of chamber B $[mm^3]$
ϕ	Porosity $[n.u.]$
v_0	Bulk molar volume $[\frac{m^3}{mol}]$
v	Molar volume $[\frac{m^3}{mol}]$
τ_1	Relaxation time of quasistationary case $[s]$

Bibliography

[1] H. E. Koschwanez and W. M. Reichert. In vitro, in vivo and post explantation testing of glucose-detecting biosensors: Current methods and recommendations. *Biomaterials*, 28(25):3687–3703, 2007. xi, 14

[2] L. Kuhn. Biosensors: Blockbuster or bomb? electrochemical biosensors for diabetes monitoring. *The Electrochemical Society Interface*, 7(4):26–31, 1998. xi, 15

[3] C. E. Ioan, T. Aberle, and W. Burchard. Structure properties of dextran. 2. dilute solution. *Macromolecules*, 33(15):5730–5739, 2000. xii, 29, 32, 34, 37

[4] G. M. Bradbrook, T. Gleichmann, S. J. Harrop, J. Habash, J. Raftery, J. Kalb, J. Yariv, I. H. Hillier, and J. R. Helliwell. X-ray and molecular dynamics studies of concanavalin-a glucoside and mannoside complexes - relating structure to thermodynamics of binding. *Journal of the Chemical Society-Faraday Transactions*, 94(11):1603–1611, 1998. xii, 33, 35, 36

[5] D. G. Castner and B. D. Ratner. Biomedical surface science: Foundations to frontiers. *Surface Science*, 500(1-3):28–60, 2002. xiii, 46, 47

[6] R. van Reis and A. Zydney. Bioprocess membrane technology. *Journal of Membrane Science*, 297(1-2):16–50, 2007. xiii, 56, 58, 59, 66

[7] Richard W. Baker. *Membrane technology and applications*. Wiley, Chichester, 2nd edition, 2004. xiii, 56

[8] W. M. Deen. Hindered transport of large molecules in liquid-filled pores. *Aiche Journal*, 33(9):1409–1425, 1987. xiii, 57, 58

[9] Leos J. Zeman and Andrew L. Zydney. *Microfiltration and ultrafiltration principles and applications*. Dekker, New York Basel etc., 1996. xiii, xix, 54, 55, 59, 61, 63, 68, 74

[10] P. Apel. Track etching technique in membrane technology. *Radiation Measurements*, 34(1-6):559–566, 2001. xiii, 65, 66

[11] T. Van Gestel, C. Vandecasteele, A. Buekenhoudt, C. Dotremont, J. Luyten, B. Van der Bruggen, and G. Maes. Corrosion properties

of alumina and titania nf membranes. *Journal of Membrane Science*, 214(1):21–29, 2003. xiii, 66, 67

[12] H. D. Tong, H. V. Jansen, V. J. Gadgil, C. G. Bostan, E. Berenschot, C. J. M. van Rijn, and M. Elwenspoek. Silicon nitride nanosieve membrane. *Nano Letters*, 4(2):283–287, 2004. xiii, 66, 69

[13] A. Carbonaro, R. Walczak, P. M. Calderale, and M. Ferrari. Nanopore silicon membrane characterization by diffusion and electrical resistance. *Journal of Membrane Science*, 241(2):249–255, 2004. xiii, 66, 69

[14] F. Keller, M. S. Hunter, and D. L. Robinson. Structural features of oxide coatings on aluminium. *Journal of the Electrochemical Society*, 100(9):411–419, 1953. xiv, 71

[15] A. T. Shawaqfeh and R. E. Baltus. Growth kinetics and morphology of porous anodic alumina films formed using phosphoric acid. *Journal of the Electrochemical Society*, 145(8):2699–2706, 1998. xiv, 71

[16] Y. Zhao, M. Chen, Y. Zhang, T. Xu, and W. Liu. A facile approach to formation of through-hole porous anodic aluminum oxide film. *Materials Letters*, 59:40–43, 2005. xiv, 72

[17] H. Uehara, T. Yoshida, M. Kakiage, T. Yamanobe, T. Komoto, K. Nomura, K. Nakajima, and M. Matsuda. Nanoporous polyethylene film prepared from bicontinuous crystalline/amorphous structure of block copolymer precursor. *Macromolecules*, 39(12):3971–3974, 2006. xiv, 65, 75, 76

[18] Stephan Morgenthaler. *Introduction à la statistique*. Presses polytechniques et universitaires romandes, Lausanne, 2e éd. revue et corr. edition, 2001. xvii, 147, 148, 149, 150

[19] N. Wisniewski and M. Reichert. Methods for reducing biosensor membrane biofouling. *Colloids and Surfaces B-Biointerfaces*, 18(3-4):197–219, 2000. xix, 46, 48

[20] S. W. Lee, H. Shang, R. T. Haasch, V. Petrova, and G. U. Lee. Transport and functional behaviour of poly(ethylene glycol)-modified nanoporous alumina membranes. *Nanotechnology*, 16(8):1335–1340, 2005. xix, 68, 72, 92, 105, 106

[21] B. Buckingham. Clinical overview of continuous glucose monitoring. *Journal of Diabetes Science and Technology*, 2(2):300–306, 2008. 9

[22] Simon Kuenzi. *Implantable glucose sensor an approach based on a rotating microviscometer combined with a sensitive liquid containing dextran and Concanavalin A*. PhD thesis, EPFL, 2007. 10, 27, 29, 40, 111, 117, 134

[23] T. Koschinsky and L. Heinemann. Sensors for glucose monitoring: technical and clinical aspects. *Diabetes-Metabolism Research and Reviews*, 17(2):113–123, 2001. 13

[24] D. C. Klonoff. Noninvasive blood glucose monitoring. *Diabetes Care*, 20(3):433–437, 1997. 16

[25] M. Rohrscheib, R. Robinson, and R. P. Eaton. Non-invasive glucose sensors and improved informatics - the future of diabetes management. *Diabetes Obesity & Metabolism*, 5(5):280–284, 2003. 16

[26] M. A. Rabinovitch, C. P. Rose, G. Chartrand, J. L. Rouleau, D. M. Wieland, L. Lepanto, L. Rosenthall, and J. H. Burgess. Noninvasive detection of cardiac sympathetic neuronal dysfunction in chronic volume-overload heart-failure. *Clinical and Investigative Medicine-Medecine Clinique Et Experimentale*, 9(3):B54–B54, 1986. 16

[27] R. Rawer, W. Stork, and C. F. Kreiner. Non-invasive polarimetric measurement of glucose concentration in the anterior chamber of the eye. *Graefes Archive for Clinical and Experimental Ophthalmology*, 242(12):1017–1023, 2004. 16

[28] R. R. Ansari, S. Bockle, and L. Rovati. New optical scheme for a polarimetric-based glucose sensor. *Journal of Biomedical Optics*, 9(1):103–115, 2004. 16

[29] S. T. Pan, H. Chung, M. A. Arnold, and G. W. Small. Near-infrared spectroscopic measurement of physiological glucose levels in variable matrices of protein and triglycerides. *Analytical Chemistry*, 68(7):1124–1135, 1996. 16

[30] I. Gabriely, R. Wozniak, M. Mevorach, J. Kaplan, Y. Aharon, and H. Shamoon. Performance of a novel near-infrared (nir) transcutaneous glucose (g) monitor during hypoglycemia. *Diabetes*, 48:A99–A99, 1999. 16

[31] M. Ren and M. A. Arnold. Comparison of multivariate calibration models for glucose, urea, and lactate from near-infrared and raman spectra. *Analytical and Bioanalytical Chemistry*, 387(3):879–888, 2007. 16, 17

[32] K. Maruo, T. Oota, M. Tsurugi, T. Nakagawa, H. Arimoto, M. Hayakawa, M. Tamura, Y. Ozaki, and Y. Yamada. Noninvasive near-infrared blood glucose monitoring using a calibration model built by a numerical simulation method: Trial application to patients in an intensive care unit. *Applied Spectroscopy*, 60(12):1423–1431, 2006. 16

[33] A. M. K. Enejder, T. G. Scecina, J. Oh, M. Hunter, W. C. Shih, S. Sasic, G. L. Horowitz, and M. S. Feld. Raman spectroscopy for noninvasive glucose measurements. *Journal of Biomedical Optics*, 10(3):–, 2005. 16

[34] J. Chaiken, W. Finney, P. E. Knudson, R. S. Weinstock, M. Khan, R. J. Bussjager, D. Hagrman, P. Hagrman, Y. W. Zhao, C. M. Peterson, and K. Peterson. Effect of hemoglobin concentration variation on the accuracy and precision of glucose analysis using tissue modulated, noninvasive, in vivo raman spectroscopy of human blood: a small clinical study. *Journal of Biomedical Optics*, 10(3):–, 2005. 16

[35] J. L. Lambert, C. C. Pelletier, and M. Borchert. Glucose determination in human aqueous humor with raman spectroscopy. *Journal of Biomedical Optics*, 10(3):–, 2005. 16

[36] D. A. Stuart, J. M. Yuen, N. S. O. Lyandres, C. R. Yonzon, M. R. Glucksberg, J. T. Walsh, and R. P. Van Duyne. In vivo glucose measurement by surface-enhanced raman spectroscopy. *Analytical Chemistry*, 78(20):7211–7215, 2006. 16

[37] R. Weiss, Y. Yegorchikov, A. Shusterman, and I. Raz. Noninvasive continuous glucose monitoring using photoacoustic technology - results from the first 62 subjects. *Diabetes Technology & Therapeutics*, 9(1):68–74, 2007. 16

[38] K. M. Quan, G. B. Christison, H. A. Mackenzie, and P. Hodgson. Glucose determination by a pulsed photoacoustic technique - an experimental-study using a gelatin-based tissue phantom. *Physics in Medicine and Biology*, 38(12):1911–1922, 1993. 16

[39] H. A. MacKenzie, H. S. Ashton, S. Spiers, Y. C. Shen, S. S. Freeborn, J. Hannigan, J. Lindberg, and P. Rae. Advances in photoacoustic noninvasive glucose testing. *Clinical Chemistry*, 45(9):1587–1595, 1999. 16

[40] G. B. Christison and H. A. Mackenzie. Laser photoacoustic determination of physiological glucose-concentrations in human whole-blood. *Medical & Biological Engineering & Computing*, 31(3):284–290, 1993. 16

[41] D. Argaman, S. Ashkenazi, L. Greenberg, and I. Raz. Evaluation of a new photoacoustic non-invasive continuous glucose monitor. *Diabetologia*, 46:A309–A309, 2003. 16

[42] K. V. Larin, M. S. Eledrisi, M. Motamedi, and R. O. Esenaliev. Noninvasive blood glucose monitoring with optical coherence tomography - a pilot study in human subjects. *Diabetes Care*, 25(12):2263–2267, 2002. 16

[43] K. V. Larin, M. Motamedi, T. V. Ashitkov, and R. O. Esenaliev. Specificity of noninvasive blood glucose sensing using optical coherence tomography technique: a pilot study. *Physics in Medicine and Biology*, 48(10):1371–1390, 2003. 16

[44] M. Schurman, W. Shakespeare, R. G. Wilkins, L. Merkle, D. Herr, and R. Wilson. Initial validation of optical coherence tomography based sensor for monitoring of blood glucose levels. *Critical Care Medicine*, 33(12):A73–A73, 2005. 16

[45] A. Caduff, C. Kapitza, R. Dewarrat, E. Hirt, and L. Heinemann. Non-invasive, continuous glucose monitoring system based on impedance spectroscopy: A proof of concept study. *Diabetologia*, 45:A279–A279, 2002. 16

[46] A. Caduff, F. Dewarrat, M. Talary, G. Stalder, L. Heinemann, and Y. Feldman. Non-invasive glucose monitoring in patients with diabetes: A novel system based on impedance spectroscopy. *Biosensors & Bioelectronics*, 22(5):598–604, 2006. 16

[47] C. Tlili, K. Reybier, A. Geloen, L. Ponsonnet, C. Martelet, H. Ben Ouada, M. Lagarde, and N. Jaffrezic-Renault. Fibroblast cells: A sensing bioelement for glucose detection by impedance spectroscopy. *Analytical Chemistry*, 75(14):3340–3344, 2003. 16

[48] G. Rao, P. Glikfeld, and R. H. Guy. Reverse iontophoresis - development of a noninvasive approach for glucose monitoring. *Pharmaceutical Research*, 10(12):1751–1755, 1993. 17

[49] G. Rao, R. H. Guy, P. Glikfeld, W. R. LaCourse, L. Leung, J. Tamada, R. O. Potts, and N. Azimi. Reverse iontophoresis: Noninvasive glucose monitoring in vivo in humans. *Pharmaceutical Research*, 12(12):1869–1873, 1995. 17

[50] R. O. Potts, J. A. Tamada, and M. J. Tierney. Glucose monitoring by reverse iontophoresis. *Diabetes-Metabolism Research and Reviews*, 18:S49–S53, 2002. 17

[51] A. Sieg, R. H. Guy, and M. B. A. Delgado-Charro. Reverse iontophoresis for noninvasive glucose monitoring: The internal standard concept. *Journal of Pharmaceutical Sciences*, 92(11):2295–2302, 2003. 17

[52] J. C. Pickup, F. Hussain, N. D. Evans, and N. Sachedina. In vivo glucose monitoring: the clinical reality and the promise. *Biosensors & Bioelectronics*, 20(10):1897–1902, 2005. 17

[53] P. Abel, U. Fischer, E. Salzsieder, and E. Brunstein. The amperometric estimation of interstitial glucose-concentration - how to interpret the electrode signal. *Diabetologia*, 30(7):A492–A492, 1987. 17

[54] B. P. Kovatchev, L. A. Gonder-Frederick, D. J. Cox, and W. L. Clarke. Evaluating the accuracy of continuous glucose-monitoring sensors. *Diabetes Care*, 27(8):1922–1928, 2004. 17

[55] W. L. Clarke, S. Anderson, L. Farhy, M. Breton, L. Gonder-Frederick, D. Cox, and B. Kovatchev. Evaluating the clinical accuracy of two continuous glucose sensors using continuous glucose-error grid analysis. *Diabetes Care*, 28(10):2412–2417, 2005. 17

[56] V. R. Kondepati and H. M. Heise. Recent progress in analytical instrumentation for glycemic control in diabetic and critically ill patients. *Analytical and Bioanalytical Chemistry*, 388(3):545–563, 2007. 18

[57] R. Ballerstadt, A. Polak, A. Beuhler, and J. Frye. In vitro long-term performance study of a near-infrared fluorescence affinity sensor for glucose monitoring. *Biosensors & Bioelectronics*, 19(8):905–914, 2004. 19

[58] R. Ballerstadt and J. S. Schultz. A fluorescence affinity hollow fiber sensor for continuous transdermal glucose monitoring. *Analytical Chemistry*, 72(17):4185–4192, 2000. 19

[59] A. Pasic, H. Koehler, L. Schaupp, T. R. Pieber, and I. Klimant. Fiber-optic flow-through sensor for online monitoring of glucose. *Analytical and Bioanalytical Chemistry*, 386(5):1293–1302, 2006. 19

[60] A. Pasic, H. Koehler, I. Klimant, and L. Schaupp. Miniaturized fiber-optic hybrid sensor for continuous glucose monitoring in subcutaneous tissue. *Sensors and Actuators B-Chemical*, 122(1):60–68, 2007. 19

[61] R. A. M. Receveur, F. W. Lindemans, and N. F. de Rooij. Microsystem technologies for implantable applications. *Journal of Micromechanics and Microengineering*, 17(5):R50–R80, 2007. 22

[62] Y. J. Zhao, S. Q. Li, A. Davidson, B. Z. Yang, Q. Wang, and Q. Lin. A mems viscometric sensor for continuous glucose monitoring. *Journal of Micromechanics and Microengineering*, 17(12):2528–2537, .2007. 22, 35

[63] M. Lei, A. Baldi, E. Nuxoll, R. A. Siegel, and B. Ziaie. A hydrogel-based implantable micromachined transponder for wireless glucose measurement. *Diabetes Technol Ther*, 8(1):112–22, 2006. 22, 48, 129

[64] F. Zhang, X. H. Liu, C. F. Pan, and J. Zhu. Nano-porous anodic aluminium oxide membranes with 6-19 nm pore diameters formed by a low-potential anodizing process. *Nanotechnology*, 18(34):–, 2007. 25, 37, 68

[65] S. Straessler, P. Ryser, K. Ganz, J. Jacot, and S. Strassler. Implantable blood glucose concentration sensor and instrument for diabetics, detects viscosity change in sensitive fluid in ampule, when glucose permeates into it, WO2004037079-A1 06 May 2004 A61B-005/00 200436 2004. 25

[66] R. Ballerstadt and R. Ehwald. Suitability of aqueous dispersions of dextran and concanavalin-a for glucose sensing in different variants of the affinity sensor. *Biosensors & Bioelectronics*, 9(8):557–567, 1994. 25, 30, 130

[67] M. S. Boyne, D. M. Silver, J. Kaplan, and C. D. Saudek. Timing of changes in interstitial and venous blood glucose measured with a continuous subcutaneous glucose sensor. *Diabetes*, 52(11):2790–2794, 2003. 26

[68] Goldstei.Ij, Hollerma.Ce, and E. E. Smith. Protein-carbohydrate interaction .2. inhibition studies on interaction of concanavalin a with polysaccharides. *Biochemistry*, 4(5):876–&, 1965. 29, 33

[69] J. Schultz and G. Sims. Affinity sensors for individual metabolites. *Biotechnol. Bioeng. Symp.*, 9:65–71, 1979. 30

[70] J. S. Schultz, S. Mansouri, and I. J. Goldstein. Affinity sensor - a new technique for developing implantable sensors for glucose and other metabolites. *Diabetes Care*, 5(3):245–253, 1982. 30

[71] U. Beyer and R. Ehwald. Compensation of temperature and concanavalin a concentration effects for glucose determination by the viscometric affinity assay. *Biotechnology Progress*, 16(6):1119–1123, 2000. 30

[72] John McMurry. *Organic chemistry*. Brooks/Cole, Pacific Grove, California, second edition, 1988. 31

[73] R. J. Dimler, I. A. Wolff, J. W. Sloan, and C. E. Rist. Interpretation of periodate oxidation data on degraded dextran. *Journal of the American Chemical Society*, 77(24):6568–6573, 1955. 32

[74] L. H. Arond and H. P. Frank. Molecular weight, molecular weight distribution and molecular size of a native dextran. *Journal of Physical Chemistry*, 58(11):953–957, 1954. 32

[75] D. Kim, J. F. Robyt, S. Y. Lee, J. H. Lee, and Y. M. Kim. Dextran molecular size and degree of branching as a function of sucrose concentration, ph, and temperature of reaction of leuconostoc mesenteroides b-512fmcm dextransucrase. *Carbohydrate Research*, 338(11):1183–1189, 2003. 32

[76] J. B. Sumner. The globulins of the jack bean, canavalia ensiformis. *Journal of Biological Chemistry*, 37(1):137–U1, 1919. 33

[77] B. A. Cunningham, J. L. Wang, M. J. Waxdal, and G. M. Edelman. Covalent and 3-dimensional structure of concanavalin-a .2. amino-acid sequence of cyanogen-bromide fragment f3. *Journal of Biological Chemistry*, 250(4):1503–1512, 1975. 33

[78] J. W. Becker, G. N. Reeke, J. L. Wang, B. A. Cunningham, and G. M. Edelman. Covalent and 3-dimensional structure of concanavalin-a .3. structure of monomer and its interactions with metals and saccharides. *Journal of Biological Chemistry*, 250(4):1513–1524, 1975. 33, 37

[79] G. N. Reeke, J. W. Becker, and G. M. Edelman. Covalent and 3-dimensional structure of concanavalin-a .4. atomic coordinates, hydrogen-bonding, and quaternary structure. *Journal of Biological Chemistry*, 250(4):1525–1547, 1975. 33, 35

[80] R. D. Poretz and Goldstei.Ij. An examination of topography of saccharide binding sites of concanavalin-a and of forces involved in complexation. *Biochemistry*, 9(14):2890–&, 1970. 33

[81] A. J. Kalb and A. Lustig. Molecular weight of concanavalin a. *Biochimica Et Biophysica Acta*, 168(2):366–&, 1968. 33

[82] A. J. Kalb and A. Levitzki. Metal-binding sites of concanavalin a and their role in binding of alpha-methyl d-glucopyranoside. *Biochemical Journal*, 109(4):669–&, 1968. 33

[83] J. L. Wang, Cunningh.Ba, and G. M. Edelman. Unusual fragments in subunit structure of concanavalin-a (gel electrophoresis/molecular weights). *Proceedings of the National Academy of Sciences of the United States of America*, 68(6):1130–&, 1971. 33, 106

[84] G. M. Edelman, G. N. Reeke, J. L. Wang, M. J. Waxdal, J. W. Becker, and Cunningh.Ba. Covalent and 3-dimensional structure of concanavalin-a. *Proceedings of the National Academy of Sciences of the United States of America*, 69(9):2580–&, 1972. 33, 35, 37

[85] G. H. Mckenzie and W. H. Sawyer. Binding of carbohydrate to concanavalin a dimer and tetramer. *Proceedings of the Australian Biochemical Society*, 5(Nmay):38–&, 1972. 35

[86] G. H. Mckenzie, W. H. Sawyer, and L. W. Nichol. Molecular-weight and stability of concanavalin-a. *Biochimica Et Biophysica Acta*, 263(2):283–&, 1972. 35

[87] D. F. Senear and D. C. Teller. Thermodynamics of concanavalin-a dimer-tetramer self-association - sedimentation equilibrium studies. *Biochemistry*, 20(11):3076–3083, 1981. 35

[88] F. J. Lopez-Jaramillo, L. A. Gonzalez-Ramirez, A. Albert, F. Santoyo-Gonzalez, A. Vargas-Berenguel, and F. Otalora. Structure of concanavalin a at ph 8: bound solvent and crystal contacts. *Acta Crystallographica Section D-Biological Crystallography*, 60:1048–1056, 2004. 35

[89] G. R. Gunther, J. L. Wang, I. Yahara, Cunningh.Ba, and G. M. Edelman. Concanavalin a derivatives with altered biological-activities. *Proceedings of the National Academy of Sciences of the United States of America*, 70(4):1012–1016, 1973. 35

[90] G. Entlicher, J. V. Kostir, and J. Kocourek. Studies on phytohemagglutinins .8. isoelectric point and multiplicity of purified concanavalin-a. *Biochimica Et Biophysica Acta*, 236(3):795–&, 1971. 35

[91] J. B. Sumner and S. F. Howell. The role of divalent metals in the reversible inactivation of jack bean hemagglutinin. *Journal of Biological Chemistry*, 115(2):582–588, 1936. 35

[92] J. W. Becker, G. N. Reeke, B. A. Cunningham, and G. M. Edelman. New evidence on location of saccharide-binding site of concanavalin-a. *Nature*, 259(5542):406–409, 1976. 35

[93] R. D. Brown, C. F. Brewer, and S. H. Koenig. Conformation states of concanavalin a - kinetics of transitions induced by interaction with mn2+ and ca2+ ions. *Biochemistry*, 16(17):3883–3896, 1977. 36, 146

[94] J. Bouckaert, F. Poortmans, L. Wyns, and R. Loris. Sequential structural changes upon zinc and calcium binding to metal-free concanavalin a. *Journal of Biological Chemistry*, 271(27):16144–16150, 1996. 36

[95] S. H. Koenig, C. F. Brewer, and R. D. Brown. Conformation as determinant of saccharide binding in concanavalin a - ca2+-concanavalin-a complexes. *Biochemistry*, 17(20):4251–4260, 1978. 36, 37

[96] J. Bouckaert, Y. Dewallef, F. Poortmans, L. Wyns, and R. Loris. The structural features of concanavalin a governing non-proline peptide isomerization. *Journal of Biological Chemistry*, 275(26):19778–19787, 2000. 36, 37

[97] C. F. Brewer, R. D. Brown, and S. H. Koenig. Stoichiometry of manganese and calcium-ion binding to concanavalin-a. *Biochemistry*, 22(15):3691–3702, 1983. 37

[98] J. C. Zahnley. Effects of manganese and calcium on conformational stability of concanavalin-a - a differential scanning calorimetric study. *Journal of Inorganic Biochemistry*, 15(1):67–78, 1981. 37

[99] F. P. Schwarz. Thermodynamics of metal cation-binding to apoconcanavalin-a. *Journal of Inorganic Biochemistry*, 52(1):1–16, 1993. 37

[100] J. B. Sumner and S. F. Howell. The identification of the hemagglutinin of the jack bean with concanavalin a. *Journal of Bacteriology*, 32(2):227–237, 1936. 37

[101] N. M. Young. Magnesium as a natural substitute for manganese in concanavalin-a and other lectins. *Febs Letters*, 161(2):247–250, 1983. 37

[102] J. Bouckaert, F. Poortmans, and L. Wyns. Concanavalin a crystallized in complex with the trisaccharide 3,6-di-o-methyl-(alpha-d-mannopyranosyl)-alpha-d-mannopyranoside. *Acta Crystallographica Section D-Biological Crystallography*, 52:879–881, 1996. 37

[103] J. N. Sanders, S. A. Chenoweth, and F. P. Schwarz. Effect of metal ion substitutions in concanavalin a on the binding of carbohydrates and on thermal stability. *Journal of Inorganic Biochemistry*, 70(2):71–82, 1998. 37

[104] J. A. Sophianopoulos, A. J. Sophianopoulos, and W. C. Macmahon. Manganese, calcium, and saccharide binding to concanavalin-a, as studied by ultrafiltration. *Archives of Biochemistry and Biophysics*, 223(2):350–359, 1983. 37

[105] A. J. Sophianopoulos and J. A. Sophianopoulos. Effect of the conformation of concanavalin-a on its affinity for manganous ion. *Archives of Biochemistry and Biophysics*, 246(2):572–580, 1986. 37

[106] R. Netrabukkana, K. Lourvanij, and G. L. Rorrer. Diffusion of glucose and glucitol in microporous and mesoporous silicate aluminosilicate catalysts. *Industrial & Engineering Chemistry Research*, 35(2):458–464, 1996. 37, 67

[107] N. Wisniewski, F. Moussy, and W. M. Reichert. Characterization of implantable biosensor membrane biofouling. *Fresenius Journal of Analytical Chemistry*, 366(6-7):611–621, 2000. 46, 48

[108] S. Tugulu and H. A. Klok. Stability and nonfouling properties of poly(poly(ethylene glycol) methacrylate) brushes-under cell culture conditions. *Biomacromolecules*, 9(3):906–912, 2008. 48, 74

[109] S. S. Praveen, R. Hanumantha, J. M. Belovich, and B. L. Davis. Novel hyaluronic acid coating for potential use in glucose sensor design. *Diabetes Technol Ther*, 5(3):393–9, 2003. 48, 92, 105, 106

[110] R. van Reis, J. M. Brake, J. Charkoudian, D. B. Burns, and A. L. Zydney. High-performance tangential flow filtration using charged membranes. *Journal of Membrane Science*, 159(1-2):133–142, 1999. 57

[111] A. Mehta and A. L. Zydney. Effect of membrane charge on flow and protein transport during ultrafiltration. *Biotechnology Progress*, 22(2):484–492, 2006. 57

[112] C. Bellona, J. E. Drewes, P. Xu, and G. Amy. Factors affecting the rejection of organic solutes during nf/ro treatment - a literature review. *Water Research*, 38(12):2795–2809, 2004. 57, 58

[113] J. R. Pappenheimer, E. M. Renkin, and L. M. Borrero. Filtration, diffusion and molecular sieving through peripheral capillary membranes a contribution to the pore theory of capillary permeability. *American Journal of Physiology*, 167(1):13–46, 1951. 57

[114] N. S. Pujar and A. L. Zydney. Electrostatic effects on protein partitioning in size-exclusion chromatography and membrane ultrafiltration. *Journal of Chromatography A*, 796(2):229–238, 1998. 58, 62

[115] Marcel Mulder. *Basic principles of membrane technology*. Kluwer, Dordrecht, repr. edition, 2000. 59

[116] I. Gitlin, J. D. Carbeck, and G. M. Whitesides. Why are proteins charged? networks of charge-charge interactions in proteins measured by charge ladders and capillary electrophoresis. *Angewandte Chemie-International Edition*, 45(19):3022–3060, 2006. 62

[117] N. S. Pujar and A. L. Zydney. Electrostatic and electrokinetic interactions during protein-transport through narrow pore membranes. *Industrial & Engineering Chemistry Research*, 33(10):2473–2482, 1994. 62

[118] M. T. Tyn and T. W. Gusek. Prediction of diffusion-coefficients of proteins. *Biotechnology and Bioengineering*, 35(4):327–338, 1990. 62

[119] M. E. Young, P. A. Carroad, and R. L. Bell. Estimation of diffusion-coefficients of proteins. *Biotechnology and Bioengineering*, 22(5):947–955, 1980. 62

[120] K. A. Granath. Solution properties of branched dextrans. *Journal of colloid science*, 13:308–328, 1958. 62

[121] A. Mehta and A. L. Zydney. Permeability and selectivity analysis for ultrafiltration membranes. *Journal of Membrane Science*, 249(1-2):245–249, 2005. 64

[122] H. Woehlecke and R. Ehwald. Characterization of size-permeation limits of cell-walls and porous separation materials by high-performance size-exclusion chromatography. *Journal of Chromatography A*, 708(2):263–271, 1995. 64

[123] J. R. Miller and W. J. Koros. Aqueous transport-properties of mesoporous gamma-al2o3 membranes. *Industrial & Engineering Chemistry Research*, 33(4):934–941, 1994. 67

[124] T. Tsuru, T. Sudoh, T. Yoshioka, and M. Asaeda. Nanofiltration in non-aqueous solutions by porous silica-zirconia membranes. *Journal of Membrane Science*, 185(2):253–261, 2001. 67

[125] J. Palmeri, P. Blanc, A. Larbot, and P. David. Hafnia ceramic nanofiltration membranes - part ii. modeling of pressure-driven transport of neutral solutes and ions. *Journal of Membrane Science*, 179(1-2):243–266, 2000. 67

[126] C. Combe, C. Guizard, P. Aimar, and V. Sanchez. Experimental determination of four characteristics used to predict the retention of a ceramic nanofiltration membrane. *Journal of Membrane Science*, 129(2):147–160, 1997. 67

[127] C. S. Cojocaru, J. M. Padovani, T. Wade, C. Mandoli, G. Jaskierowicz, J. E. Wegrowe, A. F. I. Morral, and D. Pribat. Conformal anodic oxidation of aluminum thin films. *Nano Letters*, 5(4):675–680, 2005. 68

[128] W. G. Yelton, K. B. Pfeifer, and A. W. Staton. Porous al2o3 nanogeometry sensor films - growth and analysis. *Journal of the Electrochemical Society*, 149(1):H1–H5, 2002. 68

[129] C. S. Toh, B. M. Kayes, E. J. Nemanick, and N. S. Lewis. Fabrication of free-standing nanoscale alumina membranes with controllable pore aspect ratios. *Nano Letters*, 4(5):767–770, 2004. 68

[130] D. Crouse, Y. H. Lo, A. E. Miller, and M. Crouse. Self-ordered pore structure of anodized aluminum on silicon and pattern transfer. *Applied Physics Letters*, 76(1):49–51, 2000. 68

[131] Jinsub Choi. *Fabrication of monodomain porous alumina using nanoimprint lithography and its applications*. PhD thesis, s.n., 2004. 68

[132] L. J. Heyderman, B. Ketterer, D. Bachle, F. Glaus, B. Haas, H. Schift, K. Vogelsang, J. Gobrecht, L. Tiefenauer, O. Dubochet, P. Surbled, and T. Hessler. High volume fabrication of customised nanopore membrane chips. *Microelectronic Engineering*, 67-8:208–213, 2003. 68

[133] T. A. Desai, D. J. Hansford, L. Leoni, M. Essenpreis, and M. Ferrari. Nanoporous anti-fouling silicon membranes for biosensor applications. *Biosensors & Bioelectronics*, 15(9-10):453–462, 2000. 69

[134] A. Berg van den and M. Wessling. Nanofluidics - silicon for the perfect membrane. *Nature*, 445(7129):726–726, 2007. 69

[135] C. C. Striemer, T. R. Gaborski, J. L. McGrath, and P. M. Fauchet. Charge- and size-based separation of macromolecules using ultrathin silicon membranes. *Nature*, 445(7129):749–753, 2007. 69

[136] A. T. Shawaqfeh and R. E. Baltus. Fabrication and characterization of single layer and multi-layer anodic alumina membranes. *Journal of Membrane Science*, 157(2):147–158, 1999. 72

[137] W. R. Bowen, N. Hilal, R. W. Lovitt, and P. M. Williams. Atomic force microscope studies of membranes: Surface pore structures of cyclopore and anopore membranes. *Journal of Membrane Science*, 110(2):233–238, 1996. 72

[138] G. A. Parks. Isoelectric points of solid oxides solid hydroxides and aqueous hydroxo complex systems. *Chemical Reviews*, 65(2):177–&, 1965. 74

[139] S. Sharma, K. C. Popat, and T. A. Desai. Controlling nonspecific protein interactions in silicon biomicrosystems with nanostructured poly(ethylene glycol) films. *Langmuir*, 18(23):8728–8731, 2002. 74

[140] J. H. Lee, H. B. Lee, and J. D. Andrade. Blood compatibility of polyethylene oxide surfaces. *Progress in Polymer Science*, 20(6):1043–1079, 1995. 74

[141] M. Q. Zhang, T. Desai, and M. Ferrari. Proteins and cells on peg immobilized silicon surfaces. *Biomaterials*, 19(10):953–960, 1998. 74

[142] C. J. P. Hoogervorst, J. A. P. Vandijk, and J. A. M. Smit. Nonstationary diffusion through membranes .1. transient diffusion through a membrane separating 2 unequal volumes of well-stirred solutions. *Journal of Physical Chemistry*, 82(11):1311–1318, 1978. 77, 79, 80, 81

[143] C. J. P. Hoogervorst, J. Degoede, C. W. Versluijs, and J. A. M. Smit. Nonstationary diffusion through membranes .2. transient diffusion through a membrane separating 2 semi-infinite volumes of unstirred solutions. *Journal of Physical Chemistry*, 82(11):1318–1324, 1978. 81

[144] C. W. Versluijs and J. A. M. Smit. Nonstationary diffusion through a membrane separating 2 finite volumes of stirred or unstirred solutions. *Journal of Membrane Science*, 4(2):183–207, 1978. 81

[145] A. J. Staverman. Non-equilibrium thermodynamics of membrane processes. *Transactions of the Faraday Society*, 48(2):176–185, 1952. 81

[146] H. R. Clark, T. A. Barbari, and G. Rao. Modeling the response time of an in vivo glucose affinity sensor. *Biotechnology Progress*, 15(2):259–266, 1999. 81

[147] B. J. M. Hannoun and G. Stephanopoulos. Diffusion-coefficients of glucose and ethanol in cell-free and cell-occupied calcium alginate membranes. *Biotechnology and Bioengineering*, 28(6):829–835, 1986. 92

[148] J. Milton Harris. *Poly(ethylene glycol) chemistry biotechnical and biomedical applications*. Plenum Press, New York etc., 1992. 95

[149] J. Milton Harris, American Chemical Society Division of Polymer Chemistry, American Chemical Society, and American Chemical Society Meeting. *Poly(ethylene glycol) chemistry and biological applications developed from a symposium sponsored by the Division of Polymer Chemistry, Inc., at the 213th National Meeting of the American Chemical Society, San Francisco, CA, April 13-17, 1997*. American Chemical Society, Washington, DC, 1997. 95, 107

[150] J. J. Kim and K. Park. Glucose-binding property of pegylated concanavalin a. *Pharmaceutical Research*, 18(6):794–799, 2001. 102, 129

[151] G. C. Wood, P. Skeldon, G. E. Thompson, and K. Shimizu. A model for the incorporation of electrolyte species into anodic alumina. *Journal of the Electrochemical Society*, 143(1):74–83, 1996. 105

[152] V. Kapur, J. Charkoudian, and J. L. Anderson. Transport of proteins through gel-filled porous membranes. *Journal of Membrane Science*, 131(1-2):143–153, 1997. 105

[153] A. Asatekin, A. Menniti, S. T. Kang, M. Elimelech, E. Morgenroth, and A. M. Mayes. Antifouling nanofiltration membranes for membrane bioreactors from self-assembling graft copolymers. *Journal of Membrane Science*, 285(1-2):81–89, 2006. 105, 106

[154] U. Beyer, R. Ehwald, and L. G. Fleischer. Post-stress thickening of dextran/concanavalin a solutions used as sensitive fluids in a viscosimetric affinity assay for glucose. *Biotechnology Progress*, 13(6):722–726, 1997. 123

[155] N. Singh, Z. Chen, N. Tomer, S. R. Wickramasinghe, N. Soice, and S. M. Husson. Modification of regenerated cellulose ultrafiltration membranes by surface-initiated atom transfer radical polymerization. *Journal of Membrane Science*, 311(1-2):225–234, 2008. 129

[156] L. Siqi, J. Anderson, and Q. Wang. Synthesis and preparation of a novel glucose sensitive fluid. *SERMACS 2007 Greenville*, 2007. 130

[157] International Atomic Energy Agency. Radiation sterilization of tissue allografts : requirements for validation and routine control. a code of practice., 2007. 138

[158] N. Foghandersen, B. M. Altura, B. T. Altura, and O. Siggaardandersen. Composition of interstitial fluid. *Clinical Chemistry*, 41(10):1522–1525, 1995. 146

[159] C. Yazbeck, T. Moreau, J. Sahuquillo, L. Takser, and G. Huel. Effect of maternal manganese blood levels on erythrocyte calcium-pump activity in newborns. *Science of the Total Environment*, 354(1):28–34, 2006. 146

[160] A. A. Sharkawy, B. Klitzman, G. A. Truskey, and W. M. Reichert. Engineering the tissue which encapsulates subcutaneous implants .1. diffusion properties. *Journal of Biomedical Materials Research*, 37(3):401–412, 1997. 151

Appendix A

Data sheet of Dextran PSS

Certificate of Analysis

Polymer type:	Dextran broad/branched
Part No:	PSS-dxtb3m
Lot No:	dxtb3800-3

Molar Mass Distribution

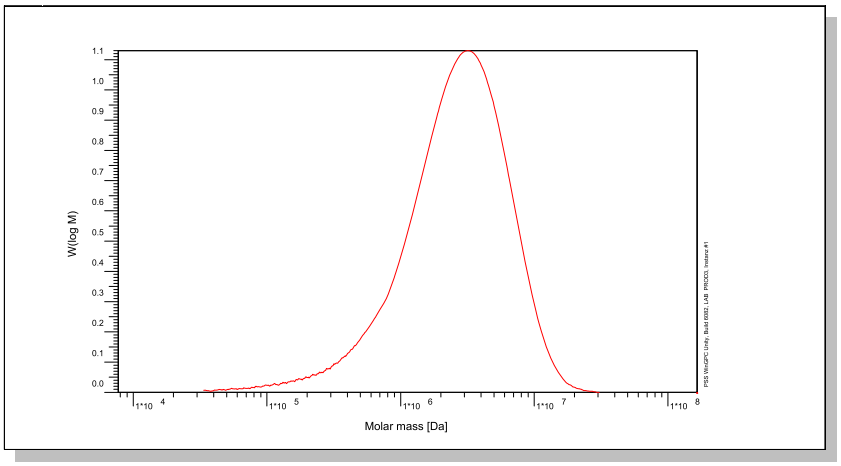

GPC/SEC - Conditions

Sample concentration	0,20 g/l	Inject volume	100 µl
Solvent	Water, 0.05% sodium azide	Flow rate	0,50 ml/min
Precolumn [8 x 50 mm]	PSS Suprema 10µm	Temperature	23,0° C
Columns [analytical, each 8 x 300 mm]	PSS SUPREMA 10µm 3 000Å / 3 000Å		
Data Acquisition Software	PSS WinGPC	Operator	G. Reinhold

GPC/SEC - Results

Detector	Mw (Da)	Mn (Da)	Mp (Da)	PDI (Mw/Mn)
Shodex RI 71	3500000	1400000	-	2,50

Light scattering - Result: Mw (Da) = 3 360 000

Note:

Mw = Weight Average Molecular Weight
Mn = Number Average Molecular Weight
Mp = Molar Mass at the Peak Maximum
PDI = Polydispersity Index

GPC/SEC - Results based on Pullulan calibration curve.

Manufacture control according to PSS method of analysis

Dr. T. Hofe
production director

Polymer Standards Service GmbH
In der Dalheimer Wiese 5 D-55120 Mainz
Tel.: +49 (0) 6131-96239-0 Fax: +49 (0) 6131-96239-11
Email: info@polymer.de www.polymer.de

DIN EN ISO 9001:2000
Zertifikat: 01 100 84065

Polymer Standards Service USA, Inc
43 Jefferson Blvd. Suite 3 Warwick, RI 02888 USA
Phone: +1 401-780-8884 Fax: +1 401-780-8824
Email: pssusa@pssgpcshop.com www.pssgpcshop.com

Appendix B

Membranes nomenclature

PPEGMA coated alumina membranes

Nomenclature in thesis	Nomenclature in experiments
WA20-NC	Whatman non-coated
WA20-10-1	lolo079-S5
WA20-20-1	lolo083-A
WA20-30-1	lolo083-D
WA20-40-1	lolo083-E
WA20-60-1	lolo080-S7
WA20-180-1	lolo79-S13
WA20-40-2	lolo79-S5
WA20-40-3	lolo83-A
WA20-40-4	lolo83-D
WA20-40-5	lolo85-5
WA20-40-7	lolo85-2
WA20-40-8	lolo85-4
WA20-40-9	lolo85-7
WA20-40-10	lolo80-S7
WA20-40-11	lolo85-3
WA20-40-12	lolo85-6
WA20-40-13	lolo80-S3
WA20-40-14	lolo85
WA20-80-1	SLL011-4
WA20-80-2	SLL6-5
WA20-80-3	SLL6-6
WA20-160-1	SLL016-3

PE films

Nomenclature in thesis	Nomenclature in experiments
PE-30-20	20060801-A
PE-30-30	20060801-B
PE-30-40	20060801-C
PE-15-05	20061222-05min
PE-15-10	20061222-10min
PE-15-30	20061222-30min
PE-15-60	20061222-60min

Appendix C

CAD drawings of demonstrator v2

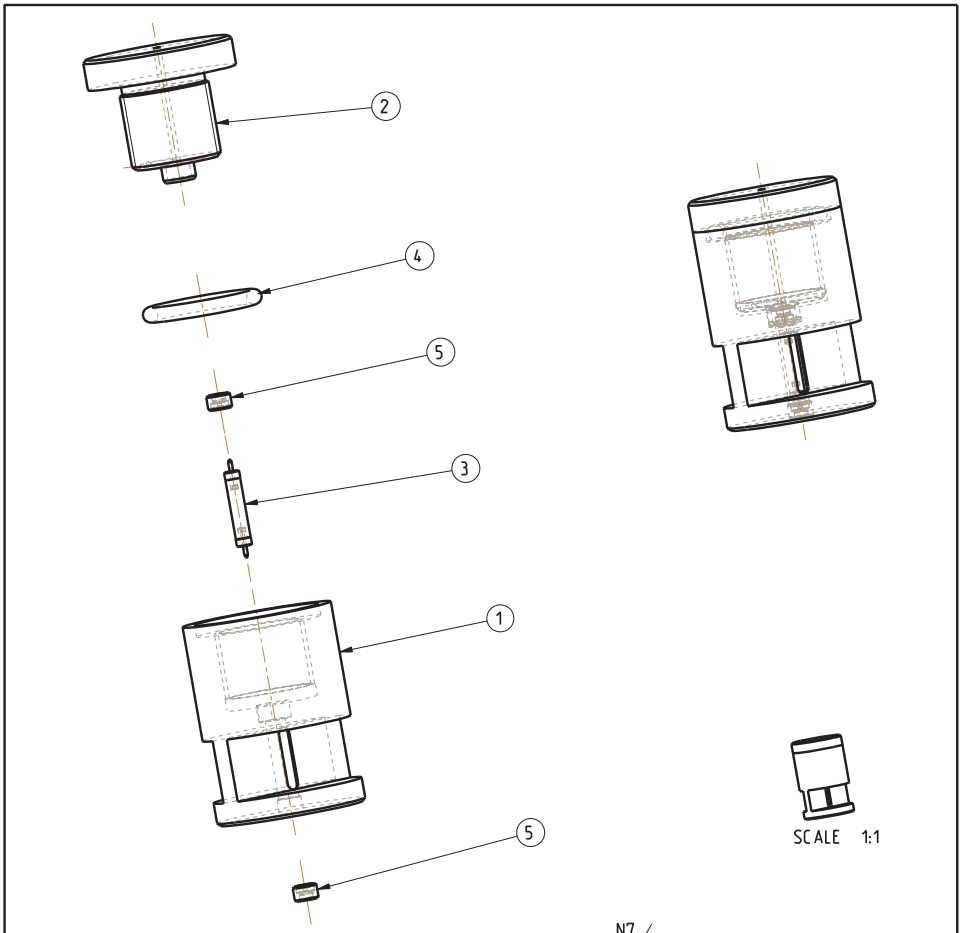

N7

Tolérances générales ISO 2768 f

Pos.	Quantite	Unite	N° d'identification	Denomination / Caracteristiques	
1	1		1001	CORPS avec slit	
2	1		1002	BOUCHON	
3	1		1003	ENSEMBLE AIMANT	
4	1		-	O-RING DE PRECISION EN NBR 70	
5	2		-	CHATON Ø1.6x0.85 PIGUET FRERES & CIE SA	

Mod	Mod	Dessine	J.Chassot	21.08.2007	Echelle 3:1
		Controle			
		Conf normes			
		Bon execution			
Sans nomenclature separee		N° commande			
Nomenclature sep de meme N°		Origine		Nb feuilles 2	Feuille N° 1
Nomenclature sep de N° different	N° ident	Remplace			
EPFL	IMPLANT			N° de dessin 1000	

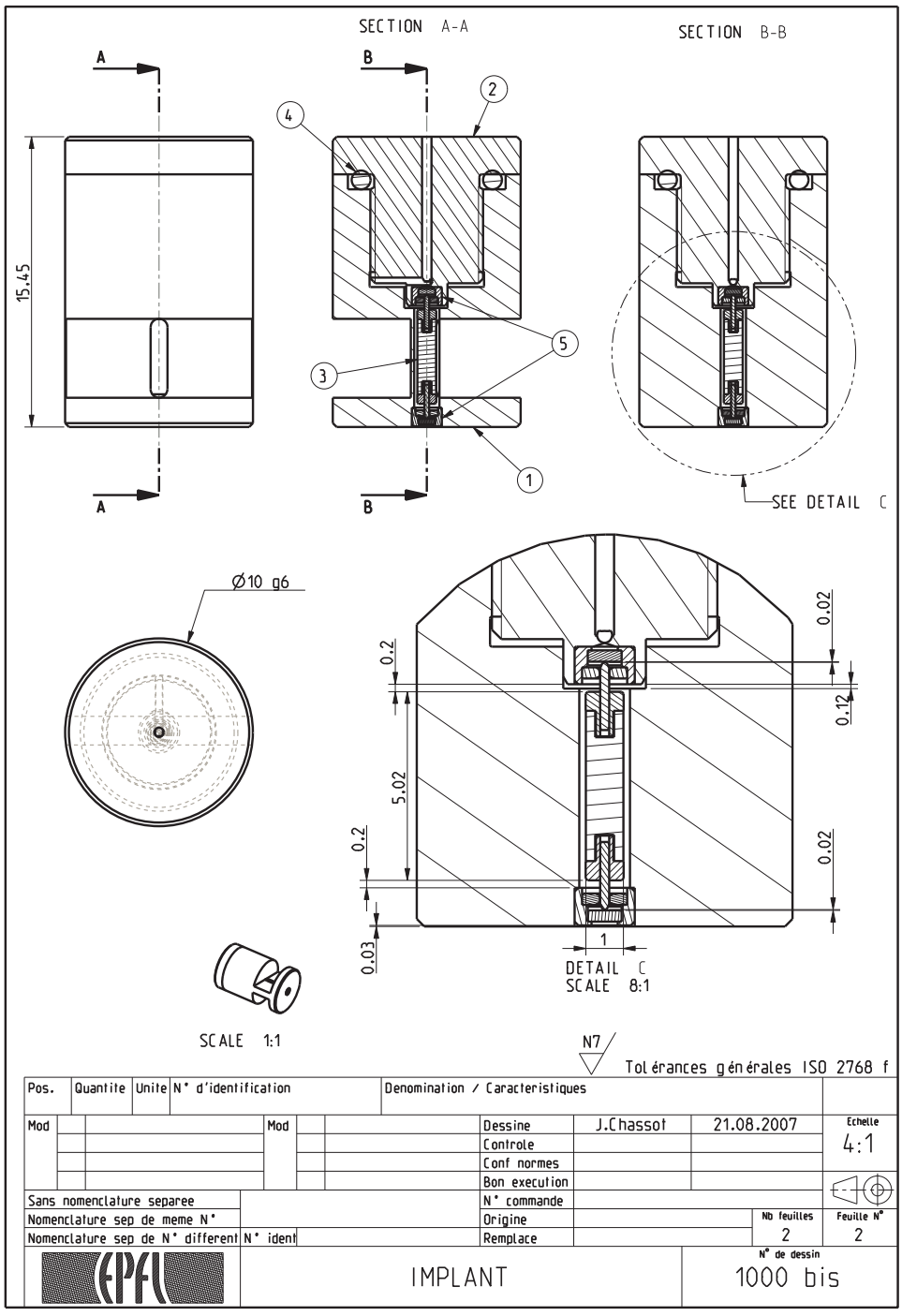
SECTION A-A
SECTION B-B
A
B
15.45
1
2
3
4
5
SEE DETAIL C
Ø10 g6
SCALE 1:1
0.2
5.02
0.2
0.03
0.02
0.12
0.02
1
DETAIL C
SCALE 8:1
N7
Tolérances générales ISO 2768 f
Pos.
Quantite
Unite
N° d'identification
Denomination / Caracteristiques
Mod
Dessine
J.Chassot
21.08.2007
Echelle
4:1
Controle
Conf normes
Bon execution
Sans nomenclature separee
N° commande
Nomenclature sep de meme N°
Origine
Nb feuilles
2
Feuille N°
2
Nomenclature sep de N° different
N° ident
Remplace
N° de dessin
IMPLANT
1000 bis

Curriculum Vitae

I was born in Meyrin (Switzerland) in 1979 and am a Swiss and Belgian citizen. I attended primary and secondary school in Lully, Tolochenaz and Morges in the vicinity of Lausanne (Switzerland). In 1997, I graduated from the Gymnase de Morges and obtained the Maturité (Swiss baccalaureat) and was awarded of the mathematics distinction. The following year, I went to Myrtle Creek (Oregon, USA) as an exchange student at the South Umpqua High School. I started studying Physics at École Polytechnique Fédérale de Lausanne (EPFL, Switzerland) in October 1998. Between October 2002 and March 2003, I accomplished my masters thesis at the IBM Research Laboratory in Zürich (Switzerland) under the supervision of Dr. Rolf Allenspach, Dr. J. Georg Bednorz and Prof. Harald Brune. I then graduated from EPFL in 2003 with a M.Sc. degree in Physics. Since September 2003, I have been working at the Laboratoire de Production Microtechnique (LPM, EPFL) as a research and teaching assistant, and as a PhD student, under the guidance of Eric Meurville and Prof. Peter Ryser. I participated in two projects in collaboration with Sensile Medical AG (Baar, Switzerland) relating to an insulin micro-pump and an implantable glucose sensor.